A stress-dependent TDP-43 SUMOylation program preserves neuronal function

Authors: Terry R. Suk[1-4], Caroline E. Part[1-4], Jenny L. Zhang[1-4†], Trina T. Nguyen[1-4†], Meghan M. Heer[1-4], Alejandro Caballero-Gómez[1-4], Veronica S. Grybas[1-4], Paul M. McKeever[5], Benjamin Nguyen[1-4], Steve M. Callaghan[1-4], John M. Woulfe[1,2,6-8], Janice Robertson[5], & Maxime W.C. Rousseaux[1-4]*.

[1]University of Ottawa Brain and Mind Research Institute, ON, Canada

[2]Department of Cellular and Molecular Medicine, University of Ottawa, ON, Canada

[3]Eric Poulin Center for Neuromuscular Diseases, ON, Canada

[4]Ottawa Institute of Systems Biology, ON, Canada

[5]Tanz Centre for Research in Neurodegenerative Diseases, University of Toronto, ON, Canada

[6]The Ottawa Hospital Research Institute, The Ottawa Hospital, ON, Canada

[7]Department of Pathology and Laboratory Medicine, University of Ottawa, ON, Canada

[8]Department of Biochemistry, Microbiology, and Immunology, University of Ottawa, ON, Canada

*Corresponding Author. Email: max.rousseaux@uottawa.ca

[†]Authors contributed equally.

Abstract: Amyotrophic Lateral Sclerosis (ALS) and Frontotemporal Dementia (FTD) are overwhelmingly linked to TDP-43 dysfunction. Mutations in TDP-43 are rare, indicating that the progressive accumulation of exogenous factors – such as cellular stressors – converge on TDP-43 to play a key role in disease pathogenesis. Post translational modifications such as SUMOylation play essential roles in response to such exogenous stressors. We therefore set out to understand how SUMOylation may regulate TDP-43 in health and disease. We find that TDP-43 is regulated dynamically via SUMOylation in response to cellular stressors. When this process is blocked *in vivo*, we note age-dependent TDP-43 pathology and sex-specific behavioral deficits linking TDP-43 SUMOylation with aging and disease. We further find that SUMOylation is correlated with human aging and disease states. Collectively, this work presents TDP-43 SUMOylation as an early physiological response to cellular stress, disruption of which may confer a risk for TDP-43 proteinopathy.

Keywords: ALS, FTD, TDP-43, SUMOylation, Pathology, Mouse Model, Post Translational Modifications, Stress

Introduction

Altered proteostasis is one of the key hallmarks of aging and is particularly prevalent in neurodegenerative diseases[1]. Despite the highly heterogenous nature of neurodegenerative diseases – likely owing to the extreme genetic and environmental diversity acting upon individuals – a select few proteins are recurringly implicated in pathology[2]. TDP-43 is an essential RNA binding protein notorious for its involvement in neurodegenerative diseases including Amyotrophic Lateral Sclerosis (ALS) and Frontotemporal Dementia (FTD). In a diseased state, TDP-43 is found mislocalized from the nucleus and aggregated in the cytoplasm of neurons within the central nervous system (CNS) in ~97% and ~45% of ALS and FTD cases, respectively[3, 4]. Additionally, ALS and FTD exist on a clinical and genetic spectrum linked by TDP-43 dysfunction often referred together as ALS/FTD[5]. Beyond ALS/FTD, TDP-43 pathology is increasingly linked to other neurological disorders including Limbic-predominant Age-related TDP-43 Encephalopathy (LATE), Alzheimer's Disease (AD), Chronic Traumatic Encephalopathy (CTE), and Stroke[6–9]. Thus, TDP-43 pathology has garnered much attention to better understand the causes of these diseases and to uncover potential routes of therapeutic intervention.

The accumulation of cytoplasmic TDP-43 aggregates is considered a late-stage event in neurodegeneration. Increasing evidence suggests that the partial mislocalization or complete depletion of TDP-43 from the nucleus to the cytoplasm is an early event in ALS/FTD pathogenesis, functioning independently – however tightly associated – with aggregation[10–16]. As a result, recent efforts have focused on the outcomes of TDP-43 mislocalization as early markers of dysfunction and/or mechanisms driving disease. Indeed, loss of function due to mislocalization of TDP-43 causes aberrant cryptic splicing in genes including *STMN2* and *UNC13A* that drive the progression of ALS[12–15, 17]. To wit, cryptic mis-splicing of *STMN2* was recently found to correlate strongly with TDP-43 pathology[18, 19]. Additionally, once in the cytoplasm, TDP-43 can exert additional toxicity through gain of function effects by sequestering critical proteins into cytoplasmic aggregates thus disrupting crucial pathways leading to cellular demise[11, 20]. Together, dysregulation of TDP-43 is sufficient to drive neuronal dysfunction ultimately leading to neurodegeneration. However, the mechanisms instigating TDP-43 pathogenesis remain convoluted.

Despite the overwhelming prevalence of TDP-43 pathology in ALS/FTD and related diseases, mutations in the gene encoding TDP-43 (*TARDBP*) are only present in less than 1% of all ALS and FTD cases[21]. It is becoming evident that not one, but many genetic and/or environmental factors affect pathways converging on TDP-43 in ALS/FTD. Many ALS/FTD causative genes exert toxicity by disruption of key pathways such as nucleocytoplasmic transport and cellular stress responses[22]. The cellular stress response is a critical pathway tightly linked to ALS/FTD and TDP-43 supported via genetic, experimental, and epidemiological evidence [23–36]. On the one hand, ALS/FTD-linked mutations disrupting various steps of the stress response pathways converge on the dysregulation of TDP-43 resulting in pathology[23–25, 30–33, 36]. On the other hand, exogenous insults such as aging, head injuries, viral infections, and other exposures may confer susceptibility or precipitate ALS/FTD and can serve as pre-clinical models of TDP-43 proteinopathy[8, 37–39]. Motor neurons, the primary vulnerable cell type in ALS, are thought to be particularly susceptible to stress due to the high levels of excitotoxicity experienced throughout one's lifetime[40]. Indeed, prolonged cellular stress due to chronic stress exposure or failures in stress recovery can result in TDP-43 pathology[28, 41]. However,

much less is known about the molecular pathways acting upon TDP-43 in the cell stress response and how they might be linked to age-related neurodegeneration. Uncovering these mechanisms will help to better understand how environmental insults that occur throughout aging converge on TDP-43 and cause susceptibility to disease.

Post translational modifications (PTMs) play key roles in regulating protein function and have been tightly linked to TDP-43 (dys)function and disease. TDP-43 is modified by an array of PTMs including phosphorylation, ubiquitination, acetylation, and polyADP-ribosylation[42–46]. Abnormal TDP-43 phosphorylation and ubiquitination are pathognomonic of ALS and TDP-43 related FTD[42]. Recent studies have suggested that SUMOylation – the covalent conjugation of a Small Ubiquitin-like Modifier (SUMO) to target lysine residues[47, 48] – by SUMO1 may have a role in regulating TDP-43 nucleocytoplasmic transport and RNA binding[49–52]. SUMO1 is best characterized for its roles in nucleocytoplasmic shuttling[53]. SUMO2 however is the only essential SUMO paralog and selectively plays roles in orchestrating cellular stress responses[54, 55]. SUMO2 has previously been observed in TDP-43 aggregates *in vitro* and is related with TDP-43 insolubility[56, 57]. However, it is unclear whether TDP-43 is a direct target of SUMO2 and what the implications are on TDP-43 function and disease pathogenesis.

Here, we show that TDP-43 is modified by SUMO2 selectively in response to cellular stressors. TDP-43 becomes SUMOylated within the nucleus early in response to stress, upstream of TDP-43 aggregation. Modification by SUMO2 is further correlated with dosage and duration of cellular stress and peaks during the recovery phase before it is cleared through the ubiquitin proteosome system. We further identified four E3 SUMO ligases that can modulate the levels of TDP-43 SUMOylation. We found that TDP-43 is SUMOylated by SUMO2 in a conserved region of the C-terminal domain at lysine (K) 408 directly adjacent to phosphorylation residues serine (S) 409/410 characteristically phosphorylated in TDP-43 aggregates. To understand the physiological consequences of blocking TDP-43 SUMOylation, we generated a knock in mouse model bearing a p.K408R point mutation in endogenous mouse *Tardbp* allele. Cortical neurons cultured from these mice display impaired stress recovery and accumulation of nuclear TDP-43. These mice do not show abnormalities in development but develop mild social and cognitive deficits as they age. Pathologically, we observe TDP-43 mislocalization and accumulation of phosphorylated TDP-43 in the spinal cord and significant denervation of neuromuscular junctions in aged mice. As SUMOylation of TDP-43 plays a protective role in mice during aging, we assessed human brain samples and observed a positive correlation between global SUMOylation and age inferring an increased demand on SUMO-related pathways during aging. Finally, we observed significant increase in TDP-43 and SUMO2 interactions in the prefrontal cortex from individuals diagnosed with ALS/FTD compared to unaffected controls suggesting SUMOylation is actively engaged in regulating TDP-43 in disease states.

Results

TDP-43 is SUMOylated in the nucleus in a context specific manner

Various acute stressors including oxidative (sodium arsenite, $NaAsO_2$), hyperosmotic (D-sorbitol and sodium chloride), and heat shock have been demonstrated to induce TDP-43 mislocalization and aggregation *in vitro*, helping to uncover key mechanisms affected in disease[24, 58, 59]. As sodium arsenite is a commonly used stressor to interrogate TDP-43 alterations, we examined whether TDP-43 became SUMOylated in response to sodium arsenite treatment. Using an immunoprecipitation assay ("SUMOylation Assay", Fig. 1A) to

immunoprecipitate HA-SUMO bound proteins under denaturing conditions to disrupt non-covalent protein interactions, we found that TDP-43 becomes SUMOylated by SUMO2 and can form polySUMO chains specifically in response to stress (Fig. 1B). Interestingly we found that sodium arsenite and heat shock stressors, but not hyperosmotic stress, induced TDP-43 SUMOylation suggesting that SUMOylation is a context specific modifier of TDP-43 (Fig. S1A).

Previous reports have suggested that TDP-43 is SUMOylated under native conditions by SUMO1 to regulate nucleocytoplasmic transport and RNA binding[49]. Strikingly, we found that TDP-43 SUMOylation was selectively modified by SUMO2 and SUMO3, but not SUMO1, specifically under stressed conditions; consistent with the conserved roles of SUMO2 and SUMO3 in response to stress (Fig. S1B). Mature (covalently bound) SUMO2 and SUMO3 share nearly 100% amino acid homology making them difficult to differentiate and thus referred together as SUMO2/3. Since SUMO2 is the only essential and most abundantly expressed SUMO paralog in the CNS and sodium arsenite is commonly used to study TDP-43 pathobiology, we focused on TDP-43 SUMOylation by SUMO2 in response to sodium arsenite stress[54, 60].

To test whether TDP-43 SUMOylation is linked with disease-like states, we expressed ALS-linked mutant TDP-43 (TDP-43^{Q331K}) and found that TDP-43 SUMOylation was significantly increased compared to wild type TDP-43 (Fig. S1C). Next, we disrupted the nuclear localization sequence in TDP-43 (TDP-43^{NLSmut}) to mislocalize TDP-43 to the cytoplasm and found that in response to sodium arsenite, TDP-43^{NLSmut} blocks SUMOylation indicating that nuclear localization is essential for TDP-43 SUMOylation (Fig. 1C,D). Classically, lysine (K) residues, in addition to arginine (R) residues, are critical components of a traditional NLS to enable the interaction with importins to facilitate nuclear import of proteins; but they may also be direct targets of SUMOylation[61]. To determine whether loss of TDP-43 SUMOylation is mediated through loss of nuclear localization or disruption of lysine (K) residues in the NLS, we sought to restore TDP-43 localization to rescue TDP-43 SUMOylation. We surveyed the literature to identify a NLS that functions independent of lysine (K) residues. Previous studies have demonstrated that the RNA binding protein HNRNPA1 contains a non-conventional PY-NLS to facilitate nuclear localization [62, 63]. We replaced the native TDP-43 NLS with an HNRNPA1 PY-NLS (TDP-43$^{PY\text{-}NLS}$) and found that TDP-43$^{PY\text{-}NLS}$ localizes to the nucleus reflecting wild type TDP-43 (Fig. 1C). By performing a GFP-Trap SUMOylation assay we found that TDP-43$^{PY\text{-}NLS}$ rescues the loss of SUMOylation observed when expressing TDP-43^{NLSmut} indicating that nuclear localization, and not the lysine (K) residues within the NLS, is required for stress-dependent TDP-43 SUMOylation (Fig. 1D).

To further validate our findings, and to visualize the interaction between TDP-43 and SUMO2 in primary cortical neurons. As TDP-43 and SUMO2 are widely expressed throughout the nucleus, co-localization analysis is challenging to infer SUMOylation events (Fig. S1D). To visualize the interaction between TDP-43 and SUMO2/3 we performed a proximity ligation assay (PLA) in murine primary cortical neurons cultures (Fig. 1E, Fig. S1E). We found that in response to sodium arsenite there is a significant increase in PLA signal between endogenous TDP-43 and SUMO2/3, consistent with the stress-dependent SUMOylation previously observed. Taken together, SUMOylation may be an important mechanism regulating nuclear TDP-43 upstream of mislocalization in response to stress.

170 ***SUMOylation is an early event in response to stress and helps clear TDP-43 through the***
171 ***ubiquitin proteasome system during recovery***

172 Prolonged cellular stress *in vitro* leads to mislocalization of TDP-43 and progressive
173 transition into insoluble aggregates resembling aspects of pathology observed in disease[16, 28,
174 31, 33, 64]. As TDP-43 SUMOylation occurs within the nucleus upstream of nuclear egress, we
175 postulated that SUMOylation would occur upstream of aggregation during prolonged sodium
176 arsenite stress. To test this hypothesis, we performed a time course assay to characterize the
177 dynamics of TDP-43 SUMOylation during prolonged treatment with sodium arsenite. We
178 observed that TDP-43 becomes readily SUMOylated in the first 15-30 minutes of the acute stress
179 response upstream of the accumulation of RIPA-insoluble, phosphorylated TDP-43 (Fig. S1F).
180 Furthermore, we observed an increase in TDP-43 SUMOylation that linearly correlated with the
181 duration of stress ($R^2 = 0.6922$, $p<0.0001$). To determine whether SUMOylation occurs in
182 response to relative stress intensity, we performed a dose response assay and found that TDP-43
183 SUMOylation is proportional to relative stress intensity (Fig. S1G). Therefore, the increase in
184 TDP-43 SUMOylation during prolonged stress is likely due to an increased stress burden over
185 time.

186 To determine the fate of SUMOylated TDP-43, we performed a stress-recovery time-
187 course assay where cells were stressed with sodium arsenite for up to 1 hour, then allowed cells
188 to recover after washout. For the first hour during stress recovery, we observed an ~3-fold
189 increase in TDP-43 SUMOylation indicating that TDP-43 continues to be SUMOylated and
190 polySUMOylated during the early stages of stress recovery (Fig. 1F). Furthermore, SUMOylated
191 TDP-43 was not detectable after 3 hours of recovery, suggesting that most of the clearance
192 occurs between 2-3 hours post stress. TDP-43 is known to interact with the SUMO-Targeted
193 Ubiquitin Ligase RNF4 which can polyUbiquitinate SUMOylated proteins to be degraded
194 through the UPS[65]. To determine whether the UPS functions to clear SUMOylated TDP-43
195 during stress recovery, we treated cells with the proteasome inhibitor MG132 and monitored
196 TDP-43 SUMOylation during stress and recovery. We observed that inhibiting the UPS system
197 by MG132 treatment prevented clearance of SUMOylated TDP-43 during post-stress recovery
198 indicating that SUMOylated TDP-43 is marked for degradation by the UPS pathway.
199 Importantly, treatment with MG132 for 1 or 4 hours was not sufficient to induce TDP-43
200 SUMOylation by itself, consistent with the stress-selective nature inducing TDP-43
201 SUMOylation. Taken together, TDP-43 SUMOylation occurs early in the stress response which
202 then leads to ubiquitin-targeted clearance during stress recovery demonstrating SUMOylation
203 may be an important mechanism regulating nuclear TDP-43 proteostasis.

204 ***Stress-dependent TDP-43 SUMOylation is mediated by select E3 SUMO ligases***
205 E3 SUMO ligases are important mediators for SUMOylation of select substrates and
206 enable spatiotemporal regulation of this modification. Thus, they may represent critical
207 modulators of TDP-43 SUMOylation. To identify potential E3 SUMO ligases that may regulate
208 TDP-43 SUMOylation, we first performed a literature search to identify potential ligases with
209 evidence of mediating SUMOylation. We prioritized 15 candidate E3 SUMO ligases and using a
210 dual sgRNA/Cas9 approach generated knockout cell lines for each of the candidate ligases and
211 performed GFP-Trap SUMOylation assays to test the effects on TDP-43 SUMOylation
212 (Fig. 1G)[66–80]. As a positive control, we knocked out the sole E2 SUMO ligase, UBC9
213 (encoded by *UBE2I*), which led to a near complete loss of TDP-43 SUMOylation demonstrating
214 the functionality of the approach. We identified four SUMO E3 ligases whose knockout

consistently reduced the levels of stress-induced TDP-43 SUMOylation: *EGR2 (KROX20), PIAS1, TRIM28 (KAP1),* and *ZNF451 (ZATT).* EGR2 is linked to the neuromuscular disorder Charcot Marie Tooth Disease and is an immediate early gene rapidly reacting to external cellular stimuli aligning with the early response of TDP-43 SUMOylation upon stress[81, 82]. PIAS1 is a canonical, highly conserved E3 SUMO ligase known to play roles in cellular stress responses[83]. TRIM28 is also a well characterized E3 SUMO ligase which is a predicted interactor of SUMOylated TDP-43 based on the GPS-SUMO2.0 algorithm[84–86]. ZNF451 is characterized as a stress dependent E3 SUMO ligase specifically promoting polySUMOylation with SUMO2/3. It is sometimes referred to as an "E4 SUMO elongase" which complements our data that TDP-43 is polySUMOylated in response to stress[80, 87]. Identification of these putative TDP-43 SUMO ligases supports the robustness of stress-induced TDP-43 SUMOylation and adds layers of nuance into the regulation of TDP-43 with variable routes of modulating TDP-43 functions.

TDP-43 SUMOylation occurs in a conserved region of the C-terminal domain

SUMOylation occurs at lysine (K) residues often residing within a consensus SUMOylation motif, Ψ-K-x-D/E (Ψ=large hydrophobic residue, x = any amino acid), however it is increasingly recognized that SUMOylation at lysine residues in non-consensus motifs is not uncommon and plays significant roles in regulating protein function[85]. Using GPS-SUMO (https://sumo.biocuckoo.cn/) to predict likely SUMOylation sites on TDP-43, we identified a consensus SUMOylation motif within the first RNA recognition motif at K136 – thought to be the site targeted by SUMO1 – and a non-consensus SUMOylation motif within the C-terminal domain at K408[85, 86].

To map the residue of stress induced TDP-43 SUMOylation, we expressed TDP-43 mutating the candidate lysine (K) residues to arginine (R) residues to maintain similar charge and structure of the native amino acid sequence while blocking SUMOylation: K136R, K408R, and K136R/K408R "2KR". By performing a GFP-trap SUMOylation assay, we observed that TDP-43^{K136R} did not block sodium arsenite-induced TDP-43 SUMOylation (Fig. 2A). Through fluorescent microscopy, we observed that TDP-43^{K136R} formed nuclear puncta with resemblance to RNA-binding deficient TDP-43 (5FL) (Fig. S2A). We predicted the structure of TDP-43 and TDP-43^{K136R} with AlphaFold3 in the presence of UG repeated RNA and found that K136R is predicted to slightly alter the tertiary structure of TDP-43 and affect the interaction with RNA (Fig. S2B and S2C). Thus, phenotypes observed in TDP-43^{K136R}, as reported by others, may be facilitated by loss of RNA binding functions independent of loss of SUMOylation[50–52]. In contrast, through GFP-trap SUMOylation assays we found that TDP-43^{K408R} mutant significantly reduced TDP-43 SUMOylation by ~50%, suggesting K408 is a major site of SUMOylation in response to sodium arsenite stress (Fig. 2A). Importantly, mining two independent unbiased mass spectrometry studies identifying sites of SUMOylation across the proteome in stressed and unstressed conditions also uncovered TDP-43 SUMOylation at K408, supporting our findings [88, 89]. Through florescent microscopy analysis, we found that expression of TDP-43^{K408R} did not induce nuclear TDP-43 puncta, but instead led to a slight albeit insignificant increase in cells presenting with mislocalized TDP-43 (Fig. S3D). However, overexpression of TDP-43^{K408R} did not uniformly induce mislocalization in all cells, consistent with the dynamic nature of TDP-43 SUMOylation and the requirement of stress to introduce TDP-43 SUMOylation responses. Finally, TDP-43^{2KR} significantly reduced TDP-43 SUMOylation to the same extent as TDP43^{K408R} suggesting that K408 and not K136 is a target of stress-induced SUMOylation (Fig.

260 2A). We further observed that TDP-43^{2KR} expression is less stable than TDP-43^{K408R} likely due
261 to the structural changes mediated by K136R. Taken together, K408 is a major target of stress-
262 induced SUMOylation.

263 To address the evolutionary conservation of TDP-43 SUMOylation at K408, we aligned
264 the amino acid sequences of TDP-43 with 300 orthologs from OrthoDB and found that human
265 K408 is nearly completely conserved throughout jawed-vertebrates concurrent with the evolution
266 of the C-terminal domain (Fig. 2B, Supplementary Table 1). While this domain harbors the
267 majority of ALS/FTD causing mutations, the residues surrounding K408 display considerably
268 high levels of conservation (~86% pairwise identity) indicating that this motif may play
269 important roles in regulating TDP-43 in vertebrates that may be altered by disease causing
270 mutations (Fig. 2C, Supplementary Table 1). Consistent with these findings, no missense
271 variants have been identified that disrupt the SUMOylation motif (based on gnomAD v4.0[90])
272 supporting its robust conservation in the healthy human population.

273 The residues surrounding TDP-43 K408, specifically S403, S404, S409, and S410 are
274 characteristically phosphorylated in patients with TDP-43 proteinopathy[42]. To determine
275 whether phosphorylation of TDP-43 at these serine residues interact with SUMOylation at K408,
276 we expressed phospho-dead "4SA" TDP-43 (S403/404/409/410A) and observed that TDP-43^{4SA}
277 does not lead to loss of SUMOylation following stress, but rather appeared to promote an
278 increase in its SUMOylation (Fig. 2D). Whether phosphorylation functions allosterically to
279 remove SUMO2/3 at K408 or antagonistically to block the SUMOylation recognition site
280 remains unclear. The independent modification by either phosphorylation or SUMOylation may
281 serve as a mechanism to differentially regulate TDP-43 function independently or sequentially in
282 response to stimuli. Thus, while TDP-43 phosphorylation has gained significant attention since
283 its initial discovery[42] – in part due to the availability of phospho-specific antibodies – we now
284 show that the C-terminal domain contains a conserved "PTM-enriched region" where
285 SUMOylation at K408 may precede phosphorylation, revealing additional complexity and
286 nuance to the stimulus-induced regulation of TDP-43.

287 ***C-terminal SUMO-mimetic destabilizes TDP-43***

288 Promoting specific protein SUMOylation is rather difficult given the size of the SUMO
289 molecule and the pleiotropy resulting from overexpressing SUMO proteins and their related
290 machinery. To overcome this limitation and to mimic SUMOylation at K408, we expressed
291 TDP-43-HA and TDP-43 with a C-terminal SUMO2 fusion (TDP-SUMO2-HA) in HEK293T
292 cells. By western blot we found that C-terminal fusion of SUMO2 led to a significant reduction
293 in TDP-43 levels (Fig. S3A). The reduction in TDP-43-SUMO2-HA suggesting that C-terminal
294 fusion of SUMO2 destabilizes TDP-43 levels, consistent with our data showing that prolonged
295 TDP-43 SUMOylation leads to its polyubiquitination and degradation (Fig. 1F). We further
296 observed that overexpression of TDP-43-HA and TDP-43-SUMO2-HA both significantly
297 increased phosphorylation of eIF2α compared to non-transfected controls despite significantly
298 lower levels of TDP-43-SUMO2-HA.

299 Next, we aimed to gain insight into how C-terminal fusion of SUMO effects TDP-43
300 localization and stress response. We did not observe constitutive changes in TDP-43 localization
301 suggesting that SUMO2 fusion does not drive TDP-43 nuclear export (Fig. S3B). By stressing
302 cells for 1 hour with sodium arsenite we observed that TDP-43-SUMO-HA cells could elicit a
303 stress response and form stress granules just like their WT counterparts. However, we were

304 surprised to find a significant increase in the proportion of stress granules colocalizing with
305 TDP-43-SUMO2-HA compared to TDP-43-HA alone. In addition, stress granules were generally
306 larger and more irregular in size and shape in cells expressing TDP-43-SUMO2-HA. Taken
307 together this suggests that SUMOylation of TDP-43 at the C-terminus converges on stress
308 response pathways involving stress granules and the integrated stress response (i.e. eIF2α
309 pathway). However, whether TDP-43 SUMOylation is involved in the upstream regulation or
310 downstream modulation of these pathways remains unclear.

311 ***Endogenous mutation of murine TDP-43 at K408 blocks stress-responsive TDP-43***
312 ***SUMOylation in the mouse brain***

313 To understand the cellular and physiological roles of TDP-43 SUMOylation, we
314 generated a knock in mouse model harboring a missense (c.1223 A>G) point mutation in the
315 endogenous mouse *Tardbp* locus resulting in the expression of Tdp-43 bearing a p.K408R
316 missense mutation thereby blocking endogenous Tdp-43 SUMOylation (Fig. 2E, Fig. S4A,B).
317 For simplicity herein, all genes/proteins will be referred to following their human nomenclature
318 (e.g. mouse Tdp-43 versus human TDP-43, collectively "TDP-43"). Although TDP-43 and
319 SUMO2 are independently essential for embryonic development, the "TDP-43^{K408R}" mice are
320 born at normal mendelian ratios without gross impairment indicating that TDP-43 SUMOylation
321 at K408 is not essential for murine development (Fig. S4C)[54, 91].

322 In order to validate that mutation of endogenous TDP-43 K408 blocks stress responsive
323 TDP-43 SUMOylation in TDP-43^{K408R} mice, we designed an ex vivo approach to test
324 endogenous stress responsive TDP-43 SUMOylation in the mouse brain (Fig. 2F). Briefly, we
325 dissected mouse embryos at E14 and divided each brain into two hemispheres. Both hemispheres
326 were maintained in neurobasal complete media for one hour, with one hemisphere at 37 °C as a
327 control, and the complementary hemisphere was heat shocked at 42 °C. The brain hemispheres
328 were lysed under denaturing conditions and endogenously SUMOylated proteins were
329 immunoprecipitated using antibodies targeted against endogenous SUMO2/3. SUMOylated
330 proteins were eluted using a synthetic peptide reflecting the antibody epitope to competitively
331 elute SUMOylated proteins. We observed that this approach reliably detects endogenous TDP-43
332 SUMOylation in response to heat shock yielding a doublet band at ~65kDa and a corresponding
333 decrease by ~50% in TDP-43^{K408R} animals reflecting previous results in HEK293T cells (Fig.
334 2G, 1B). Thus, stress-induced TDP-43 SUMOylation is impaired in the TDP-43^{K408R} mouse
335 brain.

336 ***TDP-43 SUMOylation at K408 supports cellular stress response and recovery in neurons***

337 As TDP-43 SUMOylation responds to, and is cleared during cellular stress and recovery
338 respectively, we posited that SUMOylated TDP-43 plays key roles in responding and recovering
339 from stress. We cultured murine TDP-43$^{+/+}$ and TDP-43$^{K408R/K408R}$ primary cortical neurons and
340 performed stress and recovery assays to determine how the cell stress response may be affected.
341 Since TDP-43 is critical for the formation of G3BP1 positive stress granules, we examined their
342 formation and resolution following stress and recovery[92, 93]. We found that stress granules
343 could form in TDP-43$^{K408R/K408R}$ neurons to the same degree as TDP-43$^{+/+}$ neurons, but there was
344 a significant delay in stress granule clearance during recovery (Fig. 3A, Fig. S5A-C). When
345 assessing TDP-43 solubility, we also observed a significant increase in RIPA insoluble
346 phosphorylated TDP-43 at 1 hour recovery that was cleared by 3 hours post-stress recovery (Fig.
347 3B, S6A). Based on our previous results that SUMOylation is cleared by the UPS pathway and

348 phosphorylation may function antagonistically with SUMOylation, the increase in
349 phosphorylation during recovery may serve as an alternative method of proteostasis to
350 compensate for loss of SUMOylation. We further observed a significant increase in nuclear
351 TDP-43 foci that were specific to the recovery phase and were exacerbated after 3 hours
352 recovery in the TDP-43$^{K408R/K408R}$ neurons (Fig. 3C). Various forms of nuclear TDP-43 bodies
353 are increasingly recognized to be aberrantly regulated in disease and stress states [19, 94–96].
354 We tested several likely markers of nuclear foci related to cell stress and recovery and found that
355 these foci are neither anisosomes nor paraspeckles and they do not colocalize with Ubiquitin
356 (Fig. S6B-D). Thus, these TDP-43 foci may represent a unique nuclear body related to recovery
357 from cellular stress. Together, TDP-43$^{K408R/K408R}$ neurons appropriately respond to, but not
358 efficiently resolve acute cellular stress which may render cells vulnerable to further insult.

359 Following the idea that SUMOylation of TDP-43 helps facilitate efficient recovery to
360 protect cells from further insults, we questioned whether multiple short insults exacerbate the
361 stress response in neurons. We designed a paradigm where primary cortical neurons were
362 stressed for 30 minutes with sodium arsenite then allowed to recover for 30 minutes before
363 receiving subsequent insults. We stressed and recovered the same neurons a total of 3 times over
364 3 hours and assessed stress granule dynamics in SUMO-competent (TDP-43$^{+/+}$) and
365 SUMOylation-deficient (TDP-43$^{K408R/K408R}$) neurons. In TDP-43$^{+/+}$ neurons we observed that
366 during the first stress phase, stress granules formed in a proportion of neurons which were then
367 retained during the first recovery (Fig. 3D). Subsequent rounds of stress further increased the
368 proportion of cells containing stress granules which were roughly maintained or decreased
369 during subsequent rounds of recovery suggesting that recovery pathways are being engaged and
370 subsequent stress induces an additive effect without full recovery. In TDP-43$^{K408R/K408R}$ neurons
371 however we observed the initiation of stress granule formation in the first 30 minutes of stress
372 that followed by inappropriate reactivation and recovery following subsequent rounds of stress.
373 This supports that stress responses related to stress granule dynamics are altered in
374 TDP-43$^{K408R/K408R}$ likely related to inefficient recovery from stress. Additionally, we observed a
375 striking increase in the proportion of cells presenting with nuclear TDP-43 foci after the third
376 round of stress and recovery (Fig. 3E), though increases in TDP-43 mislocalization in this
377 experimental paradigm were rather marginal and did not reach significance(Fig. S6E).

378 To better determine how blocking TDP-43 SUMOylation may respond to mild chronic
379 stress, we treated neurons with low dose of sodium arsenite for 30 hours then allowed them to
380 recovery for 3 days and assessed biochemical changes in TDP-43 solubility. In TDP-43$^{+/+}$
381 neurons we observed a significant decrease in RIPA soluble TDP-43 after chronic stress
382 followed by a marked increase in phosphorylated TDP-35 fragments in the urea-fraction (Fig.
383 S6F). Upon recovery these fragments were cleared and insoluble TDP-43 returned to unstressed
384 levels by 72 hours recovery. In TDP-43$^{K408R/K408R}$ neurons however, we observed the same
385 changes in response to chronic stress, however during recovery we observed significantly lower
386 soluble TDP-43 levels and significantly increased phosphorylated TDP-35 fragments in the urea-
387 fraction. Furthermore, we observed significant shift in the solubility of Ubiquitinated proteins
388 during recovery. Taken together, blocking TDP-43 SUMOylation impairs the ability for cells to
389 recover from cellular stress and may shift to other pathways involving phosphorylation or
390 cleavage to regulate TDP-43.

391 ***Blocking TDP-43 SUMOylation in vivo leads to sex-specific social and cognitive deficits***

392 Following on our findings that blocking TDP-43 SUMOylation affect neurons abilities to
393 recover from repeated or mild cellular stress, we posited that blocking TDP-43 SUMOylation in
394 aging may render long lived cells (i.e. neurons) vulnerable across aging as mild life stresses
395 accumulate over time [97]. Thus, we aimed to comprehensively characterize the TDP-43^{K408R}
396 mice across their lifespan to uncover the baseline phenotypic changes that occur with aging as an
397 innate stress upon cells. As TDP-43 SUMOylation is involved in supporting the normal cellular
398 stress response and maintaining TDP-43 proteostasis, we hypothesized that disrupting this
399 process leads to age-dependent physiological changes accelerated by impaired stress responses
400 and TDP-43 accumulation. To ensure that the K408R mutation did not lead to post gestational
401 developmental changes that would confound the presentation of age-related impairment, we
402 assessed the weights and motor abilities of pups at P21. We did not observe any significant
403 differences between TDP-43$^{+/+}$ and TDP-43$^{K408R/K408R}$ with respect to body weight or motor
404 abilities indicating that blocking TDP-43 SUMOylation does not lead to gross developmental
405 abnormalities (Fig. S7A-C).To determine whether blocking TDP-43 SUMOylation leads to
406 phenotypes in an age-dependent manner, we assessed general wellness biweekly, including
407 measuring body weight and hindlimb clasping scores, and performed a battery of 14 behavioral
408 tests focusing on motor, social, and cognitive function related to ALS and FTD at three time
409 points (2, 9 and 16 months, Fig. S7D-F, S8-10).Of note: TDP-43$^{K408R/+}$ mice are generally
410 omitted from figures for clarity to avoid confounding variables that may arise due to asymmetric
411 regulation of wild type and K408R alleles due to the autoregulatory nature of TDP-43 (i.e.
412 potential dominant negative effects conferred by the mutation and not partial loss of
413 SUMOylation), but are accessible in Supplementary Table 2 and typically exhibit a milder
414 phenotype than TDP-43$^{K408R/K408R}$.

415 We were surprised to observe that blocking TDP-43 SUMOylation in TDP-43^{K408R} mice
416 resulted in sex-specific cognitive and social deficits selective to female animals. Starting around
417 2 months of age, we observed significant barbering in female mice leading to alopecia in the
418 K408R mutants (Fig. 4A). Consistent with this finding, we found that aged female
419 TDP-43$^{K408R/K408R}$ mice were significantly more submissive to their TDP-43$^{+/+}$ counterparts in
420 the tube test (Fig. 4B). Thus, blocking TDP-43 SUMOylation leads to social abnormalities in
421 female mice. In assessing the cognitive behaviors, we observed significant risk taking and
422 hyperactivity in the open field test at 2 months of age (Fig. 4C). This hyperactivity was age-
423 dependent and selectively affected young female mice as they were significantly less active than
424 their TDP-43$^{+/+}$ counterparts at 9 months of age in the open field tests (Fig. 4C). Additionally,
425 these female TDP-43$^{K408R/K408R}$ mice presented with significant impairment during habituation at
426 9 months in the beam break test (Fig. 4D). As there was no change in motor abilities in the
427 rotarod and digigait tests (Fig. S9C,D), we rationalized that the activity abnormalities were likely
428 due to cognitive and anxiety impairments as opposed to motor impairments. By 16 months of
429 age, female TDP-43$^{K408R/K408R}$ mice performed significantly worse than TDP-43$^{+/+}$ mice in the
430 spontaneous Y-maze, inferring age-dependent cognitive decline in the domain of working
431 memory (Fig. 4E). Together, female mice present with social and cognitive impairment in early
432 age with slight impairments in cognitive performance with aging. There were no significant
433 cognitive effects in male TDP-43$^{K408R/K408R}$ mice, however mild impairments were observed on
434 the rotarod test at 9 months of age (2-way ANOVA p=0.0273, Supplementary Table 2). This
435 deficiency was not observed at 16 months of age, largely due to all mice performing significantly
436 worse at the rotarod task, limiting the interpretation of this assay[98]. Taken together, the age-
437 dependent cognitive and social impairment observed in female TDP-43 SUMO-deficient mutants

438 highlight interesting and unexplored aspects of TDP-43 with important implications for
439 understanding sex-specific roles of TDP-43 SUMOylation.

440 ***TDP-43^{K408R} mice present with distinct features of TDP-43 pathology related to ALS and FTD***

441 Next, we aimed to characterize regions of the nervous system vulnerable in ALS/FTD to
442 determine how loss of TDP-43 SUMOylation impacts these regions across aging. We did not
443 observe significant differences in cortical thickness of the primary motor cortex nor prefrontal
444 cortex in male or female mice across all timepoints suggesting that loss of TDP-43 SUMOylation
445 does not lead to widespread cortical degeneration occurring during normal aging (Fig. S11A,B).
446 To gain an additional layer of granularity into vulnerable neuron subpopulations in the cortex,
447 we stained for Ctip2 to highlight neurons in layer V, including upper motor neurons, in the
448 cortex and did not observe significant differences in neuron quantity across aging (Fig. S11C,D).
449 We further stained for Cux1 as a marker of layer II/III neurons which can be vulnerable to
450 TDP-43 pathology in FTD and degeneration in Alzheimer's disease. Again, we did not observe
451 significant changes in male nor female mice across the mouse lifespan supporting the absence of
452 cortical degeneration in TDP-43^{K408R} animals during native aging (Fig. S11C,D). To determine if
453 blocking TDP-43 SUMOylation results in neuroinflammation, we probed for the reactive
454 astrocyte marker Gfap and reactive microglia marker Iba1 and observed no change in
455 neuroinflammation (Fig. S11E-H). Together these data suggest the process of aging does not
456 lead to cortical neurodegeneration nor cortical neuroinflammation.

457 Cellular and molecular changes are generally thought to precede behavioral changes in
458 mouse models and human disease. Our biochemical and cellular assays show that stress-induced
459 SUMOylation helps to clear TDP-43 during recovery and blocking TDP-43 SUMOylation in
460 neurons leads to impaired recovery from stress and TDP-43 accumulation (Fig. 1E, Fig. 3, Fig.
461 S6A,F). Due to the sex-specific social and cognitive impairment in female mice, we posited that
462 TDP-43 accumulation would reflect the behavioural changes. Consistent with the sex-specific
463 social and cognitive impairment described above, we find that insoluble phosphorylated TDP-43
464 accumulated in the cortex of female, but not male mice (Fig. S12A,B). Furthermore, this
465 accumulation was observed as early as 2 months of age and was maintained throughout aging,
466 which may imply that impaired TDP-43 proteostasis is underlying the social and cognitive
467 phenotypes observed in female TDP-43^{K408R} animals. Interestingly, we observed significant
468 changes in *Mapt* splicing in the cortex of TDP-43^{K408R} mice, specifically the N2/N0 splice
469 isoform (Fig. S12C). Together, this may suggest that there is some degree of TDP-43 loss of
470 function in the TDP-43^{K408R} mice.

471 We questioned whether motor neurons in the spinal cord present with early-stage
472 pathology as they are subject to excess excitotoxic stress throughout their lifespan[40].
473 Surprisingly, we observed cytoplasmic mislocalization, but not nuclear depletion, of TDP-43
474 accompanied by insoluble, phosphorylated TDP-43 accumulation in the lumbar spinal cord of
475 both male and female mice at 9 months of age (Fig. 5A, Fig. S12D,E). Furthermore, by 16
476 months of age, male TDP-43$^{K408R/K408R}$ displayed a significant denervation of neuromuscular
477 junctions in the tibialis anterior and a reduction in ChAT positive neurons in the spinal cord
478 compared to littermate controls (Fig. 5B,C, Fig. S12F-H). Together, blocking TDP-43

479 SUMOylation results in altered proteostasis spinal motor neurons leading to neuromuscular
480 junction denervation and ChAT positive motor neuron loss in an age dependent manner.

481 As the TDP-43^{K408R} mice continued to age beyond our behaviour timepoints we observed
482 a 24.49% decrease in survival specific to male TDP-43$^{K408R/K408R}$ mice with a median survival of
483 521 days for the TDP-43$^{K408R/K408R}$ compared to 690 days for TDP-43$^{+/+}$ mice (Fig. 5D, Fig.
484 S7D). Mice were typically found dead or euthanized after reaching a humane endpoint.
485 Surprisingly, a few animals presented with classic hindlimb weakness paralysis akin to those
486 observed in other models of ALS (Supplemental Video 1). However, these results should be
487 interpreted with caution due to the low statistical power. Taken together, our data supports that
488 TDP-43 SUMOylation plays a protective role in mediating TDP-43 proteostasis in the CNS and
489 that its blockade may confer a risk for ALS/FTD-like pathogenesis in an age-dependent, and sex-
490 specific manner providing insights into molecular substrates underlying sexually dimorphic
491 clinical features of ALS and FTD.

492 ***Aberrant SUMOylation is a feature of human aging and disease***

493 Although SUMOylation is well understood to play an essential role in the CNS, its
494 involvement in human aging and neurodegenerative diseases remains largely elusive. To assess
495 how SUMOylation is normally affected in human aging, we processed samples from human
496 temporal lobe tissue ranging between 0.5 and 88 years of age from individuals unaffected by
497 neurological diseases (Fig. 6A, Supplementary Table 3, n=55). Complementing our findings that
498 SUMOylation serves as a response to increased proteostatic demands, such as those in our aging
499 TDP-43^{K408R} model, we observed that global SUMOylation was significantly increased in "aged"
500 (>60 years old) human brains (Fig. 6B).

501 To explore the extent of TDP-43 SUMOylation in human ALS/FTD cases, we performed
502 proximity ligation assays against TDP-43 and SUMO2/3 in prefrontal cortex samples from
503 ALS/FTD cases positive for TDP-43 pathology and age/sex matched unaffected controls
504 (Supplementary Table 3). Through semiquantitative analysis, patient samples collected from
505 various sites were assessed for relative TDP-43 pathology by a neuropathologist in a blinded
506 manner. We confirmed there was a significant increase in TDP-43 pathology in the prefrontal
507 cortex of ALS/FTD patients relative to controls (Fig. S13A). When assessing the interaction
508 between TDP-43 and SUMO2/3, we observed a significant increase in interactions in the
509 prefrontal cortex of ALS/FTD patients with TDP-43 pathology suggesting the TDP-43
510 SUMOylation pathway is engaged in disease (Fig. 6C, Fig. S13B). This may be a result of
511 increased stress burden throughout the prefrontal cortex in those affected by ALS/FTD with
512 TDP-43 pathology compared to age and sex matched counterparts. Taken together,
513 SUMOylation as a stress responsive modification is positively correlated with aging in the
514 human brain, potentially linked to the increase demand imposed by age-associated stress.
515 Additionally, the SUMOylation response is enhanced in the frontal cortex of those affected by
516 ALS/FTD providing further *in vivo* support for its role in disease.

517 **Discussion**

518 Although ALS and FTD are highly heterogenous diseases, the nearly universal
519 convergence on TDP-43 proteinopathy emphasizes a need to understand early drivers of this
520 pathogenic process. Mutations in various genes can lead to TDP-43 pathology, however the
521 majority of ALS and FTD cases occur sporadically without a clear genetic cause[3, 22].

522 Additionally, patients living with disease causing mutations do not present with symptoms of
523 disease until later in life suggesting exogenous factors related to aging play a role in
524 phenoconversion[99]. Cellular stressors are well characterized to induce TDP-43 pathology
525 providing a clue as to how exogenous factors may contribute to disease pathogenesis. Given the
526 postmitotic nature of neurons, maintaining proteostasis in response to lifelong stressors is critical
527 for neuronal longevity[1]. This is particularly true for motor neurons which endure constant
528 excitotoxic stress[40]. In this study, we found that SUMOylation maintains TDP-43 proteostasis
529 in the nucleus specifically in response to stress. This modification is critical to preserve neuronal
530 function, the absence of which results in neuronal demise and TDP-43 proteinopathy.

531 SUMOylation of TDP-43 occurs at K408 in a highly conserved region of the C-terminal
532 domain. This is in contrast to what was previously reported for TDP-43 and SUMO1; where it
533 was suggested, but not demonstrated, that SUMO1 modified TDP-43 at lysine 136[49, 100].
534 Indeed, mutating K136 to an arginine (R) had no effect on stress-induced TDP-43 SUMOylation
535 by SUMO2/3, though this does not discount the possibility that SUMO1 may modify TDP-43
536 under conditions where increased SUMO machinery (e.g. UBC9 overexpression) is present. In
537 our hands, expression of TDP-43^{K136R} led to the formation of nuclear TDP-43 puncta as
538 previously reported[50, 51]. However, these puncta were similar to those observed when
539 expressing RNA binding deficient TDP-43. Furthermore, prediction of TDP-43 structure
540 suggests that K136R mutation may impact the structure of the RNA recognition motif and RNA
541 binding. Thus, phenotypes observed in TDP-43 carrying the K136R mutation should be
542 interpreted with caution.

543 In genetic forms of ALS or FTD caused by mutations in TDP-43, the C-terminal domain
544 harbors the overwhelming majority of disease-causing mutations[101]. Thus, understanding the
545 involvement of the C-terminal domain in TDP-43 biology is critical to uncover pathways that
546 may be linked to disease independent of TDP-43 mutations. Phosphorylation of TDP-43 in the
547 C-terminal domain, particularly S403/404 and S409/410, have garnered much attention in this
548 regard as these residues are characteristically phosphorylated in disease [42]. However, the roles
549 for phosphorylation at these sites remains generally elusive. Few reports have suggested roles in
550 regulating liquid-liquid phase separation and solubility[102, 103]. Our findings suggest that
551 phosphorylation and SUMOylation act antagonistically on TDP-43, indicating potential distinct
552 mechanisms of regulation. We further observed that this region of the C-terminal domain
553 targeted by SUMOylation and phosphorylation is highly conserved throughout vertebrate
554 species. Thus, this PTM-enriched region may play key roles for regulating TDP-43 in vertebrate
555 biology.

556 Regulation of TDP-43 proteostasis is critical for cells as fluctuations in TDP-43 levels
557 can lead to toxicity in cell and animal models[20, 104–107]. Unsurprisingly, TDP-43 is regulated
558 in a variety of mechanisms including transcriptionally, post-transcriptionally, translationally and
559 post-translationally[11, 20, 108]. Furthermore TDP-43 can be cleared through several pathways
560 including the proteasome, endo-lysosome, autophagy, and extracellular vesicle pathways[109–
561 116]. Here we add another mechanism of regulation through SUMOylation during stress and
562 recovery. We hypothesized that blocking TDP-43 SUMOylation with K408R mutation would
563 result in its accumulation during stress recovery. Interestingly, we observed a significant increase
564 in insoluble phosphorylated TDP-43 in TDP-43$^{K408R/K408R}$ cortical neurons and a delay in stress
565 granule disassembly during stress recovery indicating TDP-43 accumulation. However, this was
566 resolved 3 hours post-stress indicating that the neurons could compensate to clear the aberrantly

accumulated TDP-43 within this acute stress paradigm. We questioned whether chronic stress may exacerbate phenotypes and found that chronic stress significantly resulted in increased phosphorylated, insoluble TDP-35 fragments which then recovered upon removal of stress. Thus phosphorylation of TDP-43, in addition to cleavage, may be additional mechanisms to regulate TDP-43 proteostasis in the event of SUMOylation-pathway failure. Thus, SUMOylation may be an early line of defense to regulate TDP-43 in response to stress and blocking TDP-43 SUMOylation shifts proteostasis leading to delayed recovery. Future studies exploring repeated and/or divergent stressors will be crucial in determining the degree to which TDP-43 SUMOylation safeguards from cellular demise.

Previous reports have emphasized the status of altered proteostasis as a hallmark of aging in the CNS, culminating in impaired removal of damaged proteins with age[97]. In TDP-43$^{K408R/K408R}$ mice, TDP-43 was found to accumulate in the CNS in an age-dependent manner, suggesting SUMOylation plays important roles during aging. Supporting these findings, in human temporal lobe samples we similarly observed a positive correlation between global SUMOylation and age supporting SUMOylation as a potential protective mechanism during aging in the CNS. Previous studies on global SUMOylation have focused on the dynamic nature of this modification playing roles during development, and associations between SUMOylation and neurodegeneration gaining traction however roles for SUMOylation in the central nervous system during the process of human aging remain understudied[117, 118]. This may be ascribed, in part, to challenges in studying SUMOylation due to the dynamic nature of the modification and lack of specific tools to study its interactions. We employed a PLA approach to assess the interaction between TDP-43 and SUMO in ALS/FTD patients and found significantly increased interactions in the prefrontal cortex relative to age/sex matched unaffected controls. It was interesting to observe that PLA signal occurred and was increased in both the nucleus and the cytoplasm in ALS/FTD patient samples. We hypothesize that SUMOylation of TDP-43 is an early event regulating TDP-43 proteostasis, however if overwhelmed other systems such as phosphorylation or protein cleavage may help respond to regulate TDP-43. As we are observing late-stage events, SUMOylation in the cytoplasm may be co-occurrent with late-stage regulation of TDP-43. Approaches that provide increased resolution for detecting TDP-43 SUMOylation events are clearly warranted. Recent studies have used RNA aptamers to reveal nuclear changes in TDP-43 in spinal and cortical neurons of ALS patients prior to traditional cytoplasmic pathology in vulnerable cells[19]. Further development of these technologies with respect to TDP-43 SUMOylation may help advance biomarker development that can provide information about TDP-43 stress-response and pathogenesis in ALS/FTD patients.

While the extent of phenotypes observed in TDP-43^{K408R} are relatively mild, they similarly reflect the magnitude of phenotypes observed in mice with significant construct validity to ALS/FTD (i.e. TDP-43^{Q331K}, TDP-43^{M337V}, and TDP-43^{K145R} models) [45, 119, 120]. These knock in models highlight potential shortcomings of other TDP-43 models relying on overexpression to induce behavioural phenotypes in mice which may not reflect the underlying biology of TDP-43 in ALS/FTD. The emergence of predominantly cognitive FTD-like phenotypes in the TDP-43^{K408R} mice is not unusual in TDP-43 knock in models such as TDP-43^{Q331K} and TDP-43^{K145R} mice which present with features of cognitive dysfunction but lacking the entire constellation of ALS/FTD-like phenotypes[45, 119]. However, we were surprised to observe that the cognitive phenotypes were specific to female mice with no behavioural phenotypes being observed in male mice. This may imply that TDP-43 plays important role regulating sex specific behaviours. Alternatively, female and male mice may experience different

613 forms of life stress that may act upon SUMOylation pathways. For example, we observed
614 differences in social behaviors which may indicate social pathways linked with female behaviour
615 may also be associated with SUMOylation. Alternatively, male mice were frequently separated
616 due to fighting behavior, which could contribute to altered baseline social features, regardless of
617 genotype. Future work exploring sex-specific roles of TDP-43 and/or SUMOylation will help
618 provide mechanistic insight into sex-specific behaviour and experience.

619 As TDP-43 SUMOylation plays roles in regulating TDP-43 clearance during recovery
620 from stress, blocking TDP-43 SUMOylation in the TDP-43$^{K408R/K408R}$ mouse line disrupts this
621 proteostasis and leads to subsequent mislocalization consistent with loss of nuclear function.
622 Additionally, we observe significant increases in insoluble phosphorylated TDP-43 and motor
623 neuron loss in male mice suggesting that gain of function may be occurring, phenocopying
624 disease pathogenesis. While we did observe some motor impairment in 9-month-old mice
625 correlating with TDP-43 mislocalization, we did not observe significant motor impairment in the
626 male mice at 16 months of age, which may be explained by the overall poor performance during
627 motor tests at this age limiting the sensitivity to detect mild changes. Despite this, we did observe
628 molecular and histological evidence supporting early motor impairment with significant
629 neuromuscular junction denervation and reduction in ChAT positive motor neurons in the ventral
630 horn. Additionally, as the male TDP-43$^{K408R/K408R}$ mice displayed a significant decrease in
631 survival, behavioral analysis at 16 months of age may have preceded the onset of significant
632 motor phenotypes. Future refined studies using key pathological centered around key
633 pathological markers of cellular dysfunction will help uncover specific points of
634 phenoconversion and phenotransition to identify the chronology of events leading to phenotypes
635 associated with neurodegeneration.

636 We have demonstrated that TDP-43 SUMOylation occurs in response to cellular stress,
637 thus careful characterization of the TDP-43^{K408R} mice is critical to determine baseline
638 phenotypes without the addition of exogenous stressors. We initially hypothesized that aging
639 may be a sufficient stressor to interrogate TDP-43 SUMOylation in mice leading to age-
640 dependent phenotypes. However, the various stressors that individuals with ALS/FTD were
641 previously exposed to during their lifetime (i.e. the "exposome") are not experienced by mice in
642 vivaria on a short timescale thus mouse aging likely does not faithfully reflect human aging. The
643 TDP-43^{K408R} model will therefore help facilitate the exploration of how the exposome synergizes
644 with TDP-43 to better understand how ALS/FTD relevant stressors that humans may experience
645 throughout aging (e.g. *C9ORF72* expansions, viral infections, and traumatic brain injury)
646 converge on TDP-43 and uniquely drive aspects of neurodegeneration.

647

648 **References**

649 1. Hipp MS, Kasturi P, Hartl FU (2019) The proteostasis network and its decline in
650 ageing. Nature Reviews Molecular Cell Biology 2019 20:7 20:421–435
651 2. Spires-Jones TL, Attems J, Thal DR (2017) Interactions of pathological proteins in
652 neurodegenerative diseases. Acta Neuropathologica 2017 134:2 134:187–205
653 3. Hardiman O, Al-Chalabi A, Chio A, Corr EM, Logroscino G, Robberecht W, Shaw
654 PJ, Simmons Z, Van Den Berg LH (2017) Amyotrophic lateral sclerosis. Nature
655 Reviews Disease Primers 2017 3:1 3:1–19
656 4. Grossman M, Seeley WW, Boxer AL, et al (2023) Frontotemporal lobar
657 degeneration. Nature Reviews Disease Primers 2023 9:1 9:1–19

5. Burrell JR, Halliday GM, Kril JJ, Ittner LM, Götz J, Kiernan MC, Hodges JR (2016) The frontotemporal dementia-motor neuron disease continuum. The Lancet 388:919–931
6. Nelson PT, Dickson DW, Trojanowski JQ, et al (2019) Limbic-predominant age-related TDP-43 encephalopathy (LATE): consensus working group report. Brain 142:1503–1527
7. Meneses A, Koga S, O'Leary J, Dickson DW, Bu G, Zhao N (2021) TDP-43 Pathology in Alzheimer's Disease. Molecular Neurodegeneration 2021 16:1 16:1–15
8. Nicks R, Clement NF, Alvarez VE, et al (2023) Repetitive head impacts and chronic traumatic encephalopathy are associated with TDP-43 inclusions and hippocampal sclerosis. Acta Neuropathol 145:395–408
9. Thammisetty SS, Pedragosa J, Weng YC, Calon F, Planas A, Kriz J (2018) Age-related deregulation of TDP-43 after stroke enhances NF-κB-mediated inflammation and neuronal damage. J Neuroinflammation 15:1–15
10. Coyne AN, Baskerville V, Zaepfel BL, Dickson DW, Rigo F, Bennett F, Patrick Lusk C, Rothstein JD (2021) Nuclear accumulation of CHMP7 initiates nuclear pore complex injury and subsequent TDP-43 dysfunction in sporadic and familial ALS. Sci Transl Med 13:1923
11. Suk TR, Rousseaux MWC (2020) The role of TDP-43 mislocalization in amyotrophic lateral sclerosis. Mol Neurodegener 15:45
12. Ma XR, Prudencio M, Koike Y, et al (2022) TDP-43 represses cryptic exon inclusion in the FTD–ALS gene UNC13A. Nature 2022 603:7899 603:124–130
13. Brown AL, Wilkins OG, Keuss MJ, et al (2022) TDP-43 loss and ALS-risk SNPs drive mis-splicing and depletion of UNC13A. Nature 2022 603:7899 603:131–137
14. Melamed Z, López-Erauskin J, Baughn MW, et al (2019) Premature polyadenylation-mediated loss of stathmin-2 is a hallmark of TDP-43-dependent neurodegeneration. Nat Neurosci 1
15. Klim JR, Williams LA, Limone F, et al (2019) ALS-implicated protein TDP-43 sustains levels of STMN2, a mediator of motor neuron growth and repair. Nat Neurosci 22:167–179
16. Gasset-Rosa F, Lu S, Yu H, Chen C, Melamed Z, Guo L, Shorter J, Da Cruz S, Cleveland DW (2019) Cytoplasmic TDP-43 De-mixing Independent of Stress Granules Drives Inhibition of Nuclear Import, Loss of Nuclear TDP-43, and Cell Death. Neuron 102:339-357.e7
17. Baughn MW, Melamed Z, López-Erauskin J, et al (2023) Mechanism of STMN2 cryptic splice-polyadenylation and its correction for TDP-43 proteinopathies. Science (1979) 379:1140–1149
18. Agra Almeida Quadros AR, Li Z, Wang X, et al (2024) Cryptic splicing of stathmin-2 and UNC13A mRNAs is a pathological hallmark of TDP-43-associated Alzheimer's disease. Acta Neuropathologica 2024 147:1 147:1–18
19. Spence H, Waldron FM, Saleeb RS, et al (2024) RNA aptamer reveals nuclear TDP-43 pathology is an early aggregation event that coincides with STMN-2 cryptic splicing and precedes clinical manifestation in ALS. Acta Neuropathol 147:1–15

703 20. Hergesheimer RC, Chami AA, De Assis DR, Vourc'h P, Andres CR, Corcia P,
704 Lanznaster D, Blasco H (2019) The debated toxic role of aggregated TDP-43 in
705 amyotrophic lateral sclerosis: A resolution in sight? Brain 142:1176–1194
706 21. Zou ZY, Zhou ZR, Che CH, Liu CY, He RL, Huang HP (2017) Genetic
707 epidemiology of amyotrophic lateral sclerosis: a systematic review and meta-
708 analysis. J Neurol Neurosurg Psychiatry 88:540–549
709 22. Ghasemi M, Brown RH (2018) Genetics of Amyotrophic Lateral Sclerosis. Cold
710 Spring Harb Perspect Med. https://doi.org/10.1101/CSHPERSPECT.A024125
711 23. Mackenzie IR, Nicholson AM, Sarkar M, et al (2017) TIA1 Mutations in
712 Amyotrophic Lateral Sclerosis and Frontotemporal Dementia Promote Phase
713 Separation and Alter Stress Granule Dynamics. Neuron 95:808-816.e9
714 24. Walker AK, Soo KY, Sundaramoorthy V, et al (2013) ALS-associated TDP-43
715 induces endoplasmic reticulum stress, which drives cytoplasmic TDP-43
716 accumulation and stress granule formation. PLoS One 8:e81170
717 25. Tam OH, Rozhkov N V., Shaw R, et al (2019) Postmortem Cortex Samples
718 Identify Distinct Molecular Subtypes of ALS: Retrotransposon Activation,
719 Oxidative Stress, and Activated Glia. Cell Rep 29:1164-1177.e5
720 26. Wolozin B, Ivanov P (2019) Stress granules and neurodegeneration. Nat Rev
721 Neurosci 20:649–666
722 27. Lin MT, Beal MF (2006) Mitochondrial dysfunction and oxidative stress in
723 neurodegenerative diseases. Nature 443:787–795
724 28. Ratti A, Gumina V, Lenzi P, et al (2020) Chronic stress induces formation of stress
725 granules and pathological TDP-43 aggregates in human ALS fibroblasts and iPSC-
726 motoneurons. Neurobiol Dis 145:105051
727 29. D'Amico E, Factor-Litvak P, Santella RM, Mitsumoto H (2013) Clinical
728 perspective on oxidative stress in sporadic amyotrophic lateral sclerosis. Free Radic
729 Biol Med 65:509–527
730 30. Colombrita C, Zennaro E, Fallini C, Weber M, Sommacal A, Buratti E, Silani V,
731 Ratti A (2009) TDP-43 is recruited to stress granules in conditions of oxidative
732 insult. J Neurochem 111:1051–1061
733 31. Zuo X, Zhou J, Li Y, et al (2021) TDP-43 aggregation induced by oxidative stress
734 causes global mitochondrial imbalance in ALS. Nature Structural & Molecular
735 Biology 2021 28:2 28:132–142
736 32. Ueda T, Takeuchi T, Fujikake N, et al (2024) Dysregulation of stress granule
737 dynamics by DCTN1 deficiency exacerbates TDP-43 pathology in Drosophila
738 models of ALS/FTD. Acta Neuropathol Commun 12:1–15
739 33. Iguchi Y, Katsuno M, Takagi S, Ishigaki S, Niwa J ichi, Hasegawa M, Tanaka F,
740 Sobue G (2012) Oxidative stress induced by glutathione depletion reproduces
741 pathological modifications of TDP-43 linked to TDP-43 proteinopathies. Neurobiol
742 Dis 45:862–870
743 34. Liu-Yesucevitz L, Bilgutay A, Zhang YJ, et al (2010) Tar DNA binding protein-43
744 (TDP-43) associates with stress granules: Analysis of cultured cells and
745 pathological brain tissue. PLoS One 5:e13250
746 35. McDonald KK, Aulas A, Destroismaisons L, Pickles S, Beleac E, Camu W,
747 Rouleau GA, Velde C Vande (2011) TAR DNA-binding protein 43 (TDP-43)

748 regulates stress granule dynamics via differential regulation of G3BP and TIA-1.
749 Hum Mol Genet 20:1400–1410
750 36. Luan W, Wright AL, Brown-Wright H, Le S, San Gil R, Madrid San Martin L,
751 Ling K, Jafar-Nejad P, Rigo F, Walker AK (2023) Early activation of cellular stress
752 and death pathways caused by cytoplasmic TDP-43 in the rNLS8 mouse model of
753 ALS and FTD. Molecular Psychiatry 2023 28:6 28:2445–2461
754 37. Fung G, Shi J, Deng H, Hou J, Wang C, Hong A, Zhang J, Jia W, Luo H (2015)
755 Cytoplasmic translocation, aggregation, and cleavage of TDP-43 by enteroviral
756 proteases modulate viral pathogenesis. Cell Death & Differentiation 2015 22:12
757 22:2087–2097
758 38. Ash PEA, Stanford EA, Al Abdulatif A, et al (2017) Dioxins and related
759 environmental contaminants increase TDP-43 levels. Mol Neurodegener 12:1–14
760 39. Dubinski A, Gagne M, Peyrard S, Gordon D, Talbot K, Vande Velde C (2023)
761 Stress granule assembly in vivo is deficient in the CNS of mutant TDP-43 ALS
762 mice. Hum Mol Genet 32:319–332
763 40. Odierna GL, Vucic S, Dyer M, Dickson T, Woodhouse A, Blizzard C (2024) How
764 do we get from hyperexcitability to excitotoxicity in amyotrophic lateral sclerosis?
765 Brain 147:1610–1621
766 41. Zhang P, Fan B, Yang P, Temirov J, Messing J, Kim HJ, Taylor JP (2019) Chronic
767 optogenetic induction of stress granules is cytotoxic and reveals the evolution of
768 ALS-FTD pathology. Elife. https://doi.org/10.7554/eLife.39578
769 42. Neumann M, Kwong LK, Lee EB, et al (2009) Phosphorylation of S409/410 of
770 TDP-43 is a consistent feature in all sporadic and familial forms of TDP-43
771 proteinopathies. Acta Neuropathol 117:137–149
772 43. Neumann M, Sampathu DM, Kwong LK, et al (2006) Ubiquitinated TDP-43 in
773 Frontotemporal Lobar Degeneration and Amyotrophic Lateral Sclerosis. Science
774 (1979) 314:130–133
775 44. Arai T, Hasegawa M, Akiyama H, et al (2006) TDP-43 is a component of
776 ubiquitin-positive tau-negative inclusions in frontotemporal lobar degeneration and
777 amyotrophic lateral sclerosis. Biochem Biophys Res Commun 351:602–611
778 45. Necarsulmer J, Simon J, Evangelista B, et al (2023) RNA-binding deficient TDP-43
779 drives cognitive decline in a mouse model of TDP-43 proteinopathy. Elife.
780 https://doi.org/10.7554/ELIFE.85921.2
781 46. McGurk L, Gomes E, Guo L, Mojsilovic-Petrovic J, Tran V, Kalb RG, Shorter J,
782 Bonini NM (2018) Poly(ADP-Ribose) Prevents Pathological Phase Separation of
783 TDP-43 by Promoting Liquid Demixing and Stress Granule Localization. Mol Cell
784 71:703-717.e9
785 47. Henley JM, Craig TJ, Wilkinson KA (2014) Neuronal SUMOylation: mechanisms,
786 physiology, and roles in neuronal dysfunction. Physiol Rev 94:1249–1285
787 48. Wilkinson KA, Henley JM (2010) Mechanisms, regulation and consequences of
788 protein SUMOylation. Biochemical Journal 428:133–145
789 49. Maraschi AM, Gumina V, Dragotto J, Colombrita C, Mompeán M, Buratti E, Silani
790 V, Feligioni M, Ratti A (2021) SUMOylation Regulates TDP-43 Splicing Activity
791 and Nucleocytoplasmic Distribution. Mol Neurobiol 58:5682–5702

792 50. Maraschi A, Gumina V, Dragotto J, Colombrita C, Mompeán M, Buratti E, Silani
793 V, Feligioni M, Ratti A (2021) SUMOylation Regulates TDP-43 Splicing Activity
794 and Nucleocytoplasmic Distribution. Mol Neurobiol 58:5682–5702
795 51. Maurel C, Chami AA, Thépault RA, Marouillat S, Blasco H, Corcia P, Andres CR,
796 Vourc'h P (2020) A role for SUMOylation in the Formation and Cellular
797 Localization of TDP-43 Aggregates in Amyotrophic Lateral Sclerosis. Mol
798 Neurobiol 57:1361–1373
799 52. Marino R, Buccarello L, Hassanzadeh K, Akhtari K, Palaniappan S, Corbo M,
800 Feligioni M (2023) A novel cell-permeable peptide prevents protein SUMOylation
801 and supports the mislocalization and aggregation of TDP-43. Neurobiol Dis
802 188:106342
803 53. Pichler A, Melchior F (2002) Ubiquitin-Related Modifier SUMO1 and
804 Nucleocytoplasmic Transport. Traffic 3:381–387
805 54. Wang L, Wansleeben C, Zhao S, Miao P, Paschen W, Yang W (2014) SUMO 2 is
806 essential while SUMO 3 is dispensable for mouse embryonic development . EMBO
807 Rep 15:878–885
808 55. Enserink JM (2015) Sumo and the cellular stress response. Cell Div 10:1–13
809 56. Seyfried NT, Gozal YM, Dammer EB, Xia Q, Duong DM, Cheng D, Lah JJ, Levey
810 AI, Peng J (2010) Multiplex SILAC analysis of a cellular TDP-43 proteinopathy
811 model reveals protein inclusions associated with SUMOylation and diverse
812 polyubiquitin chains. Molecular and Cellular Proteomics 9:705–718
813 57. Dammer EB, Fallini C, Gozal YM, et al (2012) Coaggregation of RNA-binding
814 proteins in a model of TDP-43 proteinopathy with selective RGG motif methylation
815 and a role for RRM1 ubiquitination. PLoS One.
816 https://doi.org/10.1371/JOURNAL.PONE.0038658
817 58. Dewey CM, Cenik B, Sephton CF, Dries DR, Mayer P, Good SK, Johnson BA,
818 Herz J, Yu G (2011) TDP-43 Is Directed to Stress Granules by Sorbitol, a Novel
819 Physiological Osmotic and Oxidative Stressor. Mol Cell Biol 31:1098–1108
820 59. Chang HY, Hou SC, Way T Der, Wong CH, Wang IF (2013) Heat-shock protein
821 dysregulation is associated with functional and pathological TDP-43 aggregation.
822 Nat Commun 4:1–11
823 60. Suk TR, Nguyen TT, Fisk ZA, et al (2023) Characterizing the differential
824 distribution and targets of Sumo1 and Sumo2 in the mouse brain. iScience
825 26:106350
826 61. Lu J, Wu T, Zhang B, Liu S, Song W, Qiao J, Ruan H (2021) Types of nuclear
827 localization signals and mechanisms of protein import into the nucleus. Cell
828 Communication and Signaling 19:1–10
829 62. Lange A, Mills RE, Devine SE, Corbett AH (2008) A PY-NLS Nuclear Targeting
830 Signal Is Required for Nuclear Localization and Function of the Saccharomyces
831 cerevisiae mRNA-binding Protein Hrp1. Journal of Biological Chemistry
832 283:12926–12934
833 63. Sun Y, Zhao K, Xia W, et al (2020) The nuclear localization sequence mediates
834 hnRNPA1 amyloid fibril formation revealed by cryoEM structure. Nature
835 Communications 2020 11:1 11:1–8
836 64. Mann JR, Gleixner AM, Mauna JC, et al (2019) RNA Binding Antagonizes
837 Neurotoxic Phase Transitions of TDP-43. Neuron 102:321-338.e8

838 65. Keiten-Schmitz J, Wagner K, Piller T, Kaulich M, Alberti S, Müller S (2020) The
839 Nuclear SUMO-Targeted Ubiquitin Quality Control Network Regulates the
840 Dynamics of Cytoplasmic Stress Granules. Mol Cell 79:54-67.e7
841 66. Kagey MH, Melhuish TA, Wotton D (2003) The polycomb protein Pc2 is a SUMO
842 E3. Cell 113:127–137
843 67. Garcáa-Gutiérrez P, Juárez-Vicente F, Gallardo-Chamizo F, Charnay P, García-
844 Domínguez M (2011) The transcription factor Krox20 is an E3 ligase that
845 sumoylates its Nab coregulators. EMBO Rep 12:1018–1023
846 68. Oh SM, Liu Z, Okada M, Jang SW, Liu X, Chan CB, Luo H, Ye K (2009) Ebp1
847 sumoylation, regulated by TLS/FUS E3 ligase, is required for its anti-proliferative
848 activity. Oncogene 2010 29:7 29:1017–1030
849 69. Eisenhardt N, Chaugule VK, Koidl S, et al (2015) A new vertebrate SUMO enzyme
850 family reveals insights into SUMO-chain assembly. Nature Structural & Molecular
851 Biology 2015 22:12 22:959–967
852 70. Payne F, Colnaghi R, Rocha N, et al (2014) Hypomorphism in human NSMCE2
853 linked to primordial dwarfism and insulin resistance. J Clin Invest 124:4028–4038
854 71. Kahyo T, Nishida T, Yasuda H (2001) Involvement of PIAS1 in the Sumoylation of
855 Tumor Suppressor p53. Mol Cell 8:713–718
856 72. Kotaja N, Karvonen U, Jänne OA, Palvimo JJ (2002) PIAS Proteins Modulate
857 Transcription Factors by Functioning as SUMO-1 Ligases. Mol Cell Biol 22:5222–
858 5234
859 73. Nakagawa K, Yokosawa H (2002) PIAS3 induces SUMO-1 modification and
860 transcriptional repression of IRF-1. FEBS Lett 530:204–208
861 74. Sachdev S, Bruhn L, Sieber H, Pichler A, Melchior F, Grosschedl R (2001) PIASy,
862 a nuclear matrix–associated SUMO E3 ligase, represses LEF1 activity by
863 sequestration into nuclear bodies. Genes Dev 15:3088–3103
864 75. Chu Y, Yang X (2010) SUMO E3 ligase activity of TRIM proteins. Oncogene 2011
865 30:9 30:1108–1116
866 76. Pichler A, Gast A, Seeler JS, Dejean A, Melchior F (2002) The Nucleoporin
867 RanBP2 Has SUMO1 E3 Ligase Activity. Cell 108:109–120
868 77. Reynolds A, Qiao H, Yang Y, et al (2013) RNF212 is a dosage-sensitive regulator
869 of crossing-over during mammalian meiosis. Nature Genetics 2013 45:3 45:269–
870 278
871 78. Liang Q, Deng H, Li X, Wu X, Tang Q, Chang T-H, Peng H, Rauscher FJ, Ozato
872 K, Zhu F (2011) Tripartite Motif-Containing Protein 28 Is a Small Ubiquitin-
873 Related Modifier E3 Ligase and Negative Regulator of IFN Regulatory Factor 7.
874 The Journal of Immunology 187:4754–4763
875 79. Yamashita D, Moriuchi T, Osumi T, Hirose F (2016) Transcription Factor hDREF
876 Is a Novel SUMO E3 Ligase of Mi2α*. Journal of Biological Chemistry
877 291:11619–11634
878 80. Karvonen U, Jääskeläinen T, Rytinki M, Kaikkonen S, Palvimo JJ (2008) ZNF451
879 Is a Novel PML Body- and SUMO-Associated Transcriptional Coregulator. J Mol
880 Biol 382:585–600
881 81. Warner LE, Mancias P, Butler IJ, McDonald CM, Keppen L, Koob KG, Lupski JR
882 (1998) Mutations in the early growth response 2 (EGR2) gene are associated with
883 hereditary myelinopathies. Nature Genetics 1998 18:4 18:382–384

884 82. Garcáa-Gutiérrez P, Juárez-Vicente F, Gallardo-Chamizo F, Charnay P, García-
885 Domínguez M (2011) The transcription factor Krox20 is an E3 ligase that
886 sumoylates its Nab coregulators. EMBO Rep 12:1018–1023
887 83. Nishida T, Yasuda H (2002) PIAS1 and PIASxα Function as SUMO-E3 Ligases
888 toward Androgen Receptor and Repress Androgen Receptor-dependent
889 Transcription. Journal of Biological Chemistry 277:41311–41317
890 84. Liang Q, Deng H, Li X, Wu X, Tang Q, Chang T-H, Peng H, Rauscher FJ, Ozato
891 K, Zhu F (2011) Tripartite Motif-Containing Protein 28 Is a Small Ubiquitin-
892 Related Modifier E3 Ligase and Negative Regulator of IFN Regulatory Factor 7.
893 The Journal of Immunology 187:4754–4763
894 85. Zhao Q, Xie Y, Zheng Y, Jiang S, Liu W, Mu W, Liu Z, Zhao Y, Xue Y, Ren J
895 (2014) GPS-SUMO: A tool for the prediction of sumoylation sites and SUMO-
896 interaction motifs. Nucleic Acids Res 42:W325–W330
897 86. Ren J, Gao X, Jin C, Zhu M, Wang X, Shaw A, Wen L, Yao X, Xue Y (2009)
898 Systematic study of protein sumoylation: Development of a site-specific predictor
899 of SUMOsp 2.0. Proteomics 9:3409–3412
900 87. Eisenhardt N, Chaugule VK, Koidl S, et al (2015) A new vertebrate SUMO enzyme
901 family reveals insights into SUMO-chain assembly. Nature Structural & Molecular
902 Biology 2015 22:12 22:959–967
903 88. Lumpkin RJ, Gu H, Zhu Y, Leonard M, Ahmad AS, Clauser KR, Meyer JG,
904 Bennett EJ, Komives EA (2017) Site-specific identification and quantitation of
905 endogenous SUMO modifications under native conditions. Nature Communications
906 2017 8:1 8:1–11
907 89. Hendriks IA, Lyon D, Su D, Skotte NH, Daniel JA, Jensen LJ, Nielsen ML (2018)
908 Site-specific characterization of endogenous SUMOylation across species and
909 organs. Nature Communications 2018 9:1 9:1–17
910 90. Chen S, Francioli LC, Goodrich JK, et al (2023) A genomic mutational constraint
911 map using variation in 76,156 human genomes. Nature 2023 625:7993 625:92–100
912 91. Kraemer BC, Schuck T, Wheeler JM, Robinson LC, Trojanowski JQ, Lee VMY,
913 Schellenberg GD (2010) Loss of Murine TDP-43 disrupts motor function and plays
914 an essential role in embryogenesis. Acta Neuropathol 119:409–419
915 92. Khalfallah Y, Kuta R, Grasmuck C, Prat A, Durham HD, Vande Velde C (2018)
916 TDP-43 regulation of stress granule dynamics in neurodegenerative disease-
917 relevant cell types. Sci Rep 8:7551
918 93. Sidibé H, Khalfallah Y, Xiao S, et al (2021) TDP-43 stabilizes G3BP1 mRNA:
919 relevance to amyotrophic lateral sclerosis/frontotemporal dementia . Brain.
920 https://doi.org/10.1093/brain/awab217
921 94. Shelkovnikova TA, Kukharsky MS, An H, Dimasi P, Alexeeva S, Shabir O, Heath
922 PR, Buchman VL (2018) Protective paraspeckle hyper-assembly downstream of
923 TDP-43 loss of function in amyotrophic lateral sclerosis. Mol Neurodegener 13:1–
924 17
925 95. Wang C, Duan Y, Duan G, et al (2020) Stress Induces Dynamic, Cytotoxicity-
926 Antagonizing TDP-43 Nuclear Bodies via Paraspeckle LncRNA NEAT1-Mediated
927 Liquid-Liquid Phase Separation. Mol Cell 79:443-458.e7
928 96. Yu H, Lu S, Gasior K, et al (2021) HSP70 chaperones RNA-free TDP-43 into
929 anisotropic intranuclear liquid spherical shells. Science (1979).

930 https://doi.org/10.1126/SCIENCE.ABB4309/SUPPL_FILE/ABB4309_YU_SM.PD
931 F
932 97. Hipp MS, Kasturi P, Hartl FU (2019) The proteostasis network and its decline in
933 ageing. Nature Reviews Molecular Cell Biology 2019 20:7 20:421–435
934 98. Geertsma HM, Suk TR, Ricke KM, Horsthuis K, Parmasad JLA, Fisk ZA,
935 Callaghan SM, Rousseaux MWC (2022) Constitutive nuclear accumulation of
936 endogenous alpha-synuclein in mice causes motor impairment and cortical
937 dysfunction, independent of protein aggregation. Hum Mol Genet 31:3613–3628
938 99. Yu B, Pamphlett R (2017) Environmental insults: Critical triggers for amyotrophic
939 lateral sclerosis. Transl Neurodegener 6:1–10
940 100. Maurel C, Chami AA, Thépault RA, Marouillat S, Blasco H, Corcia P, Andres CR,
941 Vourc'h P (2020) A role for SUMOylation in the Formation and Cellular
942 Localization of TDP-43 Aggregates in Amyotrophic Lateral Sclerosis. Mol
943 Neurobiol 57:1361–1373
944 101. Kirola L, Mukherjee A, Mutsuddi M (2022) Recent Updates on the Genetics of
945 Amyotrophic Lateral Sclerosis and Frontotemporal Dementia. Molecular
946 Neurobiology 2022 59:9 59:5673–5694
947 102. Wang A, Conicella AE, Schmidt HB, et al (2018) A single N-terminal
948 phosphomimic disrupts TDP-43 polymerization, phase separation, and RNA
949 splicing. EMBO J 37:e97452
950 103. Brady OA, Meng P, Zheng Y, Mao Y, Hu F (2011) Regulation of TDP-43
951 aggregation by phosphorylation andp62/SQSTM1. J Neurochem 116:248–259
952 104. Wegorzewska I, Bell S, Cairns NJ, Miller TM, Baloh RH (2009) TDP-43 mutant
953 transgenic mice develop features of ALS and frontotemporal lobar degeneration.
954 Proc Natl Acad Sci U S A 106:18809–18814
955 105. Campbell KM, Xu Y, Patel C, et al (2021) Loss of TDP-43 in male germ cells
956 causes meiotic failure and impairs fertility in mice. Journal of Biological
957 Chemistry. https://doi.org/10.1016/j.jbc.2021.101231
958 106. Milstead RA, Link CD, Xu Z, Hoeffer CA (2023) TDP-43 knockdown in mouse
959 model of ALS leads to dsRNA deposition, gliosis, and neurodegeneration in the
960 spinal cord. Cerebral Cortex (New York, NY) 33:5808
961 107. Yang C, Qiao T, Yu J, et al (2022) Low-level overexpression of wild type TDP-43
962 causes late-onset, progressive neurodegeneration and paralysis in mice. PLoS One
963 17:e0255710
964 108. Buratti E (2018) TDP-43 post-translational modifications in health and disease.
965 Expert Opin Ther Targets. https://doi.org/10.1080/14728222.2018.1439923
966 109. Chatterjee M, Özdemir S, Fritz C, et al (2024) Plasma extracellular vesicle tau and
967 TDP-43 as diagnostic biomarkers in FTD and ALS. Nature Medicine 2024 30:6
968 30:1771–1783
969 110. Feiler MS, Strobel B, Freischmidt A, et al (2015) TDP-43 is intercellularly
970 transmitted across axon terminals. Journal of Cell Biology 211:897–911
971 111. Iguchi Y, Eid L, Parent M, et al (2016) Exosome secretion is a key pathway for
972 clearance of pathological TDP-43. Brain 139:3187–3201
973 112. Leibiger C, Deisel J, Aufschnaiter A, Ambros S, Tereshchenko M, Verheijen BM,
974 Büttner S, Braun RJ (2018) TDP-43 controls lysosomal pathways thereby
975 determining its own clearance and cytotoxicity. Hum Mol Genet 27:1593–1607

113. Liu G, Byrd A, Warner AN, Pei F, Basha E, Buchanan A, Buchan JR (2019) Cdc48/VCP and Endocytosis Regulate TDP-43 and FUS Toxicity and Turnover. Mol Cell Biol. https://doi.org/10.1128/mcb.00256-19
114. Liu G, Coyne AN, Pei F, Vaughan S, Chaung M, Zarnescu DC, Buchan JR (2017) Endocytosis regulates TDP-43 toxicity and turnover. Nat Commun 8:2092
115. Scotter EL, Vance C, Nishimura AL, et al (2014) Differential roles of the ubiquitin proteasome system and autophagy in the clearance of soluble and aggregated TDP-43 species. J Cell Sci 127:1263–1278
116. Wang X, Fan H, Ying Z, Li B, Wang H, Wang G (2010) Degradation of TDP-43 and its pathogenic form by autophagy and the ubiquitin-proteasome system. Neurosci Lett 469:112–116
117. Yau TY, Molina O, Courey AJ (2020) SUMOylation in development and neurodegeneration. Development. https://doi.org/10.1242/DEV.175703
118. Princz A, Tavernarakis N (2017) The role of SUMOylation in ageing and senescent decline. Mech Ageing Dev 162:85–90
119. White MA, Kim E, Duffy A, et al (2018) TDP-43 gains function due to perturbed autoregulation in a Tardbp knock-in mouse model of ALS-FTD. Nat Neurosci 21:1138
120. Fratta P, Sivakumar P, Humphrey J, et al (2018) Mice with endogenous TDP-43 mutations exhibit gain of splicing function and characteristics of amyotrophic lateral sclerosis. EMBO J. https://doi.org/10.15252/embj.201798684
121. Abramson J, Adler J, Dunger J, et al (2024) Accurate structure prediction of biomolecular interactions with AlphaFold 3. Nature 2024 630:8016 630:493–500
122. Dereeper A, Guignon V, Blanc G, et al (2008) Phylogeny.fr: robust phylogenetic analysis for the non-specialist. Nucleic Acids Res 36:W465–W469
123. Gertsenstein M, Nutter LMJ (2018) Engineering Point Mutant and Epitope-Tagged Alleles in Mice Using Cas9 RNA-Guided Nuclease. Curr Protoc Mouse Biol 8:28–53
124. Miedel CJ, Patton JM, Miedel AN, Miedel ES, Levenson JM (2017) Assessment of Spontaneous Alternation, Novel Object Recognition and Limb Clasping in Transgenic Mouse Models of Amyloid-β and Tau Neuropathology. JoVE (Journal of Visualized Experiments) 2017:e55523
125. Guyenet SJ, Furrer SA, Damian VM, Baughan TD, la Spada AR, Garden GA (2010) A Simple Composite Phenotype Scoring System for Evaluating Mouse Models of Cerebellar Ataxia. JoVE (Journal of Visualized Experiments) e1787
126. Lê S, Josse J, Husson F (2008) FactoMineR: An R Package for Multivariate Analysis. J Stat Softw 25:1–18
127. Alboukadel K, Fabian M (2020) Extract and Visualize the Results of Multivariate Data Analyses [R package factoextra version 1.0.7]. https://CRAN.R-project.org/package=factoextra. Accessed 8 Apr 2024

Acknowledgements:

This project was supported in part by an NSERC Discovery Grant and Discovery Launch Supplement to M.W.C.R. (RGPIN-2019-04133 and DGECR-2019-00369); the Canada Research Chairs program to M.W.C.R; the ALS Society of Canada in partnership with the Brain Canada Foundation through the Brain Canada Research Fund, with the financial support of Health

1022 Canada, for financial support through the ALS Trainee Award Program 2019 (T.R.S.) and the
1023 Discovery Grants Program 2021 (M.W.C.R.); the J.P. Bickell Medical Research Fund
1024 (M.W.C.R.); Canadian Institute of Health Research Project Grant (PJT-195691, M.W.C.R.). The
1025 Eric Poulin Center for Neuromuscular Disease through the Student Translational Research
1026 Awards (T.R.S., V.S.G.); The Canadian Institute of Health Research through the CGS-M award
1027 (C.E.P., J.L.Z., V.S.G.); The Ontario Graduate Scholarship Program Award (C.E.P.); NSERC
1028 Undergraduate Summer Research Award (T.T.N.); Medical Student Summer Research Program
1029 Award (T.T.N); Rising Star in ALS Research 2024 Award in memory of Madeleine Blanc
1030 through the Brain Canada Foundation (J.L.Z.); Christopher Chiu senior postdoctoral fellowship
1031 (P.M.M.); James Hunter and Family ALS Initiative (J.R.). Human tissue was received from the
1032 NIH NeuroBioBank at the University of Maryland, University of Pittsburgh, and Sepulveda
1033 sites. The authors also thank all members of the Rousseaux lab for important discussions and
1034 critical feedback on the manuscript. The authors also thank the following Core facilities from the
1035 University of Ottawa and the Ottawa Hospital Research Institute (OHRI) for use of their facility,
1036 equipment, and expertise: the Cell Biology and Imaging Acquisition Core (RRID:SCR_021845),
1037 STEMCore Laboratories (RRID:SCR_012601), Genome Engineering and Molecular Biology
1038 (GEM) Core (RRID:SCR_022954), Animal Behaviour and Physiology Core
1039 (RRID:SCR_022882), Louise Pelletier Histology Core (RRID: SCR_021737), Figs. 1, 2, 6, and
1040 S4 were generated in part with Biorender.com.

1041 **Author Contributions**

1042 Conceptualization: TRS, CEP, MWCR

1043 Methodology: TRS, CEP, TTN, JLZ, VSG, PMM, BN, SMC, JR

1044 Investigation: TRS, CEP, TTN, JLZ, MMH, ACG, VSG, PMM, BN, JR

1045 Visualization: TRS, CEP, JLZ, MWCR

1046 Funding acquisition: TRS, CEP, MWCR

1047 Project administration: JMW, JR, MWCR

1048 Supervision: JR, MWCR

1049 Writing – original draft: TRS, MWCR

1050 Writing – review & editing: TRS, MWCR

1051

1052 **Declaration of Interests:** Authors declare that they have no competing interests.

1053

1054 **Figure Captions**

1055 **Fig. 1: SUMOylation dynamically regulates nuclear TDP-43 in a stress-responsive manner.**
1056 **(A)** Schematic of immunoprecipitation assays to detect TDP-43 SUMOylation. **(B)**
1057 Representative SUMOylation Assay western blot detecting TDP-43 SUMOylation specifically in
1058 response to 1 hour sodium arsenite (250 µM) stress. * = SUMOylated TDP-43, ** =
1059 PolySUMOylated TDP-43. **(C)** Schematic TDP-43-GFP Nuclear Localization Sequence (NLS)
1060 variants and representative florescent microscopy analysis of their subcellular localization.
1061 (Scalebar = 10 µm). Yellow amino acids represent those critical for PY-NLS function. Teal

1062 arginine residue was mutated from the native HNRNPA1. **(D)** Representative GFP-trap
1063 SUMOylation assay detecting loss of SUMOylation in response to TDP-43 mislocalization in
1064 response to 1 hour sodium arsenite stress (250 µM). (N=3) RM One-Way ANOVA with Fisher's
1065 LSD test data presented as mean ± SEM, * p<0.05, ** p<0.005, *** p<0.0005. **(E)**
1066 Representative image and quantification of relative proximity ligation signal between TDP-43
1067 and SUMO2/3 in murine primary cortical neuron cultures in response to 1 hour sodium arsenite
1068 (250 µM) treatment. Scalebar = 20 µm. (N = 4 per condition) Unpaired T-test data presented as
1069 mean ± SEM, *** p<0.0005 **(F)** Representative SUMOylation Assay of TDP-43 SUMOylation
1070 dynamics during stress (250 µM sodium arsenite) and recovery demonstrating a dependency on
1071 the ubiquitin proteosome for clearance of polySUMOylated TDP-43 by treatment with
1072 proteasome inhibitor MG132 (2µM). **(G)** Schematic and representative GFP-Trap SUMOylation
1073 assay screening for potential E3 ligases regulating TDP-43 SUMOylation in response to 1 hour
1074 sodium arsenite stress (250 µM). (N = 3) RM One-Way ANOVA with Fisher's LSD test data
1075 presented as mean ± SEM, * p<0.05, ** p<0.005, *** p<0.0005, **** p<0.0001.

1076

1077 **Fig. 2: TDP-43 is SUMOylated at K408 in a conserved region of the C-terminal domain.**
1078 **(A)** Representative GFP-Trap SUMOylation assay to map the site of TDP-43 SUMOylation in
1079 response to 1 hour sodium arsenite (250 µM) stress. One-Way ANOVA with Fisher's LSD test
1080 data presented as mean ± SEM, ** p<0.005, **** p<0.0001. **(B)** Phylogenetic representation
1081 from alignment of representative TDP-43 paralogs highlighting the emergence and conservation
1082 of [human] K408 (Blue). **(C)** Pairwise identity of the [human] TDP-43 C-terminal domain from
1083 MUSCLE alignment of 300 amino acid sequences for TDP-43 paralogs from Humans to
1084 Actinopterygii from OrthoDB. Red represents the TDP-43 C-terminal domain (Intrinsically
1085 disordered domain). Cyan represents PTM- enriched region at the extreme C-terminus. **(D)**
1086 Representative GFP-Trap SUMOylation assay with phospho-dead TDP-43 "4SA"
1087 (S403/404/409/410A) highlighting antagonism between SUMOylation and phosphorylation.
1088 (N=3) Unpaired T-test data presented as mean ± SEM. **(E)** Schematic and sanger sequencing of
1089 the TDP-43^{K408R} knock in mouse line. **(F)** Schematic of endogenous SUMOylation assay from
1090 embryonic mouse brains. **(G)** Validation of loss of TDP-43 SUMOylation in the brains of TDP-
1091 43^{K408R} mice. 2-Way ANOVA with Fisher's LSD test. Data presented as mean ± SEM, ****
1092 p<0.0001.

1093 **Fig. 3: Blocking TDP-43 SUMOylation at K408 impairs the cellular stress response in**
1094 **neurons. (A)** Representative images and quantification of G3BP1 stress granule dynamics in
1095 mouse primary cortical neurons (7 DIV) during stress (1 hour 250 µM sodium arsenite) and
1096 recovery. G3BP1 contrast was set for optimal visualization of stress granules. Scale Bar = 25 µm
1097 N=5, 2-Way ANOVA with Fisher's LSD test data presented as mean ± SEM, * p<0.05, **
1098 p<0.005. **(B)** Representative western blot and quantification of RIPA and UREA fractions from
1099 mouse primary cortical neurons (7 DIV) during stress (1 hour 250 µM sodium arsenite) and
1100 recovery. Quantification found in Fig. S6A. **(C)** Representative images and quantification of
1101 TDP-43 nuclear foci formation in mouse primary cortical neurons (7 DIV) during stress (1 hour
1102 250 µM sodium arsenite) and recovery. Cyan arrowheads denote cells with nuclear TDP-43 foci.
1103 Scale Bar = 25 µm. N=5, 2-Way ANOVA with Fisher's LSD test data presented as mean ± SEM,
1104 ** p<0.005. **(D)** Representative images and quantification of G3BP1 stress granule dynamics in
1105 mouse primary cortical neurons (7 DIV) during repeated stress (30-minute 250 µM sodium
1106 arsenite treatment) and recovery (30-minute washout), repeated 3 times. Scale Bar = 25 µm.

1107 N=3, 2-Way ANOVA with Fisher's LSD test data presented as mean ± SEM, * $p<0.05$, **
1108 $p<0.005$. **(E)** Representative images and quantification of TDP-43 nuclear foci formation in
1109 mouse primary cortical neurons (7 DIV) during repeated stress (30-minute 250 µM sodium
1110 arsenite treatment) and recovery (30-minute washout), repeated 3 times. Cyan arrowheads denote
1111 cells with nuclear TDP-43 foci. Scale Bar = 25 µm. N=3, 2-Way ANOVA with Fisher's LSD test
1112 data presented as mean ± SEM, ****$p<0.0001$. For all immunofluorescent assays at least 50
1113 cells were imaged and quantified per replicate (N=3-5).

1114 **Fig. 4: Blocking TDP-43 SUMOylation *in vivo* leads to sex-specific social and cognitive**
1115 **impairment. (A)** Representative image of a barbered female mouse and quantification of
1116 cumulative barbering probability. 2-Way ANOVA with Tukey's Multiple Comparisons, ***
1117 $p<0.0005$. **(B)** Tube test of social dominance at 16 months of age (16MO) displaying the total
1118 head-to-head battles and win percentage by genotype comparing wild type against K408R
1119 (K408R/+ and K408R/K408R animals). Binomial Test of Observed vs. Expected with Expected
1120 due to random chance set to 50%, * $p<0.05$. **(C)** Quantification of total distance traveled (cm)
1121 and total time in center (s) in the open field test. Mixed Effects Analysis with Tukey's multiple
1122 comparison data presented as mean ± SEM, *** $p<0.0005$, * $p<0.05$. **(D)** Quantification of
1123 percent alternations in the spontaneous Y-maze test at 2, 9, and 16 months of age (2MO, 9MO,
1124 16MO, respectively). Mixed-Effects Analysis with Tukey's multiple comparison data presented
1125 as mean ± SEM, * $p<0.05$. **(E)** Quantification of relative ambulatory activity normalized to wild
1126 type at 1 hour at 2, 9, and 16 months of age (2MO, 9MO, and 16MO, respectively). Grey shading
1127 between hours 2 and 14 indicate "lights off" with respect to day/night light cycle. 2-Way
1128 ANOVA with Tukey's multiple comparison data presented as mean ± SEM, * $p<0.05$.

1129 **Fig. 5: Male TDP-43^{K408R} mice present with age-specific features of ALS. (A)** Representative
1130 images and quantification of TDP-43 mislocalization in the lumbar spinal cord of 9-month-old
1131 TDP-43^{K408R} mice. Each datapoint represents the average of 4 serial sections 40 µm apart per
1132 individual mouse. Scalebar = 100 µm. (N = 4 per sex/genotype) Unpaired t-test, *** $p<0.0005$.
1133 See Fig. S12C for sex comparisons. **(B)** Representative images and quantification of
1134 neuromuscular junction (NMJ) innervation in the tibialis anterior of male 16-month-old TDP-
1135 43^{K408R} mice. >80 NMJs were quantified per animal (N = 4 per genotype). 2-Way ANOVA with
1136 Tukey's multiple comparison analysis, *$p<0.05$, ****$p<0.0001$. **(C)** Representative images and
1137 quantification of ChAT+ motor neurons in the ventral horn of the lumbar spinal cord of male
1138 mice. Each datapoint is the average of 4 serial sections spaced 40 µm apart through the lumbar
1139 enlargement of the lumbar spinal cord. Unpaired t-test, ** $p<0.005$. **(D)** Survival curve for male
1140 TDP-43^{K408R} mice (Females found in Fig. S7D). Curve comparisons analyzed using Log-Rank
1141 test and Gehan-Breslow-Wilcoxon test. *$p<0.05$.

1142 **Fig. 6: SUMOylation correlates with aging and is enriched in the prefrontal cortex of**
1143 **ALS/FTD patients. (A)** Demographic composition of temporal lobe samples from aging cohort.
1144 **(B)** Representative western blot and box plot of SUMO2/3 across binned age groups. Average
1145 Age: "Young" = 6.32yrs, N = 14; "Adult" = 31.11yrs, N = 20; "Aged" = 64.00yrs, N = 19.
1146 Kruskall-Wallis with Uncorrected Dunn's multiple comparisons test. * $p<0.05$, ** $p<0.005$. **(C)**
1147 Representative images and quantification from proximity ligation assay (PLA) between
1148 SUMO2/3 and TDP-43 in the prefrontal cortex from 3 patients diagnosed with ALS/FTD and
1149 unaffected controls. (N = 7-8) Unpaired T-test data presented as mean ± SEM, * $p<0.05$.

1150

1151 **Supplemental Figures**

1152 **Fig. S1: Characterizing stress responsive TDP-43 SUMOylation. (A)** Representative western
1153 blot from SUMOylation assays testing whether various stressors that cause TDP-43 aggregation
1154 induce TDP-43 SUMOylation: NaAsO2 (250 µM), D-Sorbitol (400 mM), NaCl (300 mM), Heat
1155 Shock (42 °C) in HEK293T HA-SUMO2 stable cells. One-Way ANOVA with Fisher's LSD
1156 test. Data presented as mean ± SEM. *p<0.05, **p<0.005, ****p<0.0001. **(B)** Representative
1157 western blot from SUMOylation assays testing the selectivity of SUMO paralogs to SUMOylate
1158 TDP-43 in response to 1 hour sodium arsenite (250 µM) in HEK293T cells with transient
1159 expression of SUMO paralogs. **(C)** Representative GFP-Trap SUMOylation assay depicting
1160 increased SUMOylation with ALS-causing Q331K mutation in response to 250 µM sodium
1161 arsenite stress in HEK293T cells with transient expression of HA-SUMO2. Unpaired T-test.
1162 *p<0.05. Data presented as mean ± SEM. **(D)** Representative images of SUMO2/3 and TDP-43
1163 in the nucleus of mouse cortical neurons (7 DIV) in unstressed and 1 hour sodium arsenite
1164 (250µM) stressed conditions. **(E)** Representative control imaged from Proximity Ligation Assay
1165 (PLA) in mouse primary cortical neurons. Scalebar = 20 µm. (N = 4). **(F)** Representative western
1166 blot and quantification from GFP-Trap SUMOylation assays testing the kinetics of TDP-43
1167 SUMOylation in response to sodium arsenite stress (250 µM) and its relationship to insoluble
1168 phosphorylated TDP-43 in HEK293T HA-SUMO2 stable cells. (N = 3). Linear regression
1169 analysis of Relative SUMOylation against time in response to stress. **(G)** Representative dose-
1170 response assay to detect TDP-43 SUMOylation after 1 hour of sodium arsenite stress (1 = 250
1171 µM, 1/2 = 125 µM, 1/4 = 62.5 µM, etc.) in HEK293T HA-SUMO2 stable cells. One-Way
1172 ANOVA with Fisher's LSD test. Data presented as mean ± SEM. *p<0.05, **p<0.005,
1173 ****p<0.0001.

1174 **Fig. S2: Analysis of TDP-43 lysine to arginine mutation at K136 and K408. (A)**
1175 Representative fluorescent microscopy images expressing TDP-43-GFP with K136R and RNA
1176 binding deficient (5FL) mutations. Scale bar = 10 µm. **(B)** Predicted alignment error output from
1177 AlphaFold3 prediction of TDP-43 structure (residues 1-414) interacting with UG (x6) RNA
1178 (residues 415-426). **(C)** Predicted structure of TDP-43 with annotated domains. Color annotates
1179 predicted local difference test (plDDT)j scores. NTD = N-Terminal Domain; RRM1/RRM2 =
1180 RNA Recognition Motif 1/2; CTD = C-Terminal Domain. **(D)** Predicted structure of TDP-
1181 43^{K408R} highlighting no addition of secondary structure at the C-terminus surrounding residue
1182 408 upon mutation. **(E)** Representative image and quantification of TDP-43-GFP expression
1183 denoting mislocalization in a subset of cells overexpressing TDP-43 with K408R mutation.
1184 (N=3) Students T-test. Data presented as mean ± SEM.

1185 **Fig. S3: Characterization of SUMO2 fusion to the C-terminus of TDP-43**. **(A)**
1186 Representative western blot and quantification of TDP-43-HA and TDP-43-SUMO2-HA
1187 expression in HEK293T cells. (N=3) 2-way ANOVA with Fishers LSD test. Data presented as
1188 mean ± SEM. *p<0.05, **p<0.005. **(B)** Representative immunofluorescence microscopy images
1189 of TDP-43-HA and TDP-43-SUMO2-HA fusion in HEK293T cells in response to cellular stress
1190 (250 µM sodium arsenite for 1 hour). (N=3) Students T-test. Data presented as mean ± SEM.
1191 *p<0.05**.**

1192 **Fig. S4: Generation of the TDP-43^{K408R} mouse line. (A)** Schematic of the knock in approach to
1193 edit the endogenous *Tardbp* to express TDP-43^{K408R}. **(B)** Schematic of LNA probe based
1194 genotyping approach and allelic discrimination assay to genotype TDP-43^{K408R} mouse line. **(C)**
1195 Sex and mendelian ratios of F3 generation TDP-43^{K408R} mice from K408R/+ and K408R/+

1196 breeding pairs used to generate behaviour and histology cohorts. Observed vs Expected
1197 statistical analysis assuming an expected 1:1 ratio sex ratio and 1:2:1 mendelian ratio.

1198 **Fig. S5: Characterizing the stress response in TDP-43^{K408R} primary cortical neuron**
1199 **cultures. (A)** Classification and quantification of G3BP1 stress granule (SG) intensity in
1200 response to 1 hour sodium arsenite stress (250 μM) and recovery. Data presented as mean ±
1201 SEM. (N = 5 per genotype) 2-Way ANOVA with Tukey's multiple comparisons analysis.
1202 *p<0.05, ***p<0.0005. **(B)** Quantification of the localization of G3BP1 stress granules (SGs) in
1203 response to 1 hour sodium arsenite stress (250 μM) and recovery. Data presented as mean ±
1204 SEM. (N = 5 per genotype) 2-Way ANOVA with Tukey's multiple comparisons analysis.
1205 ***p<0.0005. **(C)** Quantification of the percentage of neurons with positive TDP-43 nuclear foci
1206 in G3BP1 stress granule positive and G3BP1 stress granule negative neurons in response to 1
1207 hour sodium arsenite stress (250 μM) and recovery. Data presented as mean ± SEM. (N = 5 per
1208 genotype) 2-Way ANOVA with Tukey's multiple comparisons analysis. ***p<0.0005. **(D)**
1209 Quantification of the average number of TDP-43 nuclear foci in neurons positive for TDP-43
1210 nuclear foci in response to 1 hour sodium arsenite stress (250 μM) and recovery. Data presented
1211 as mean ± SEM. (N = 5 per genotype) 2-Way ANOVA with Tukey's multiple comparisons
1212 analysis. *p<0.05.

1213 **Fig. S6: Characterizing the effect of blocking TDP-43 SUMOylation in primary cortical**
1214 **neurons. (A)** Quantification of RIPA and UREA fractions from mouse primary cortical neurons
1215 (7 DIV) during stress (1 hour 250 μM sodium arsenite) and recovery related to Fig. 3B. N=3-5,
1216 2-Way ANOVA with Fisher's LSD test. Data presented as mean ± SEM, * p<0.05, ** p<0.005.
1217 **(B-D)** Representative immunofluorescent images of primary cortical neurons (7 DIV) treated
1218 with 250 μM sodium arsenite for 1 hour then recovered for 3 hours to induce TDP-43 foci
1219 formation to analyze colocalization with nuclear markers: (B) HSPA1L was visualized through
1220 lentiviral transduction of HSPA1L-mRuby2; (C) paraspeckle marker PSPC-1; and (D) Ubiquitin.
1221 (N=3). At least 10 cells positive for TDP-43 foci and foci of interest were imaged and analyzed
1222 per replicate. **(E)** Quantification of primary cortical neurons with TDP-43 mislocalization in
1223 response to repeated stress (30 minutes 250 μM sodium arsenite) and recovery (30 minutes
1224 washout) related to Fig. 3E. (N=3) 2-Way ANOVA with Fishers LSD test. Data presented as
1225 mean ± SEM. **(F)** Representative western blot and analysis of RIPA soluble and UREA fractions
1226 from primary cortical neurons in response to chronic stress (30 hours of 15 μM sodium arsenite)
1227 and recovery. Data presented as mean ± SEM. 2-Way ANOVA with Fishers LSD test. *p<0.05,
1228 **p<0.005.

1229 **Fig S7: General wellness of TDP-43^{K408R} mice during development and aging. (A)** Genotype
1230 and sex composition of mice subject to behaviour testing. **(B)** Weight of mice at P21. Unpaired
1231 T-test (Males); Mann-Whitney test (Females and All) **(C)** Quantification of the duration hanging
1232 on a wire at P21. Mann-Whitney test (Males, Females, and All). **(D)** Survival curve for female
1233 TDP-43^{K408R} mice (Males found in Fig. 5d). Curve comparisons analyzed using Log-Rank test
1234 and Gehan-Breslow-Wilcoxon test. **(E)** Weights of male and female TDP-43^{K408R} mice from 3
1235 weeks to 64 weeks of age. Mixed-effects analysis. **(F)** Hindlimb clasping scores of male and
1236 female TDP-43^{K408R} mice from 3 weeks to 64 weeks of age. Mixed-effects analysis. See table S2
1237 for raw data details on statistical tests. Data presented as mean ± SEM

1238 **Fig. S8: Characterizing the cognitive and social behaviour of TDP-43^{K408R} mice.**
1239 Quantification of cognitive and social behaviours in the **(A)** Light/Dark Box, **(B)** Y-maze, **(C)** 3
1240 Chamber Social Interaction, **(D)** Marble Burying, and **(E)** Tail Suspension behaviour tasks at 2,

9, and 16 months of age (2MO, 9MO, and 16MO, respectively) in male and female TDP-43^{K408R} mice. All behaviour tests were analyzed with a Mixed-Effects Model with Tukey's multiple comparison analysis, see table S2. Data presented as mean ± SEM.

Fig. S9: Characterizing the motor behaviour of TDP-43^{K408R} mice. Quantification of motor abilities in the **(A)** Hanging Wire, **(B)** Grip Strength, and **(C)** Rotarod behaviour tasks at 2, 9, and 16 months of age (2MO, 9MO, and 16MO, respectively) in male and female TDP-43^{K408R} mice. **(D)** Digigait behaviour tasks at 16 months of age in male and female TDP-43^{K408R} mice. Behaviour tests were analyzed with 2-Way ANOVA or Mixed-Effects Models, see table S2. Data presented as mean ± SEM.

Fig. S10: Characterizing the activity of TDP-43^{K408R} mice. Quantification of **(A)** total distance traveled (cm) and time in center (s) during the Open Field behaviour test and **(B)** the relative ambulatory activity (males) of TDP-43^{K408R} mice at 2, 9, and 16 months of age (2MO, 9MO, and 16MO, respectively). Behaviour tests were analyzed with 2-Way ANOVA or Mixed-Effects models, see table S2. Data presented as mean ± SEM.

Fig. S11. Absence of overt neurodegenerative or neuroinflammatory phenotypes in TDP-43$^{K408R/K408R}$ mice. Cresyl violet staining used to measure cortical thickness in the prefrontal cortex (PFC) and motor area 1 (M1) of female **(A)** and male **(B)** TDP-43$^{K408R/K408R}$ mice and littermate controls. Cux1 and Ctip2 staining and quantification in the motor cortex of female **(C)** and male **(D)** TDP-43$^{K408R/K408R}$ mice and littermate controls. Iba1 staining of microglia **(E, F)** and GFAP staining of astrocytes **(G, H)** in female **(E,G)** and male **(F,H)** TDP-43$^{K408R/K408R}$ mice and littermate controls. Quantification represents evaluation of N=4 mice per genotype, per sex, per time point. Micrographs are representative of the 16-month time point. Students T-test. Data presented as mean ± SEM. ns denotes p>0.05.

Fig. S12: Characterizing the molecular and histological affects of blocking TDP-43 SUMOylation in vivo. (A) Representative western blot and quantification of TDP-43 and phosphorylated TDP-43 in the RIPA and UREA fractions of the cortex from male mice at 2, 9, and 16 months of age (2MO, 9MO, and 16MO, respectively). Data presented as mean ± SEM. (N = 4 per genotype) 2-Way ANOVA with Fisher's LSD test. **(B)** Representative western blot and quantification of TDP-43 and phosphorylated TDP-43 in the RIPA and UREA fractions of the cortex from male mice at 2, 9, and 16 months of age (2MO, 9MO, and 16MO, respectively). Data presented as mean ± SEM. (N = 4 per genotype) 2-Way ANOVA with Fisher's LSD test. *p<0.05, **p<0.005, ***p<0.0005. **(C)** Quantitative RT-PCR from 16 month old mouse cortex for splicing isoforms of *Mapt*. (N=8, 4 per sex, per genotype) 2-Way ANOVA with Fisher's LSD Test. Data presented as mean ratios of ΔCt normalized to wild type ± SEM. **p<0.005. **(D)** Quantification of TDP-43 mislocalization in the lumbar spinal cord of 9-month-old from Fig. 5a split by sex. Each datapoint represents the average of 4 serial sections 40 µm apart from an individual mouse. Unpaired t-test. * = p<0.05, ** = p<0.005. **(E)** Representative western blot and quantification of TDP-43 and phosphorylated TDP-43 in the RIPA and UREA fractions of the lumbar spinal cord at 2, 9, and 16 months of age (2MO, 9MO, and 16MO, respectively). Data presented as mean ± SEM. (N = 8 per genotype; 4 per sex/genotype) 2-Way ANOVA with Fisher's LSD test, *p<0.05, ***p<0.0005, ****p<0.0001 **(F)** Example images of neuromuscular junctions (NMJs) for scoring criteria to assess fully innervated, partially innervated, and fully denervated NMJs. **(G)** Representative images and quantification of neuromuscular junction (NMJ) innervation in the tibialis anterior of female 16-month-old TDP-43^{K408R} mice. >80 NMJs were quantified per animal. Data presented as mean ± SEM. (N = 4 per genotype) 2-Way

1286 ANOVA with Tukey's multiple comparison analysis, *p<0.05, ****p<0.0001. (H)
1287 Representative images and quantification of ChAT+ motor neurons in the ventral horn of the
1288 lumbar spinal cord of male and female mice. Each datapoint is the average of 4 serial sections
1289 spaced 40 µm apart through the lumbar enlargement of the lumbar spinal cord. Data presented as
1290 mean ± SEM. Unpaired t-test, ** p<0.005.

1291 **Fig. S13 : Optimization of proximity ligation assay in human tissue. (A)** Quantification of
1292 neuropathology score of PPFE prefrontal cortex (PFC) tissue sections (5um) from patients
1293 diagnosed with ALS/FTD and unaffected controls. Data presented as mean ± SEM. (N = 6-8)
1294 Unpaired t-test, ** p<0.005. **(B)** Representative images of proximity ligation assay (PLA)
1295 between TDP-43 and SUMO2/3 in human PPFE hippocampus tissue sections (5um). Yellow
1296 arrows indicate TDP-43:SUMO2/3 interactions where the signal specific to the PLA channel and
1297 not identified in the autofluorescence channel. Scalebar = 18 µm.

1298

1299 **Supplementary Information**

1300 Supplementary Tables 1-4

1301 Supplementary Video 1

1302

1303 **Materials and Methods**

1304 ***Materials availability***

1305 Plasmids generated in this study will be deposited to Addgene by the time of publication.

1306 Mouse lines generated in this study are available upon request.

1307 ***Data and code availability***

1308 Human tissue data reported in this paper will be shared by the lead contact upon request.

1309 Any additional information required to reanalyze the data reported in this paper is available from
1310 the lead contact upon request.

1311 ***Cloning of pEGFP-TDP-43 plasmid and variants***

1312 For expression of C-terminally tagged TDP-43-EGFP, human TDP-43 was subcloned out of a
1313 wtTDP-43tdTOMATOHA (gift from Zoushang Xu, Addgene # 28205) via XhoI and Kpn1
1314 double digest and inserted into a pEGFP-N3 (Clontech) backbone and validated by sanger
1315 sequencing. Site directed mutagenesis was performed using QuikChange II XL (Agilent 200521)
1316 following manufacturer instructions. Primers for site directed mutagenesis can be found in table
1317 S4. Several TDP-43 variants were generated through the uOttawa Genome Engineering and
1318 Molecular Biology facility or designed and ordered through twist bioscience and were subcloned
1319 into the pEGFP-TDP-43 backbone for consistency using XhoI and HindIII double digest, see
1320 table S4 for plasmids used/generated in this study.

1321 ***Cell culture***

1322 HEK293T cells were cultured in DMEM outgrowth media containing 10% FBS (unless
1323 otherwise stated) and antibiotic/antimycotics at 37°C with 5% CO_2.

1324 ***Generation of pL302-HA-SUMO2 stable HEK293T cell line***

1325 To generate a pL302-HA-SUMO2 lentivirus-compatible vector for stable HA-SUMO2
1326 expression, HA-SUMO2 was subcloned from pcDNA-HA-SUMO2 (gift from Guy Salvesen,
1327 Addgene #48967) and inserted into the pL302 lentiviral backbone (gift from Jacqueline Burré
1328 and Thomas Südhof at Stanford). Briefly, extension PCR was performed to add an Xba1
1329 restriction site to the 5' and 3' ends of the HA-SUMO2 insert using PCR amplification using
1330 forward primer sequence*: 5'- ggctgcaggtcgactctagaaagcttatggatgcctaccc-3'*, and reverse primer
1331 sequence*: 5'- tggctgcaggtcgactctagatgcatgctcgagtcaacct-3'.* The PCR amplicon and pL302
1332 backbone were digested with XbaI and the amplicon was ligated into the pL302 backbone.
1333 Colonies were screened by sanger sequencing to ensure proper orientation and copy number of
1334 the insert. Next the pL302-HA-SUMO2 plasmid was packaged into lentivirus by co-transfection
1335 of psPAX2 (Gift from Didier Trono, Addgene #12259), and pMD2-G (Gift from Didier Trono,
1336 Addgene #12260) into HEK293T cells and subsequent media collections. Viral media was
1337 filtered through a 0.45 μm filter then concentrated by centrifugation at 100,000G for 2 hours at 4
1338 °C and the pellet was resuspended in 1X PBS. Fresh HEK293T cells were transduced with
1339 pL302-HA-SUMO2 virus to generate a stable polyclonal cell line.

1340 ***GFP-trap SUMOylation assay***

1341 ~250,000 HEK293T and/or pL302-HA-SUMO2 HEK293T cells were seeded (experiment
1342 dependent) in a 6-well plate. The following day, plasmids were transfected to express TDP-43-
1343 GFP (or mutant variants) and/or HA-SUMO variants and allowed to incubate for 48 hours for
1344 optimal expression. Cells were treated with 250 μM $NaAsO_2$ for one hour (or variations of time,
1345 concentration, or chemical depending on assay), after which cells were immediately collected by
1346 scraping the bottom of the well and pelleting the samples by centrifugation at 2500G for 5 minutes
1347 at room temperature. The supernatant was then aspirated, and the cells were flash frozen or
1348 immediately lysed in 450 uL of ice cold 1X Denaturing Lysis buffer (1X RIPA, supplemented
1349 with 1X protease inhibitor, 1X phosphatase inhibitor, 50mM N-Ethylmalamide, and 5% 2-
1350 mercaptoethanol) and boiled at 95 °C for 5 minutes. After boiling, 450 uL of ice cold 1X Lysis
1351 buffer (1X RIPA, supplemented with 1X protease inhibitor, 1X phosphatase inhibitor, 50mM N-
1352 Ethylmalamide) was then added to the sample, and cells were left on ice for 20 minutes with
1353 vortexing every 5 minutes for 10 second. Next, the cell lysates are centrifuged at ~21000G for 20
1354 minutes at 4 °C and during this time, 30 uL of GFP-Trap beads (Bulldog Bio) per sample were
1355 washed 3 times in cold 1X RIPA buffer then aliquoted equally into microcentrifuge tubes for each
1356 sample. Following the centrifugation, 1-3% of the supernatant was transferred into a
1357 microcentrifuge tube to be used as the *Input* sample. The remainder of the supernatant was
1358 transferred into a microcentrifuge tube containing the GFP-Trap beads as the immunoprecipitation
1359 sample and was then placed on a rotator for 45 minutes at 4 °C. After the incubation, the solution
1360 was aspirated, and the beads were washed using cold 1X RIPA buffer 5 times. Samples were eluted
1361 in 30 μL of 2X Laemmli buffer containing 10% Beta-Mercaptoethanol and boiled at 85 °C for 10
1362 minutes at 1250 rpm on a thermomixer. The input samples were prepared with 4X Laemmli buffer
1363 containing 10% Beta-Mercaptoethanol and then boiled at 85 °C for 10 minutes. Samples were then
1364 analyzed by Western Blot. Quantification of SUMOylation assays was performed through
1365 densitometry analysis using ImageLab (BioRad) to quantify the volume of the ~95kDa anti-HA
1366 bands from the immunoprecipitation standardized to the anti-GFP pulldown. For quantification of
1367 changes in TDP-43 SUMOylation response, conditions were normalized to the 1 hour sodium
1368 arsenite treatment for wild type TDP-43.

1369 ***SUMOylation assay***

1370 ~500,000 HEK293T and/or pL302-HA-SUMO2 HEK293T cells were seeded (experiment
1371 dependent) in a 6-well plate. The following day, cells were treated respective of their experiment
1372 after which cells were immediately collected by scraping the bottom of the well and pelleting the
1373 samples by centrifugation at 2500G for 5 minutes at room temperature. The supernatant was then
1374 aspirated, and the cells were flash frozen or immediately lysed in 100 uL of 1% SDS buffer (1%
1375 SDS in IP Lysis Buffer supplemented with 1X protease inhibitor, 1X phosphatase inhibitor,
1376 100mM N-Ethylmalamide), vortexed for 20 seconds then boiled at 95C for 10 minutes. After
1377 boiling, 900 µL of ice-cold IP Lysis buffer was then added to the sample, and cells were left on
1378 ice for 20 minutes with vortexing every 5 minutes for 10 second. Next, the cell lysates are
1379 centrifuged at ~21000G for 20 minutes at 4 C. Following the centrifugation, 1-3% of the
1380 supernatant was transferred into a microcentrifuge tube to be used as the *Input* sample. The
1381 remainder of the supernatant was transferred into a microcentrifuge tube containing 1 to 10 ug of
1382 antibody per sample (See table S5 for concentrations) and incubated overnight rotating at 4 °C.
1383 The next day, 50 µL of Protein G Dynabeads (Thermo Fisher Scientific) per sample were washed
1384 3X in ice cold IP Lysis Buffer. The beads were resuspended in 50 µL IP Lysis Buffer per sample
1385 which was then added to each of the samples incubated with antibody. The samples were left to
1386 rotate at 4 °C for 45 minutes. Next, the solution was added to a magnetic rack kept at 4 °C and the
1387 supernatant was collected for *flowthrough* to test immunodepletion or aspirated. The beads were
1388 washed 5X in ice cold IP Lysis buffer. Samples were eluted using 5 ug of synthetic HA peptide
1389 (Sino Biological) per 1ug of antibody and incubating at 37 °C for 15 minutes at 900rpm on a
1390 thermomixer (for anti-HA immunoprecipitations). The input/flowthrough and HA
1391 immunoprecipitation samples were prepared with 4X Laemmli buffer containing 10% Beta-
1392 Mercaptoethanol and then boiled at 85 °C for 10 minutes. Samples were then analyzed by Western
1393 Blot using light chain specific secondary antibodies. Quantification of SUMOylation assays was
1394 performed through densitometry analysis using ImageLab (BioRad) to quantify the volume of the
1395 ~65kDa anti-TDP-43 bands from the immunoprecipitation standardized to the loading control of
1396 the input. For quantification of changes in TDP-43 SUMOylation response, conditions were
1397 normalized to the 1 hour sodium arsenite treatment.

1398 ***Serial protein extraction from cell culture***

1399 Soluble protein was extracted using RIPA buffer (supplemented with protease inhibitor,
1400 phosphatase inhibitor, and 50mM N-Ethylmalamide) during immunoprecipitation assays (taken
1401 as *Input* prior to immunoprecipitation) or from lysate in cortical neuron experiments. The
1402 remaining pellet after the centrifugation step post-lysis was washed in 1mL RIPA buffer with
1403 vortexing for 10 seconds followed by centrifugation at ~21000G for 20 minutes at 4 °C. The
1404 supernatant was carefully removed, and the pellet was resuspended in 300 µL of 2% SDS buffer
1405 in PBS for immunoprecipitation assays, or in 300 µL of 8M UREA in PBS with 10mM Tris-HCl
1406 pH 7.4. Samples were left to solubilize overnight at room temperature before 2X Laemmli was
1407 added prior to Western Blot analysis.

1408 ***Western blot analysis***

1409 Protein sample prepared in Laemmli loading buffer was loaded onto 8% polyacrylamide gel,
1410 TGx Mini-PROTEAN 4-15% precast gel (BioRad), or Bolt Bis-Tris Plus mini-Protein Gel 4-
1411 12% (Invitrogen) and run at 100-140 constant voltage in Tris-Glycine or MES buffer for their
1412 respective gels. Proteins were transferred onto a 0.45 µm nitrocellulose membrane at a constant
1413 340 mA for 2 hours at 4 °C. The membranes were blocked in 10% milk diluted in TBS-T,

1414 washed 5 x 5 minutes in TBS-T then incubated in primary antibody overnight (table S5). The
1415 following day the membranes were washed for 5 x 5 minutes in TBS-T, then incubated in
1416 secondary antibody for 1-2 hours at room temperature. Finally, the secondary antibody is washed
1417 5 x 5 minutes in TBS-T before being imaged using chemiluminescence Clarity Western ECL or
1418 Clarity Max Western ECL on an LAS4000 (GE). Densitometry was performed using the
1419 volumes function of the ImageLab (BioRad) software.

1420 **Immunofluorescent microscopy analysis in HEK293T cells**

1421 Micro Coverglass #1.5 coverslips (Electron Microscopy Sciences) coverslips were washed in 2M
1422 HCl overnight at 55 °C, washed 5 times in sterile H_2O, then pre-coated with 300 µL poly-D-
1423 lysine (10 µg/mL) overnight at 37 °C, then washed with distilled water three times and air-dried
1424 at room temperature for at least 2 hours or stored at 4 °C until required. 400 000 HEK293T cells
1425 were seeded in a 6 well dish and incubated overnight. 1000 ng of plasmid for protein expression
1426 was transfected into cells using Lipofectamine 3000 protocol (Thermo Fisher Scientific). Media
1427 was changed 4 hours post transfection to reduce toxicity. The following day transfected
1428 HEK293T cells were split onto coverslips plating ~50 000 cells per coverslip. Cells were
1429 allowed to adhere for 24 hours. Cells were fixed using 10% buffered formalin for 10 minutes,
1430 then permeabilized in blocking buffer (10% serum, 1% Triton X-100, in 1X PBS) for 1 hour,
1431 then primary antibody diluted in blocking buffer was applied overnight (See supplemental table
1432 5 for antibody concentrations). The following day coverslips were washed 5X in 1X PBS for 5
1433 minutes then secondary antibody diluted in blocking buffer was applied for 2 hours at room
1434 temperature. Samples were stained with 1X DAPI (and/or 1:10000 dilution of CellMask
1435 Membrane Stain) in PBS for 10 minutes. Samples were washed 4 more times in PBS for 5
1436 minutes each. Coverslips were briefly air dried and then mounted on slides using Vectashield
1437 Antifade Mounting Medium with DAPI. Z-stack images were obtained on a Zeiss
1438 AxioObserverZ1 LSM800 Confocal Microscope at 40× magnification with a 5× digital zoom or
1439 63x magnification with 2X digital zoom through a Z distance of 10-12 µm per image using
1440 optimal spacing per slice with dimensions set to 1024 x 1024 pixels with 4X averaging per
1441 frame. At least 10 cells were imaged per replicate. Images were analyzed and quantified using
1442 ImageJ.

1443 ***E3 SUMO ligase screen***

1444 One day prior to transfection 62,000 HEK293T or HEK293T stably expressing HA-SUMO2
1445 were plated in a 6 well dish. Samples were co-transfected using 800 ng of pCLIP-Dual-sgRNA
1446 for each of the SUMO E3 ligases alongside 1200ng pLenti-Cas9-BLAST and media was
1447 changed after 4 hours to minimize toxicity. Forty-eight hours after transfection, cells were
1448 selected using 2 µg/mL puromycin for 2-3 days. After selection was complete, cells were
1449 recovered in outgrowth media. On day 7 post transfection, 6-well plates were coated with 10
1450 µg/mL poly-D-lysine for 1 hour at 37 °C then washed 3X in 1X PBS. 200,000 cells were plated
1451 into a 6 well dish for each knockout condition and respective controls. The following day, 500ng
1452 of pEGFP-N3 or pEGFP-TDP-43 was transfected for each respective condition and media was
1453 changed after 4 hours. Cells were incubated for 48 hours (10 days post Cas9/sgRNA
1454 transfection). Cells were then stressed for 1 hour using 250 µM sodium arsenite and GFP-Trap
1455 SUMOylation Assay and Western Blot analysis was performed as previously described. Samples
1456 were quantified using densitometry normalizing each condition to the stressed positive control
1457 condition on each respective gel.

AlphaFold3 TDP-43 structure prediction

TDP-43 structure was predicted using the AlphaFold3 server (https://alphafoldserver.com/) using FASTA sequence of Human TDP-43 (Uniprot TADBP_HUMAN, Q13148) with relevant mutations. UG x6 (5'-UGUGUGUGUGUG-3') RNA sequence was included for structure predictions.[121]

Conservation analysis of TDP-43 K408

Representative FASTA amino acid sequences of TDP-43 paralogs were aligned for phylogenetic analysis using MUSCLE multiple alignment and PhyML maximum likeliness for phylogenetic tree generation[122]. Pairwise alignment of the C-terminal domain was performed using Geneious Prime 2022.1.1 (https://geneious.com) performing a MUSCLE multiple alignment of 300 FASTA amino acid sequences of TDP-43 paralogs between Humans and Actinopterygii representing the emergence of [human] K408 curated from the OrthoDB database (table S1).

TDP-43^{K408R} **mouse line generation**

At The Centre of Phenogenomics (SickKids, Toronto, ON, Canada), the *TDP-43^{K408R}* mice were generated on a C57BL6/N background based on previous methods[123] using CRISPR/Cas9-mediated gene editing of the endogenous *Tardbp* locus. In brief, spCas9 loaded with an sgRNA to target exon 6 of *Tardbp (MGI:2387629; 5'-TGGGGGCTTTGGCTCGAGCA-3')* was electroporated into embryos alongside a single stranded oligonucleotide (ssODN) repair template (5'-C*TAAATCTACCTAACCTAATAACCAACCTACTAACCACCCCCCACCACCTACATTCCCCAG CCAGAAGAC**c**TAGAATCCATG**ga**CGAGCCAAAGCCCCCATTAAAACCACTGCCCGATCCTG CATTTGATGCTGACCCCCAACCAAGGGGGGC-3'*). Embryos were screened via allelic discrimination (see "TDP-43^{K408R} genotyping" below) to identify founders. Four founders were crossed to C57BL6/N mice to ensure germline transmission of knock-in allele.

Mouse husbandry

All mouse procedures were carried out in accordance with the Canadian Council on Animal Care and approved by the University of Ottawa Animal Care Committee. All mice were group housed (3-5 per mice cage) with access to food and water *ad libitum* on a standard 12-hour light dark cycle. Exceptions included adult male mice who were separated and single housed if persistent fighting and fight wounds were observed in the cage. All experimental mice were given crinkle paper in addition to the standard nestlet and hut enrichment material. Husbandry was completed by University of Ottawa Animal Care and Veterinary Services except for cohorts actively undergoing behavior testing for which husbandry was completed by the experimenter.

Mouse wellness monitoring

Mice were monitored weekly starting at age P21 and included assessment of hindlimb clasping, kyphosis, weight, and general health. The hindlimb function was assessed following previous methods [124]. Briefly, the mouse was suspended in the air for approximately 5-10 seconds by the base of the tail. Features of the limbs were assessed to give a score from 0-4. Kyphosis was assessed by allowing the mice to briefly walk on the flat table top in the housing room and visually observing the straightness of the spine. A score of 0-3 was given based on previously described methods[125]. Weight was measured every other week by placing individual mice on a digital weigh scale. Notably, mice exhibiting barbered patches were monitored and recorded.

1500 ***Sex and age of experimental mice***

1501 Experiments were performed using both male and female mice sufficiently powered to detect sex
1502 differences. In some instances where no sex differences were observed, male and female mice
1503 were grouped together to assess genotypic differences independent of sex. Experiments
1504 involving primary cortical neurons cultures dissected from individual embryos were used
1505 involving a mixture of male and female embryos. Experimental animals underwent behavioral
1506 testing as early as P21 and as late as 16 months of age. See Table S2 for number of animals used
1507 (distinguished by sex and genotype), raw behavior data, and specific statistical analyses for each
1508 behavior experiment.

1509 ***TDP-43^{K408R} genotyping***

1510 Tail samples were collected prior to weaning and again postmortem for genomic DNA (gDNA)
1511 isolation and genotyping. Tails were solubilized in 300 µL solubilization buffer (10X SET, 100
1512 mM NaCl, 100 µg/mL Proteinase K (Bio Basic PB0451-250)) at 55 °C overnight. Cell debris
1513 was precipitated by adding 150 µL of "Tail Salts Buffer" (4.31M NaCl, 0.63M HCl, 10 mM
1514 Tris-HCl, pH7.4) then samples were centrifuged at ~21,000*g* for 15 minutes at 4 °C. Supernatant
1515 containing gDNA was transferred into 600 µL of chilled 100% ethanol to precipitate nucleic
1516 acids which were then pelleted by centrifugation for 10 minutes at ~21,000*g* at 4 °C. The
1517 supernatant was carefully removed, and the pellet was washed in 600 µL of chilled 70% ethanol
1518 then centrifuged at ~21,000*g* at 4 °C for 5 minutes. The supernatant was carefully removed, and
1519 residual supernatant was left to evaporate for 5 minutes. The gDNA pellet was resuspended in
1520 double distilled H2O at 55 °C for 10 minutes. Genotyping reaction was prepared in a 10 µL
1521 reaction containing ~5ng of gDNA, 250nM *K408R Genotyping Forward* primer (5'-
1522 *CCACCATTCTAAATCTACCTAACCTAATA-3'*), 250nM *K408R Genotyping Reverse* primer (5'-
1523 *GGATCGGGCAGTGGTTTTA-3'*), 125nM wild type Locked Nucleic Acid (LNA) probe (*HEX-*
1524 *TCT+A+A+GT+CT+TCT+GGC-IowaBlack FQ),* 125nM K408R LNA probe (*FAM-*
1525 *TCT+A+G+GT+CT+T+CT-IowaBlack FQ),* and 2X PerfeCTa qPCR Tough Mix (QuantaBio).
1526 Reactions were run on a BioRad CFX96 qPCR thermocycler with the following cycling
1527 parameters: Initial annealing at 95 °C for 2 minutes, followed by 40 cycles of 95 °C for 15
1528 seconds then 60 °C for 60 seconds. Results were analyzed via allelic discrimination in the
1529 BioRad Maestro software. See Fig. S2b.

1530 ***Primary cortical neuron cultures***

1531 Pregnant mice were euthanized between gestation E13.5–15.5 with 120 mg/kg Pentobarbital
1532 Sodium (Bimeda-MTC, 8015E) delivered via intraperitoneal injection. The embryos were
1533 removed and placed into ice cold 1X PBS. For each embryo, the cortices were carefully isolated
1534 and meninges removed and then placed in ice cold HBSS (Sigma Aldrich). Cortices were
1535 dissociated for 20 minutes with trypsin (Thermo Scientific) at room temperature on a rotator
1536 before trypsin inhibitor with DNase solution was added to quench the reaction. Cells were
1537 pelleted at 2,500 x *g* for 5 minutes at 4°C. The supernatant was carefully removed and the pellet
1538 was washed with trypsin inhibitor plus DNase solution. Cortical neurons were pelleted at 2,500
1539 x *g* for 5 minutes at 4°C. The supernatant was carefully removed and the neurons were
1540 resuspended in 1 mL of ice cold outgrowth media (Neurobasal media (Thermo Scientific),
1541 supplemented with 1X B-27 (Thermo Scientific), 1X N-2 (Thermo Scientific), 500 µM L-
1542 Glutamine (Wisent Bioproducts), and 0.5% penicillin/streptomycin (GE Healthcare Life
1543 Sciences)). Culture dishes and coverslips were prepared in advanced coated with 50 µg/mL Poly-

1544 D-Lysine overnight at 37 °C specific to each experiment detailed below. Cultures were
1545 maintained for 7-9 days *in vitro* prior (DIV) to experimentation.

1546 ***Murine primary neuron culture maintenance***

1547 Primary cortical neurons were dissected and maintained in Neurobasal media (Thermo
1548 Scientific), supplemented with 1X B-27 (Thermo Scientific), 1X N-2 (Thermo Scientific),
1549 500 µM L-Glutamine (Wisent Bioproducts), and 0.5% penicillin/streptomycin (GE Healthcare
1550 Life Sciences) at 37 °C with 5% CO_2. Each neuron culture was harvested from a single embryo
1551 representing one biological replicate. The sex of the embryos/cultures were not determined thus
1552 experiments contain a mix of both male and female replicates.

1553 ***Endogenous SUMOylation assay from ex vivo embryonic mouse brains***

1554 Mouse embryos were harvested following *Cortical Primary Neuron Culture* methods described
1555 above. Brains were dissected from embryos and stored in ice cold HBSS (Sigma Aldrich). Brains
1556 were cut using a razor blade down the midline evenly to separate hemibrains and each hemibrain
1557 was transferred into a 1.5 mL microcentrifuge tube containing neurobasal complete media used in
1558 cortical *Primary Cortical Neuron Culture Maintenance* described above. One hemibrain was
1559 subjected to 42 °C heat shock for 1 hour while the complementary hemibrain was maintained at
1560 37 °C for 1 hour as a control. Samples were briefly centrifuged at 2000g for 2 minutes to pellet
1561 hemibrain, then supernatant was carefully removed. The hemibrain pellets were immediately lysed
1562 in 100 µL of 1% SDS buffer (1% SDS in IP Lysis Buffer supplemented with 1X protease inhibitor,
1563 1X phosphatase inhibitor, 100mM N-Ethylmalamide), and homogenized with a pestle then boiled
1564 at 95 °C for 10 minutes. After boiling, 900 µL of ice-cold IP Lysis buffer was then added to the
1565 sample then samples were vortexed aggressively for 10 seconds and passed through a 18G insulin
1566 needle. Lysates were left on ice for 20 minutes with vortexing every 5 minutes for 10 second to
1567 ensure complete lysis. Next, the lysates were centrifuged at ~21000G for 20 minutes at 4 °C.
1568 Following the centrifugation, 1-3% of the supernatant was transferred into a microcentrifuge tube
1569 to be used as the *Input* sample. The remainder of the supernatants were equally divided (~450 uL
1570 each) into two separate 1.5 mL microcentrifuge tubes containing 10 µg of normal mouse IgG
1571 (Alpha Diagonstic 20008-250) or 10 ug of anti-SUMO2/3 clone [8A2] (Abcam ab8137) per
1572 sample. Samples were incubated overnight rotating at 4 °C. The next day, 50 µL of Protein G
1573 Dynabeads (Thermo Fisher Scientific) per sample were washed 3X in ice cold IP Lysis Buffer.
1574 The beads were resuspended in 50 µL IP Lysis Buffer per sample which was then added to each
1575 of the samples incubated with antibody. The samples were left to rotate at 4 °C for 45 minutes.
1576 The solution was added to a magnetic rack kept at 4 °C and the supernatant was collected for
1577 *flowthrough* to test immunodepletion or aspirated. The beads were washed 5X in ice cold IP Lysis
1578 buffer. Samples were eluted using 30uL (at 1mg/mL) of synthetic SUMO2/3 peptide (Amino Acid
1579 Sequence: *IRFRFDGQPI,* synthesized through Genscript) per sample and incubating at 37 °C for
1580 15 minutes at 900rpm on a thermomixer. The input/flowthrough and immunoprecipitation samples
1581 were prepared with 4X Laemmli buffer containing 10% Beta-Mercaptoethanol and then boiled at
1582 85 °C for 10 minutes. Samples were then analyzed by Western Blot using light chain specific
1583 secondary antibodies. Quantification of SUMOylation assays was performed through densitometry
1584 analysis using ImageLab (BioRad) to quantify the volume of the ~62kDa anti-TDP-43 bands from
1585 the immunoprecipitation standardized to the loading control of the input. For quantification of
1586 changes in TDP-43 SUMOylation response, conditions were normalized to the 1 hour sodium
1587 arsenite treatment.

1588 ***Immunofluorescence in primary cortical neurons***

1589 Micro Coverglass #1.5 coverslips (Electron Microscopy Sciences) coverslips were washed in 2M
1590 HCl overnight at 55 °C, washed 5 times in sterile H_2O, then pre-coated with poly-D-lysine
1591 (50 µg/mL) overnight at 37 °C, then washed with distilled water three times and air-dried at
1592 room temperature for at least 2 hours. Primary mouse cortical neurons were seeded at 75,000-
1593 100,000 cells per coverslip and cultured as described above. On day 7, neurons were fixed for 10
1594 minutes using 10% phosphate buffered formalin for (Fisher Chemical, SF100-4) followed by 3 x
1595 5-minutes washes in 1 mL of 1X PBS. Neurons were blocked in 500 µL of blocking buffer (1%
1596 Triton X-100, 10% cosmic calf serum in 1X PBS) for 1 hour, then incubated in 300 µL of
1597 primary antibody diluted in blocking buffer overnight at 4 °C. The following day, the neurons
1598 were washed for 5 x 5-minutes in 1 mL of 1X PBS then incubated in 300 µL of secondary
1599 antibody diluted in blocking buffer for 2 hours at room temperature. Neurons were then washed
1600 in 1 mL 1X PBS, then stained with DAPI for 10 minutes at room temperature followed by 4 x 5-
1601 minutes washes in 1X PBS before being mounted using antifade fluorescence mounting media
1602 (Dako, S3023). Z-stack images were obtained on a Zeiss AxioObserverZ1 LSM800 Confocal
1603 Microscope at 40× magnification with a 2× digital zoom through a Z distance of 10-12 µm per
1604 image using optimal spacing per slice with dimensions set to 1024 x 1024 pixels with 4X
1605 averaging per frame. At least 50 cells were imaged and quantified per replicate. For TDP-43 foci
1606 colocalization, Z-stack images were obtained on a Zeiss AxioObserver Z1 LSM880 AiryScan2
1607 confocal microscope at 63x magnification with 3X digital zoom at 512 x 512 resolution. At least
1608 10 cells presenting with TDP-43 foci were imaged per replicate. Images were analyzed and
1609 quantified using ImageJ.

1610 ***TDP-43 colocalization with HSPA1L***

1611 HSPA1L colocalization experiment was designed similar to previous approaches that identified
1612 TDP-43 forming anisosomes in response to stress[96]. HSPA1L-mRuby2 was designed and
1613 synthesized in a pTwist-Lenti-Puro backbone (Twist Bioscience). Next the pTwist-Lenti-
1614 HSPA1L-mRuby2 plasmid was packaged into lentivirus by co-transfection of psPAX2 (Gift
1615 from Didier Trono, Addgene #12259), and pMD2-G (Gift from Didier Trono, Addgene #12260)
1616 at equimolar concentrations into HEK293T cells. After 24 hours, media was changed and
1617 discarded. Media was collected 48 hour and 72 hours post transfection. Viral media was filtered
1618 through a 0.45 µm filter then concentrated by centrifugation at 100,000g for 2 hours at 4 °C and
1619 the pellet was resuspended in 1X PBS. Cortical primary neurons were cultured as previously
1620 described and lentiviral infection was performed at the time of plating (0 DIV). Cells were
1621 cultured to 7 DIV then were stressed with 250 µM sodium arsenite for 1 hour and recovered for 3
1622 hours to induce TDP-43 foci formation. Cells were fixed in 10% formalin for 10 minutes and
1623 immunoflurescent staining was performed for TDP-43 as described above. Z-stack images were
1624 obtained on a Zeiss AxioObserver Z1 LSM880 AiryScan2 confocal microscope at 63x
1625 magnification with 3X digital zoom at 512 x 512 resolution. At least 10 cells presenting with
1626 TDP-43 foci and HSPA1L foci were imaged per replicate. Images were analyzed and quantified
1627 using ImageJ.

1628 ***Proximity ligation assay in primary cortical neurons***

1629 Primary mouse cortical neurons were cultured and fixed as described in *primary cortical neuron*
1630 *cultures* and *immunofluorescence in primary cortical neurons*. Fixed coverslips were transferred
1631 into 12-well plates and outlined with a hydrophobic pen and blocked using 40 µL of Duolink

1632 blocking buffer (Sigma Aldrich, DUO82007) at 37 °C for 1 hour. Coverslips were then washed
1633 for 3 × 5 minutes in 1 mL 1X PBS. Next, coverslips were incubated in 300 µL of primary
1634 antibody (anti-TDP-43 1:750, PTGLabs; anti-SUMO2/3 [8A2] 1:500 Sigma) diluted in blocking
1635 buffer (1.5% Triton X-100, 10% cosmic calf serum in 1X PBS) overnight at 4 °C. The next day,
1636 the coverslips were washed for 3 × 5 minutes in 1 mL of Duolink Wash Buffer A (0.01 M Tris-
1637 Base, 0.15 M NaCl, 0.05% Tween-20, pH 7.4) followed by incubation at 37°C for 1 hour in
1638 40 µL of dilute probe mixture containing a 1:5 dilution of Duolink PLA MINUS (Sigma Aldrich,
1639 DUO82004) and PLUS probes (Sigma Aldrich, DUO82002) in antibody diluent (Sigma Aldrich,
1640 DUO82008). Duolink PLA probes were diluted in antibody diluent (Sigma Aldrich, DUO82008)
1641 at a 1:5 dilution. Coverslips were washed for 3 × 5 minutes in Duolink Wash Buffer A and then
1642 incubated in 40 µL of ligase (Sigma Aldrich, DUO82027) diluted in 1X ligation buffer (Sigma
1643 Aldrich, DUO82009) at a 1:40 dilution at 37 °C for 30 minutes. The coverslips were then
1644 washed for 3 x 5-minutes washes in Duolink Wash Buffer A and then incubated in 40 µL of
1645 polymerase (Sigma Aldrich, DUO82028) diluted 1:80 in 1X amplification buffer (Sigma
1646 Aldrich, DUO82011) at 37°C for 90 minutes. Next, the coverslips were washed 2 × 10 minutes
1647 in Duolink Wash Buffer B (0.2 M Tris-Base, 0.1 M NaCl, pH 7.5) and then again in 1 mL of
1648 Duolink Wash Buffer B diluted at 1:100 in 1X PBS for 1 minute. Coverslips were briefly air
1649 dried and then mounted on slides using Vectashield Antifade Mounting Medium with DAPI. Z-
1650 stack images were obtained on a Zeiss AxioObserverZ1 LSM800 Confocal Microscope at 63×
1651 magnification with a 5× digital zoom through a Z distance of 10-12 µm per image using optimal
1652 0.27 µm spacing per slice with dimensions set to 512 × 512 pixels with 2X averaging per frame.
1653 ~5 images were randomly obtained around the coverslip sampling >15 cells per condition per
1654 replicate. Images were analyzed and quantified using the Spots function on the Imaris (ver. 9.9.1
1655 Bitplane, Switzerland) software.

1656 ***Behavior testing general information***

1657 All adult behavior testing was performed in the University of Ottawa Behaviour and Physiology
1658 Core. During behavior testing periods the mice were minimally disturbed: food and water were
1659 only added/changed as needed and cages were changed by the experimenter with a transfer of
1660 old bedding material. Apart from nesting and Beam Break testing, all behavior tests were
1661 performed in the light phase of the cycle. The experimenter was blinded to the genotype of the
1662 mice during behavior testing and until the mice were end pointed. Mice were brought to the
1663 testing room to habituate in dim white light at least 30 minutes prior to commencing testing with
1664 the exceptions of nest building and fear conditioning for which there was no habituation period.
1665 The behavior cohort consisted of males and females with 12-15 animals per sex per genotype.
1666 These mice had been backcrossed three times to C57BL/6N background. All mice used for
1667 histology, biochemistry, and RNA analyses performed the fear conditioning test 1 week prior to
1668 dissections to control for potential molecular changes induced by this behavior test.

1669 ***Developmental testing***

1670 A small battery of behavior tests was completed at P8 and P21. At P8, these tested included (I)
1671 weight, (II) righting reflex, (III) hindlimb suspension, and (IV) forelimb suspension. (I) Weight
1672 was measured every other week by placing individual mice on a digital weigh scale. (II) Mice
1673 were placed on their back on a tabletop and timed for how long it took them to right themselves
1674 onto their paws. (III) Mice were placed facing downward in a 50mL Falcon tube (VWR 21008-
1675 940) and timed for their latency to fall. (IV) Mice were placed to grasp a wire suspended by a
1676 pencil holder and timed for latency to fall. At P21, hanging wire was performed in which the

mouse was allowed to grasp a wire 30 cm off the ground and time for its latency to fall. Each mouse completed three trials with a maximum time of 60 seconds.

Beam break

The Beam Break test was used to assess general locomotor activity and habituation to a novel cage environment. The apparatuses used to record and analyze the mice activity included the Micromax analyzer/Fusion Software (Omnitech Electronics; Columbus, OH, USA) at the 2-month time point and the Photobeam Activity System (San Diego Instruments; San Diego, CA, USA) at the 9 and 16-month timepoints. Clean cages with only a thin layer of corncob bedding, food, and water were loaded into the recording frame. Mice were singly housed in one of these cages 2 hours prior to the start of their dark cycle. For a 24-hour period at the standard 12-hour dark/light cycle, the activity of the mice was monitored by infrared beam emitters and receptors. When the test was completed, the sum of the infrared beam breaks in 5-minute, 1-hour, and 24-hour sampling bins was analyzed.

Digigait

The Digigait treadmill Imager and Analysis Software (Mouse Specifics Inc.) were used to record and analyze parameters of gait, respectively. Mice were placed on the unmoving treadmill surface and once recording was started the speed was increased to 18 cm/s with 0 degree incline. A 3 second video of each mouse walking continuously, with no stopping or starting, was captured. A mouse was excluded from the test if it was unable to walk for 3 seconds at the 18 cm/s speed. Digiait data was analyzed using FactoMinR [126] and visualized using FactoExtra [127] packages in R (version 4.2.3).

Fear conditioning

Contextual and cued fear conditioning were tested using a 3-day protocol to assess associative fear learning and memory. Naïve age and sex matched mice were initially used to determine the optimal shock value. On day 1 (training), the mice were placed into a Phenotyper box (Noldus Information Technology) with a grid shock floor (Med Associates). The testing room was set to 60 lux light level and 70 dB of white noise (context A). The mice were left in the apparatus for 6 minutes during which they receive 3 tone-shock pairings (30 seconds tone co-terminated with a 2 second foot shock). On day 2 (Context), the mice were placed in the same apparatus (Context A) with no tone or foot shock delivered for the 6-minute trial. On day 3 (cue), the animals were placed in the test apparatus with an altered context (context B) including red light, no white noise, vanilla scent, textured mat covering the shock floor and plastic inserts in the apparatus. The mice are allowed to explore this context with no tone for 3 minutes, and then are presented with the same tone from Day 1 for the last 3 minutes. The time freezing was analyzed with EthoVision software for all 3 testing days.

Grip strength

A grip strength meter (Chatillon DFE II, Columbus Instruments) was used to assess the maximal forelimb grip strength of the mice. The grip strength meter was rotated vertically and temporarily mounted on a flat surface prior to testing. The mouse was brought near the triangular attachment and allowed to grasp the lower bar with its forepaws. The mouse was pulled directly downward, by the tail, in one smooth motion. Each mouse was tested, and the grip strength recorded for 5 consecutive trials with a 1-minute intertrial interval. If a trial was deemed unsuccessful by the blinded experimenter, the trial was redone. Causes of an unsuccessful trial included the mouse

prematurely losing its grip on the bar or grasping the bar with its hindfoot. The average grip strength for the 5 successful trials was analyzed.

Hanging wire

The hanging wire test was used to assess muscle strength and coordination. A metal wire was secured to the top of a tall plastic box with padding on the bottom. The mouse was brought near and allowed to grasp the wire with its forepaws. A timer was started once the experimenter released the mouse to allow it to hang freely. When the mouse fell from the wire the time was recorded. Mice had three trials and were allowed to hang for a maximum of 600 seconds with a 60 second intertrial interval in between. If a mouse hung for 600 seconds, it did not complete any additional trials. The maximum hanging time from the trials was used for analysis.

Light/dark box

The light dark paradigm was used to assess anxiety-like or disinhibited, exploratory behavior. The testing apparatus (Med Associates) has two equal sized rectangular compartments the mouse can move freely between. The one is fully illuminated whereas the other is covered by a black plastic insert. The position of the mouse in the apparatus testing field is recorded using infrared beams. To start the test, the mice are placed into the lit side and allowed to explore for 10 minutes. The time spent in each compartment and number of entries into each compartment was recorded and analyzed by Activity Monitor software (Med Associates).

Marble burying

The marble burying assay can assess the motor function required to bury objects as well as cognitive changes related to apathy or perseverance. Cages were filled with 10cm of fresh corncob bedding and one mouse was placed to habituate for 5 minutes. After habituation, 20 glass marbles were laid out evenly in a 4 by 5 pattern. The mouse was returned to the cage and left alone for 30 minutes in 60 lux light. With the completion of the trial, the number of marbles buried by at least two thirds was scored by a blinded experimenter.

Nest building

Nest building is an innate behavior of mice in their daily lives. This complex behavior requires both executive planning and sensorimotor coordination. Directly following Beam Break testing, a single square nestlet (5 cm^2 cotton pad) was placed in each Beam Break cage for 16 – 18 hours, of which 12 of these hours was during the dark cycle. At the end of the test, images were taken of the nests and scored blindly for quality as previously described on a scale from 1-5.

Open field

The open field test was used to assess anxiety and locomotor activity in a novel environment. The apparatus consists of white plastic square arenas measuring 45cm on each side. The mice were placed in a corner of the arena and allowed to freely explore for 10 minutes with light levels at 300 lux. The distance travelled, time spent in the corners and center of the field was recorded and analyzed by EthoVision software (Noldus Information Technology).

Rotarod

The rotarod (IITC Life Science, Ugo Basile) was used to test the motor performance of mice including coordination and resistance to fatigue. Mice were placed in the stationary rotarod bar for 10 seconds before the rotarod program was initiated. The bar accelerated from 4 rpm to 40

1761 rpm for 5 minutes and the latency to fall for each mouse was recorded. The time was stopped
1762 when the mouse fell from the bar or rotated passively. Mice were completed four trials per day,
1763 with a 10-minute intertrial interval in their home cage, for 3 consecutive days.

1764 ***Spontaneous Y-maze***

1765 The spontaneous Y-Maze test was used to assess spatial working memory. The Y-shaped maze
1766 has three identical arms at 120°C around a center point triangle. The mice were placed in the
1767 center point and allowed to freely explore the arms for 8 minutes. The movement of the mouse
1768 was tracked including the sequence of arm entries by EthoVision (Noldus Information
1769 Technology). An alternation is defined as the mouse making consecutive, sequential entries into
1770 each of the three arms without revisiting an arm. The alternation index was calculated as
1771 (number of alternations/(total number of arm entries minus two)) and reported as a percent.

1772 ***Tail suspension***

1773 The automated Tail Suspension apparatus (Med Associates) was used to assess apathetic-like
1774 behaviors of the mice. Mice were taped and suspended by the tail to a vertical steel bar which
1775 measures strain gauge as the mouse moves during a 6-minute trial. The cumulative time spent
1776 immobile, hanging passively (below lower threshold) was measured by the Tail Suspension
1777 software.

1778 ***Three chamber sociability***

1779 The Three Chamber test was conducted to measure the sociability of mice when allowed to
1780 interact with a novel mouse or a similarly sized inanimate object. The testing apparatus is a 19 x
1781 45 cm plastic box divided into three equal chambers with clear plastic wall dividers. The two
1782 external chambers each have a single weighted metallic mesh pencil holder and the central
1783 chamber is empty. The mice are habituated to the apparatus for 5 minutes by being placed in the
1784 central chamber and allowed to freely explore and enter all chambers. The mouse has a 5-minute
1785 intertrial interval in its home cage. In the test trial, a sex and age matched wild type mouse
1786 (social target) is placed beneath one mesh pencil holder, and an inanimate plastic toy (non-social
1787 target) is placed beneath the other. To commence the test trial, the mouse is paced in the central
1788 chamber. The time spent in each chamber and interacting with the social or non-social target is
1789 recorded and analyzed by EthoVision software (Noldus Information Technology).

1790 ***Tube test of social dominance***

1791 Tube test was used to assess social dominance and within cage social hierarchy. Cage mates
1792 were paired against each other for testing in a round-robin design. The tube test was conducted
1793 on a flat tabletop, which the mice were allowed to run around on for 5 minutes prior to
1794 commencing the testing. One foot of vinyl tubing was used. Mice were habituated to the tube
1795 prior to testing on the same day by encouraging them to run through the empty tube from either
1796 side 5 times. A blinded experimenter placed a mouse on either end of the tube, and released their
1797 tales when they completely entered the tube. The first mouse to step its hind paws out of the tube
1798 lost the battle. The battle was redone if after 2 minutes no mouse had won.

1799 ***Collection and preparation of mouse tissue***

1800 Mice were harvested for both histology and biochemistry/molecular analyses to reduce total
1801 animal numbers. Mice were first acclimated for 2 hours prior to dissection to help control for
1802 activity-induced changes and all dissections were performed at zeitgeber hours ZT6 to ZT11 to

1803 control for potential circadian affects. Mice were randomly dissected by cage to limit batch
1804 effects and additional stress. Mice were anesthetized using isoflurane inhalation, blood was
1805 collected, and then mice were sacrificed via decapitation and the brains were quickly isolated,
1806 weighted, then cut into 2 hemispheres where the left hemisphere was drop fixed in 10% buffered
1807 formalin and the right hemisphere was dissected by region and flash frozen on dry ice. Spinal
1808 cords were removed using hydraulic extrusion and the lumbar spinal cord was isolated. The
1809 lumbar enlargement was isolated for histology whereas the remaining lumbar spinal cord was
1810 used for molecular analysis. Tibialis anterior and soleus muscles were isolated and drop fixed in
1811 10% buffered formalin for imaging studies and gastrocnemius muscle was flash frozen.

1812 ***Preparation of mouse tissue for analysis by histology***

1813 Tissue was collected as described in *Collection and preparation of mouse tissue*. Following
1814 fixation for 48 hours, samples were transferred to a 70% ethanol solution and sent to the Louise
1815 Pelletier Histology Core facility at the University of Ottawa for paraffin embedding and
1816 microtome sectioning. The samples were sectioned at a thickness of 5 µm. Serial sectioning was
1817 performed at four levels within the tissue each separated by 40 µm. For staining, slide-mounted
1818 sections were deparaffinized in 100% xylenes (Fisher Scientific X3P-1GAL) for 10 minutes,
1819 then transferred into a second container of fresh 100% xylenes for an additional 10 minutes. The
1820 slides were then rehydrated in descending ethanol solutions: two 5 minutes treatments in 100%
1821 ethanol, 5 minutes in 70% ethanol, and 5 minutes in 50% ethanol. The slides were then
1822 immersed in 1X PBS for at least 5 minutes to rinse residual ethanol.

1823 ***Cresyl violet staining***

1824 *Slides containing PPFE mounted sections were slowly dipped 20 times in 70% ethanol followed*
1825 *by 95% ethanol, 100% ethanol, 95% ethanol, and 70% ethanol. Slides were then submerged in*
1826 *ddH2O for 1 minute. Next the sections were incubated in 0.25% Cresyl Violet stain for 2*
1827 *minutes. Samples were then dipped 10 times in ddH2O followed by 70% ethanol, 95% ethanol,*
1828 *0.25% glacial acetic acid, 95% ethanol, and finally 100% ethanol. Permount was applied to*
1829 *sections and mounted with coverslips.*

1830 ***Immunofluorescence analysis in mouse tissue***

1831 Antigen was performed by placing slides in 1X sodium citrate buffer (2.94g sodium citrate
1832 0.5mL Tween-20 in 1L 1X PBS, pH6) at 95°C for 30 minutes then rinsed in 1X PBS. Tissue
1833 sections were then blocked in blocking buffer containing 1% Triton-X and serum (5% horse
1834 serum, 5% cosmic calf serum, or 1% bovine serum albumin) in 1X PBS for 2 hours at room
1835 temperature. Next the tissue sections were incubated with primary antibody (table S5) overnight
1836 at 4°C. The next day, the sections were washed twice in PBS 1X + 0.1% Triton-X for 5 minutes
1837 each and then 3X in 1X PBS for 5 minutes each. The slides were then incubated in secondary
1838 antibody at room temperature for 2 hours. The slides were then washed in 1X PBS + 0.1%
1839 Triton-X for 5 x 5-minutes, before mountin with #1.5 coverslips (Thermo Fisher Scientific 12-
1840 544E) and fluorescent mounting media (Dako S3023). The coverslips were sealed with clear nail
1841 polish and allowed to dry before imaging. Images of each ventral horn were taken on a Zeiss
1842 Axio Imager 2 at 20X magnification. Cells were counted manually per image using Fiji
1843 (ImageJ).

1844 ***Neuromuscular junction analysis***

1845 Tissue was collected as described in *Collection and preparation of mouse tissue*. After 24 hours
1846 of fixation, tibialis anterior muscles were stored in a solution of 1X PBS. Muscle bundles were
1847 carefully teased apart from the tissue into 4-5 bundles with forceps. The muscle bundles were
1848 transferred to 6-well plate cell culture plate containing 1% Triton-X in 1X PBS overnight at 4°C
1849 under gentile agitation for permeabilization. The next day, the muscle bundles were washed three
1850 times in 1X PBS for 5 minutes at room temperature. They were placed in a blocking buffer
1851 solution of 4% bovine serum albumin and 1% Triton-X in 1X PBS at 4°C overnight. The
1852 following day, the muscles were incubated in primary antibody (BTX and NfL/SV2 cocktail, see
1853 table S5) diluted in blocking buffer solution overnight at 4°C. The next day, the muscle bundles
1854 were washed with 1X PBS three times for 5 minutes and incubated with secondary antibody
1855 diluted in blocking buffer solution at room temperature for 2 hours. The muscle bundles were
1856 then washed 3 times in 1X PBS for 5 minutes. The bundles were then placed on slides, mounted
1857 with VECTASHIELD® HardSet™ Antifade Mounting Medium (#H-1400), and #1.5 coverslips
1858 placed above the muscle bundles. The slides were left at room temperature overnight in the dark
1859 to allow the mounting media to cure. Images were taken on a Zeiss LSM800 Confocal
1860 Microscope at 20X through a Z-stack with optimal spacing (0.61 µm). Images were taken
1861 throughout the entirety of the muscle tissue such that at least 80 neuromuscular junctions per
1862 animal were captures. Images were scored manually per image using Fiji (ImageJ). See Fig. S8E
1863 for scoring examples.

1864 ***SUMOylation analysis in human brain tissue***

1865 20 mg of frozen human brain tissue was homogenized in 300 µL of RIPA buffer supplemented
1866 with protease inhibitor, phosphatase inhibitor, and 50mM N-Ethylmalamide and vortexed every
1867 5 minutes for 20 minutes while incubating on ice. The samples were centrifuged at 21000G for
1868 20 minutes at 4°C and the supernatant (RIPA soluble fraction) was carefully removed. 4X
1869 laemmli buffer was added and samples were boiled for 5 minutes at 95 °C then stored overnight
1870 at 4 °C. The remaining pellet after the centrifugation step post-lysis was washed in 1mL RIPA
1871 buffer with vortexing for 10 seconds followed by centrifugation at ~21000G for 20 minutes at 4
1872 °C. The supernatant was carefully removed, and the pellet was resuspended in 300 µL of of 8M
1873 UREA in PBS with 10mM Tris-HCl pH 7.4. Samples were vortexed and left to solubilize
1874 overnight at room temperature before 4X Laemmli was added prior to Western Blot analysis.
1875 RIPA and UREA samples were randomly loaded onto gels (separated by fraction) with 4 control
1876 samples consistently loaded (aged 20-30) on each gel for normalization. Western blot was
1877 performed as described above. Samples were standardized to ponceau signal then normalized to
1878 control samples.

1879 ***Collection and preparation of FFPE human brain tissue***

1880 Frontal cortex tissues were collected antemortem from three sporadic ALS/FTLD patients (a 74-
1881 year-old male, 67-year-old female and 59-year-old female) obtained through the ALS Clinic at
1882 Sunnybrook Health Sciences Centre, Toronto. ALS was diagnosed using the revised El Escorial
1883 Criteria (Brooks et al., 2000) and informed consent was obtained with approval from the local
1884 ethical review board. The presence of TDP-43 proteinopathy within the frontal cortex was
1885 verified through immunohistochemical labeling using rat anti-phosphorylated TDP-43
1886 (p409/410) antibody on formalin fixed paraffin embedded sections. Genetic analyses confirmed
1887 absence of mutations in key ALS/FTD-associated genes: *C9orf72*, *SOD1*, *FUS* and *TARDBP*.

1888 ***Neuropathological assessment of all human PFC tissues from various sites***

Human FFPE PFC samples collected from the NIH Neurobiobank, CHEO, and University of Toronto were independently assessed and scored by a neuropathologist to verify TDP-43 pathology. Immunohistochemistry staining was performed on FFPE tissue sections using the Leica bond system. Sections were pre-treated using sodium citrate buffer (pH 7.0, epitope retrieval solution 1) for 20 minutes and then incubated using a 1:2000 dilution of anti-phosphorylated TDP-43 S409/410 (Cosmo Bio Co. Ltd, #TIP-PTD-P07) for 40 minutes at room temperature and detected using an HRP conjugated compact polymer system. Slides were then stained using DAB as the chromogen, counterstained with Hematoxylin, mounted on slides and covered with coverslips. TDP-43 pathology was assessed by a score of 0-4 looking for neuronal cytoplasmic inclusions and glial cytoplasmic inclusions, particularly within layers II and V/VI. Scoring: 0 = negative, 1 = very rare inclusions, 2 = inclusions readily visible, 3= moderate density of inclusions, 4= highest density of inclusions.

Proximity ligation assay in human FFPE tissue

Formalin fixed paraffin-embedded human brain sections (5 µm sections) were deparaffinized using two 10-minute washes with xylenes, two 5-minute washes with 100% ethanol, one 5-minute wash with 70% ethanol, and one 5-minute was with 50% ethanol. Deparaffinized sections then underwent sodium citrate antigen retrieval (10mM sodium citrate, 0.05% Tween-20, pH 6) for 2 hours at 80°C. Sections were then blocked with Duolink blocking buffer (Sigma Aldrich, DUO82007) for 1 hour at room temperature. Next, sections were incubated with primary antibodies (anti-TDP-43 1:750, PTGLabs; anti-SUMO2/3 [8A2] 1:500 Sigma) diluted in blocking buffer (1.5% Triton X-100, 10% cosmic calf serum in 1X PBS) overnight at 4°C. The following day, the sections were washed in Duolink Wash Buffer A (0.01M Tris-Base, 0.15M NaCl, 0.05% Tween-20, pH 7.4), followed by incubation in Duolink PLA MINUS (Sigma Aldrich, DUO82004) and PLUS probes (Sigma Aldrich, DUO82002) at 37°C for 1 hour. Duolink PLA probes were diluted in antibody diluent (Sigma Aldrich, DUO82008) at a 1:5 dilution. Sections were washed in Duolink Wash Buffer A and then incubated in ligase (Sigma Aldrich, DUO82027) at 37°C for 30 minutes. Ligase was diluted in 1X ligation buffer (Sigma Aldrich, DUO82009) at a 1:40 dilution. Then, the sections were washed in Duolink Wash Buffer A and then incubated in polymerase (Sigma Aldrich, DUO82028) at 37°C for 90 minutes. Polymerase was diluted in 1X amplification buffer (Sigma Aldrich, DUO82011) at a 1:80 solution. The sections were then washed in Duolink Wash Buffer B (0.2M Tris-Base, 0.1M NaCl, pH 7.5) and then again in Duolink Wash Buffer B diluted at 1:1000. Finally, sections were incubated with DAPI at room temperature for 15 minutes. DAPI was diluted at 1:1000 in PBS. Fluorescent mounting media (Dako, S3023) and #1.5 coverslips were then placed over the sections and sealed using clear nail polish. Images were taken on a Zeiss LSM800 Confocal Microscope. 5 images per tissue were randomly collected from grey matter at 63X magnification and 2X digital zoom through a Z stack of 10-12 µm with optimal spacing (0.27 µm) at a resolution of 512 x 512 pixels. PLA foci were manually counted per image using Fiji (ImageJ).

Statistical analyses

Statistical tests were performed using PRISM 10.2.2. Test type was selected based on the number of comparisons made, repeated measures, and gaussian distribution of the data. Levels of statistical significance are indicated in figure legends.

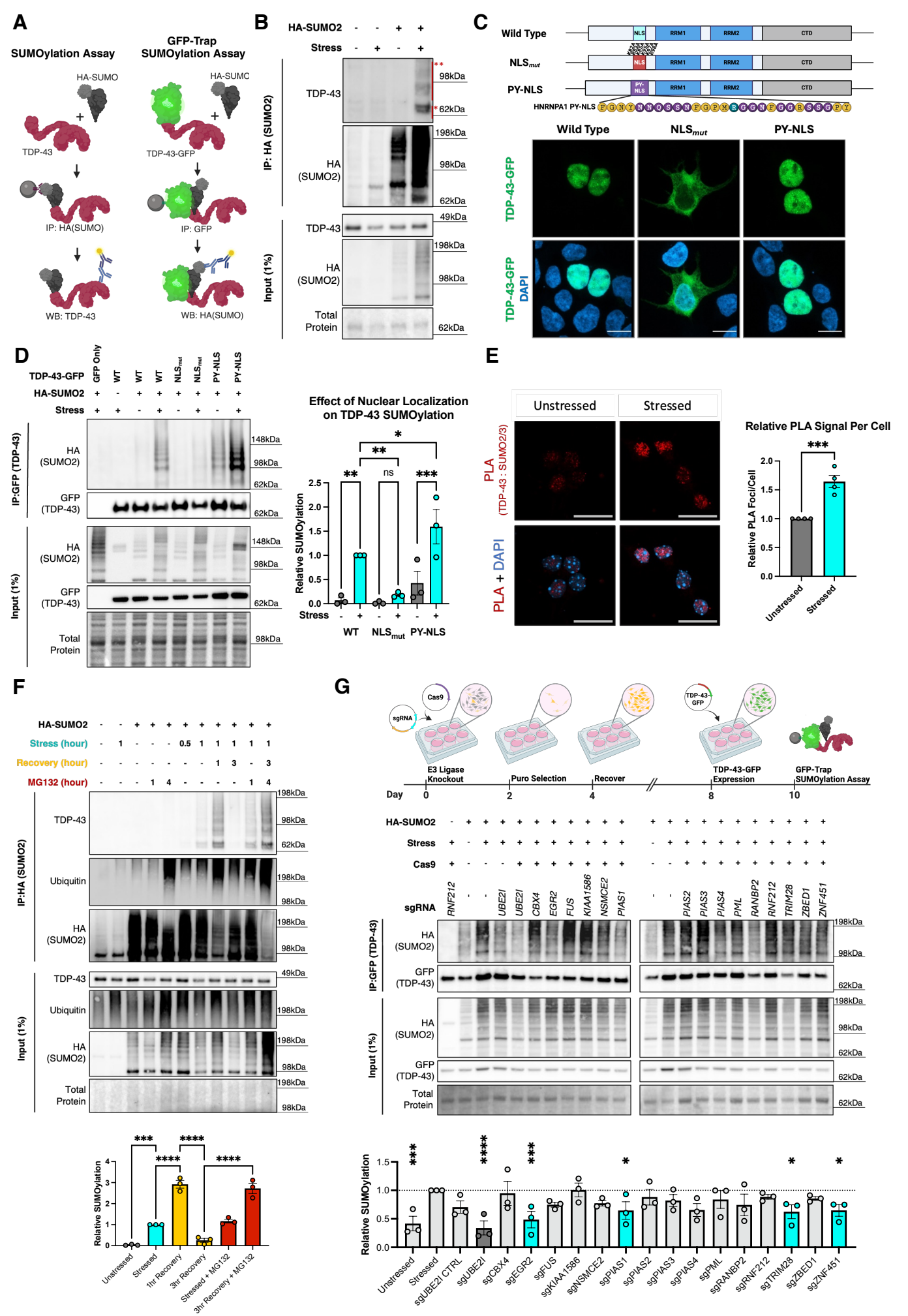

Fig. 1: SUMOylation dynamically regulates nuclear TDP-43 in a stress-responsive manner.

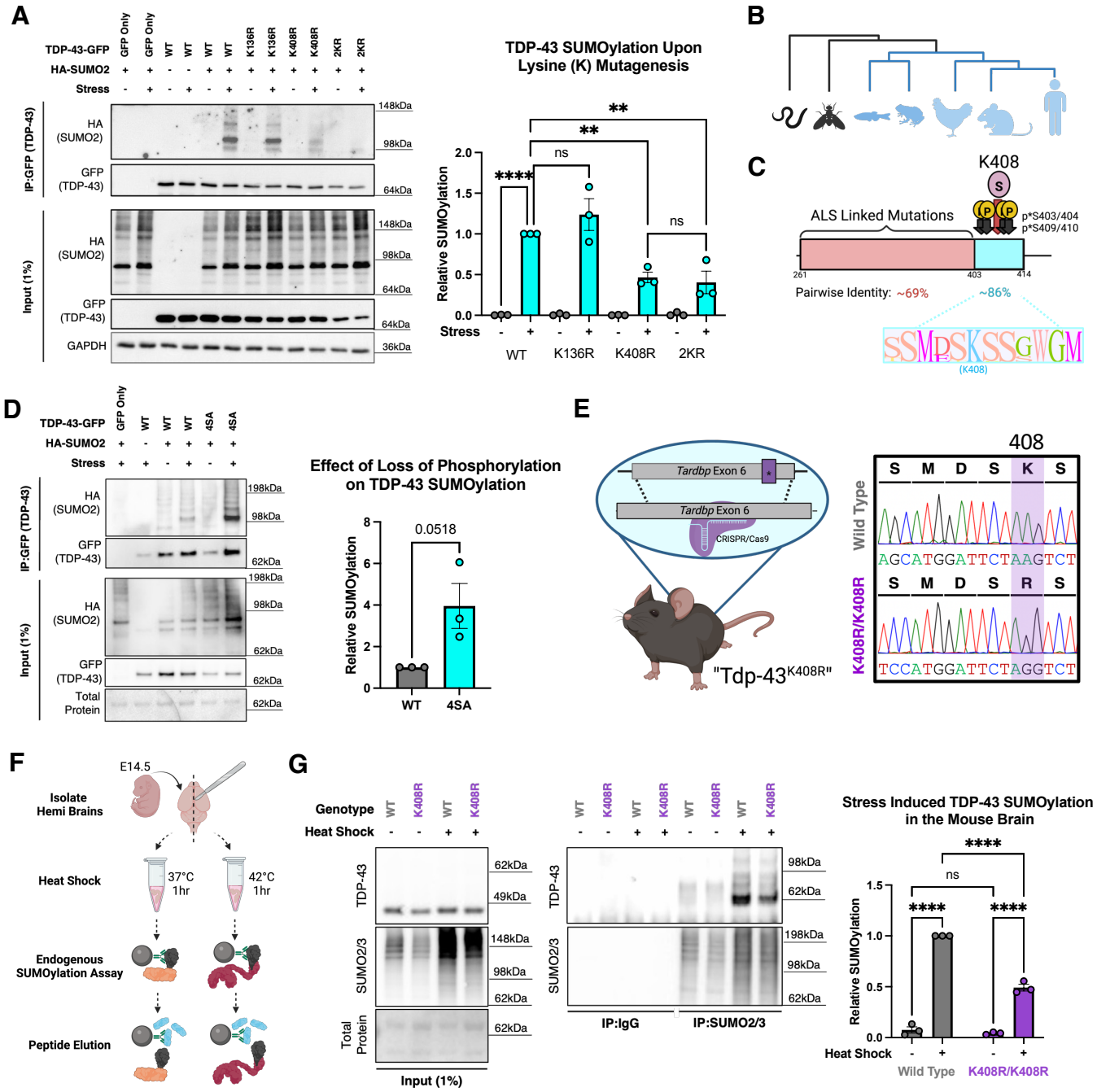

Fig. 2: TDP-43- is SUMOylated at K408 in a conserved region of the C-terminal domain.

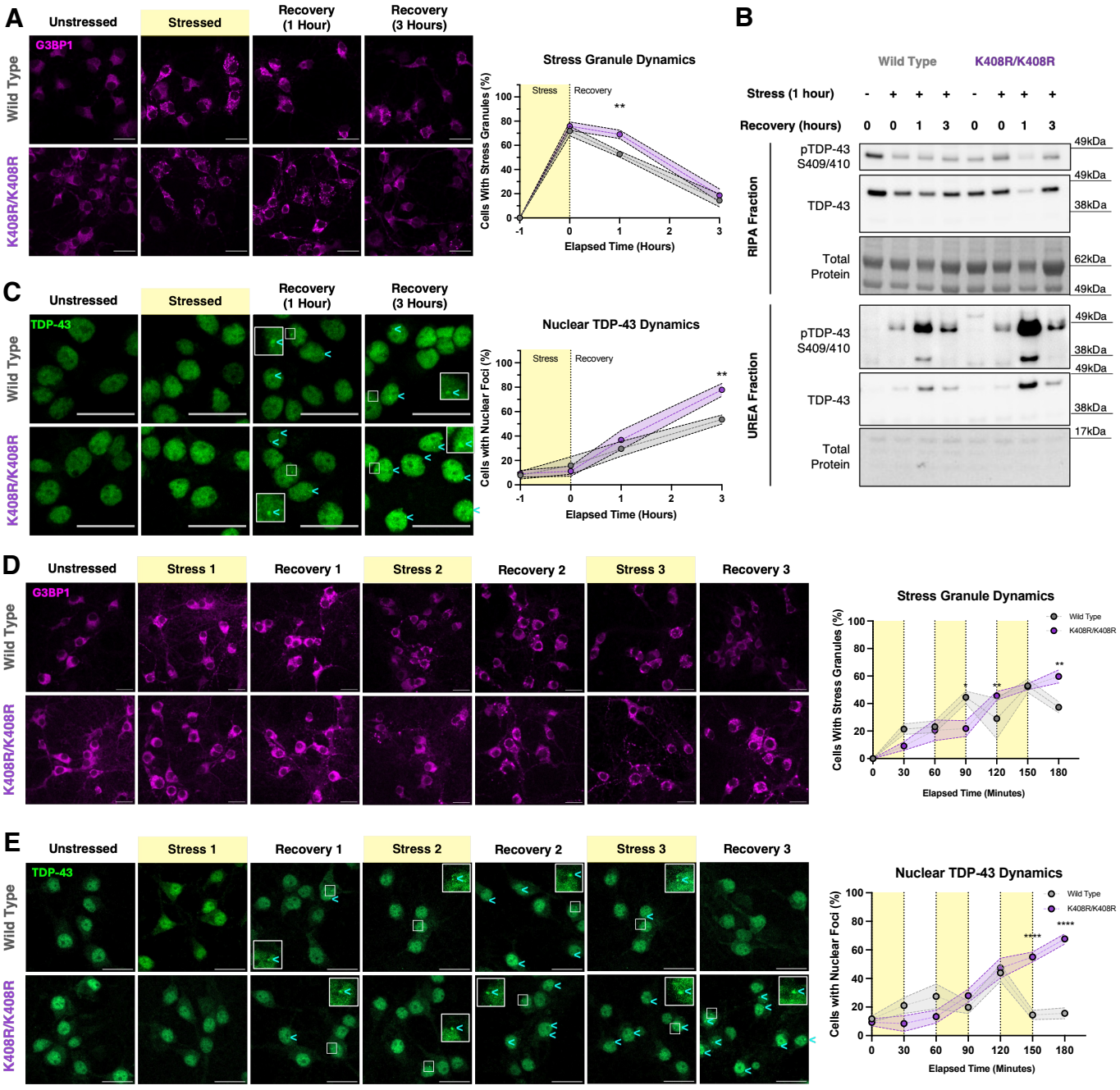

Fig. 3: Blocking TDP-43 SUMOylation at conserved K408 impairs the cellular stress response.

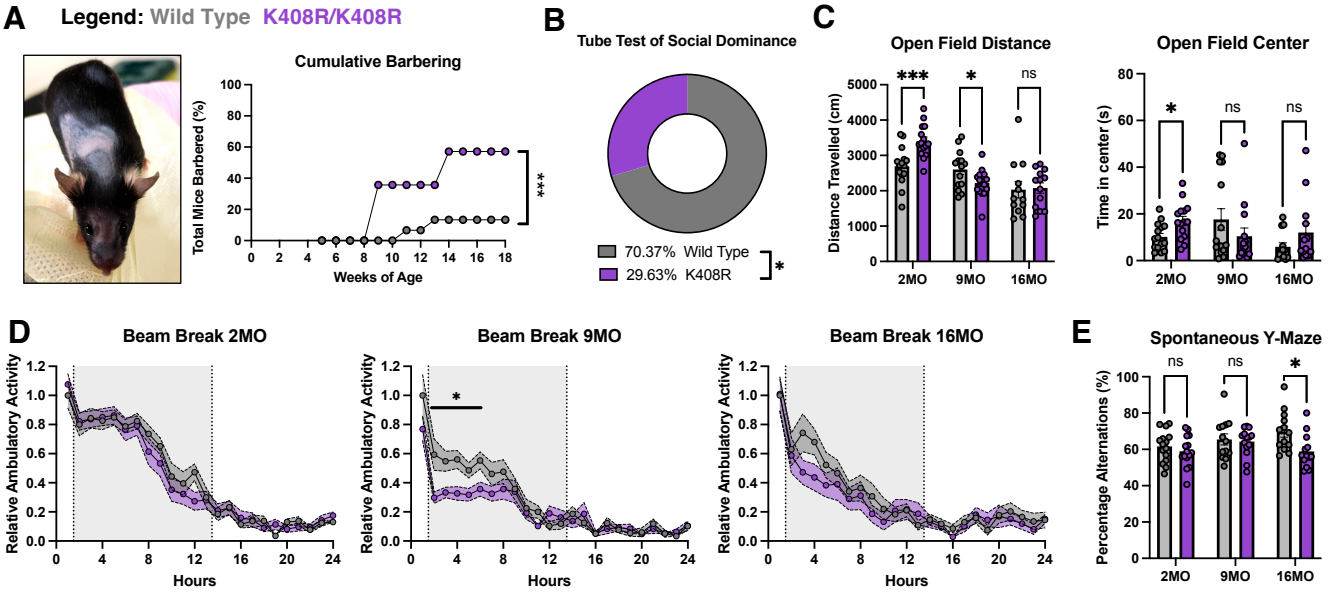

Fig. 4: Blocking TDP-43 SUMOylation *in vivo* leads to sex-specific social and cognitive impairment.

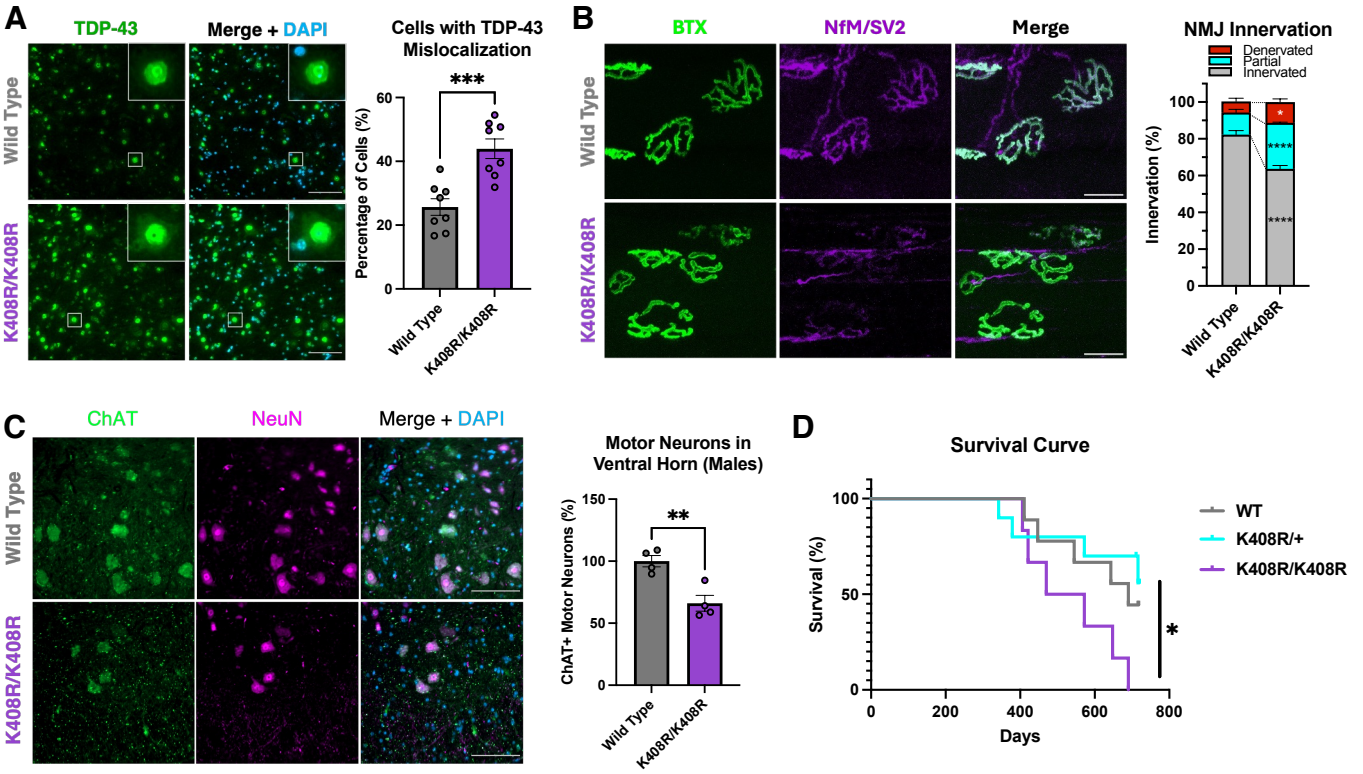

Figure 5: Male TDP-43^{K408R} mice present with age-specific features of ALS.

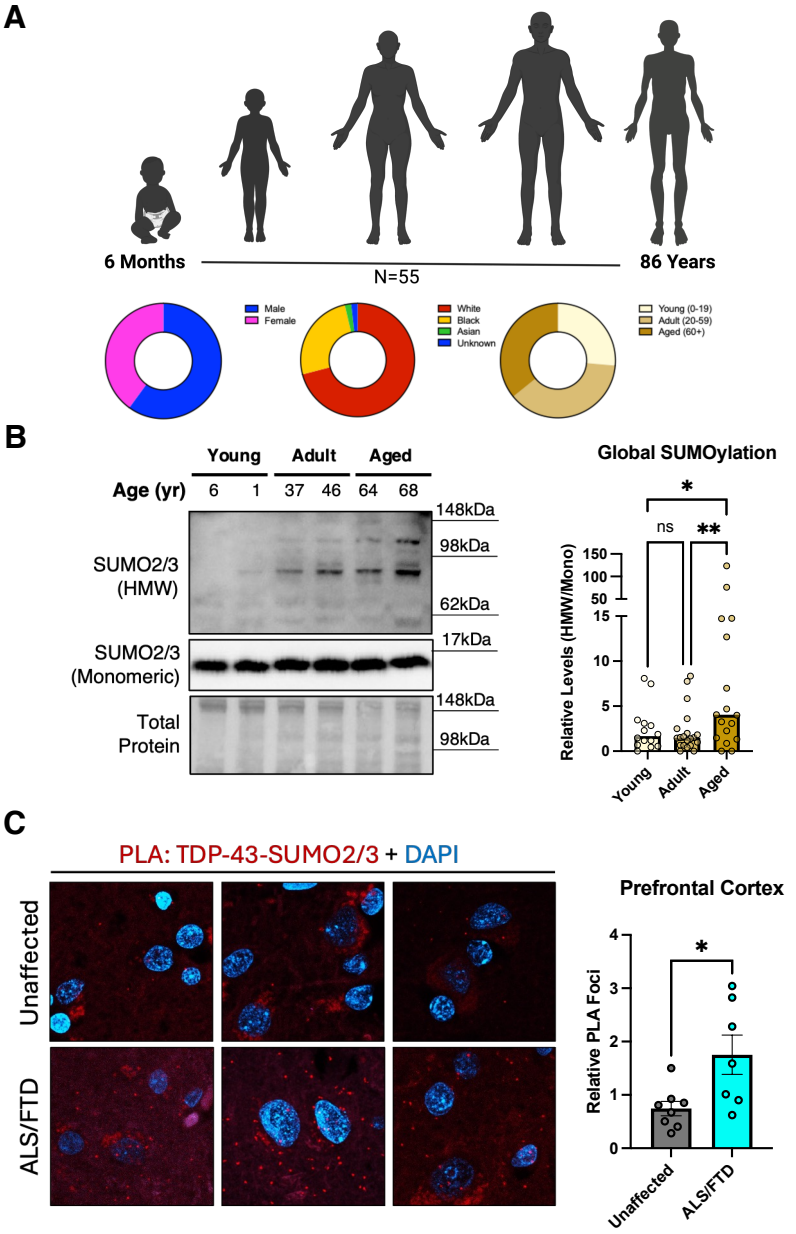

Fig. 6: SUMOylation correlates with aging and is enriched in the prefrontal cortex of ALS/FTD patients.

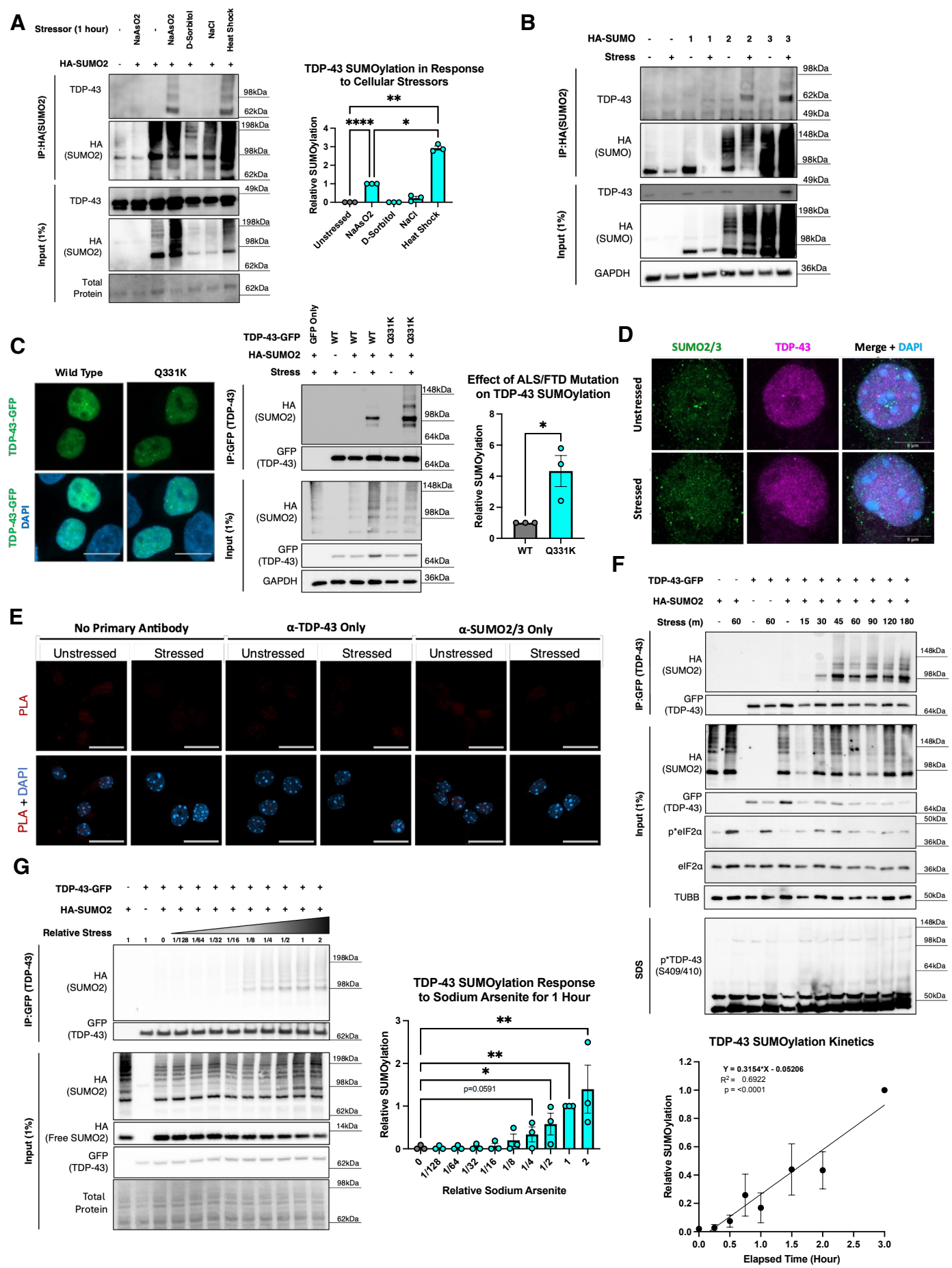

Fig. S1: Characterizing stress responsive TDP-43 SUMOylation.

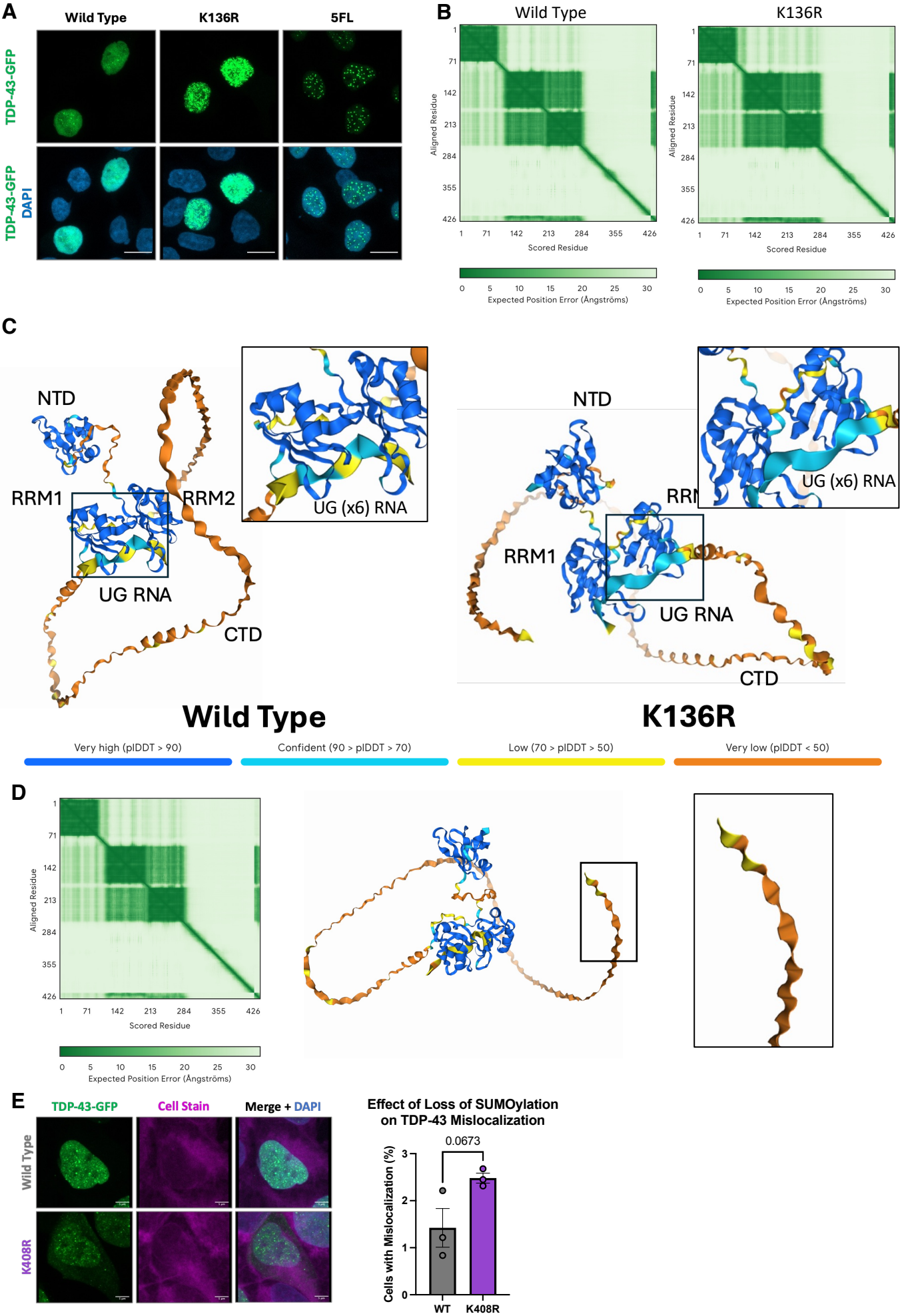

Fig. S2: Analysis of TDP-43 lysine to arginine mutation at K136 and K408.

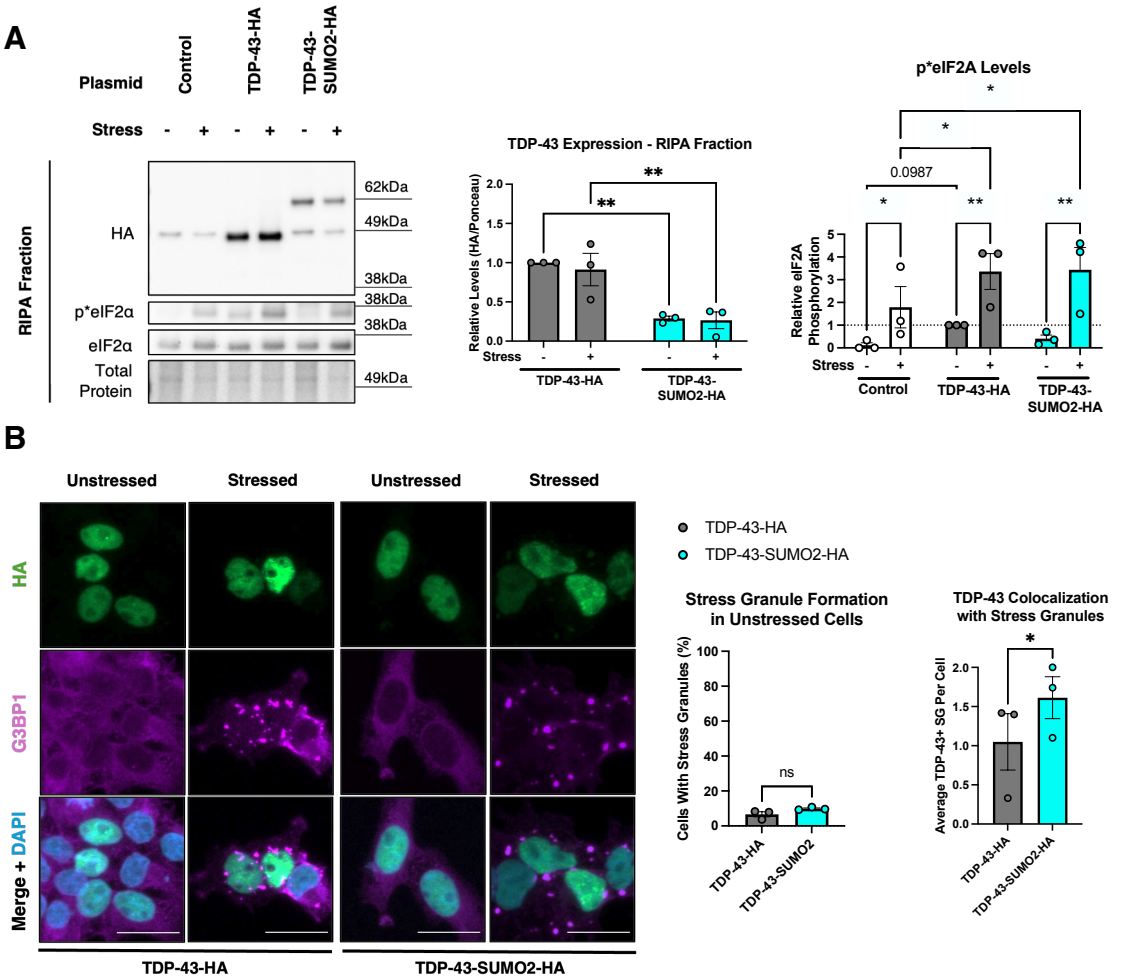

Fig. S3: Characterization of SUMO2 fusion to the C-terminus of TDP-43.

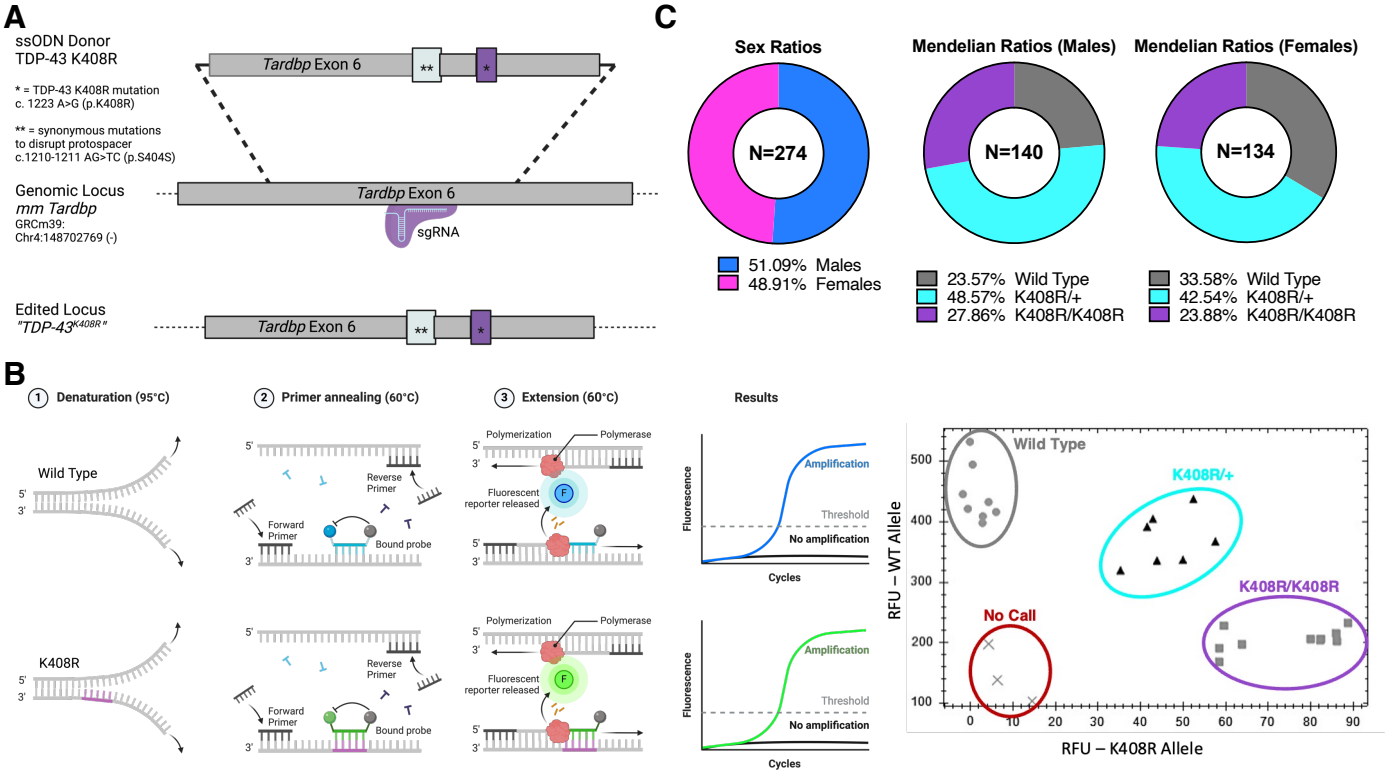

Fig. S4: Generation of the TDP-43^{K408R} mouse line.

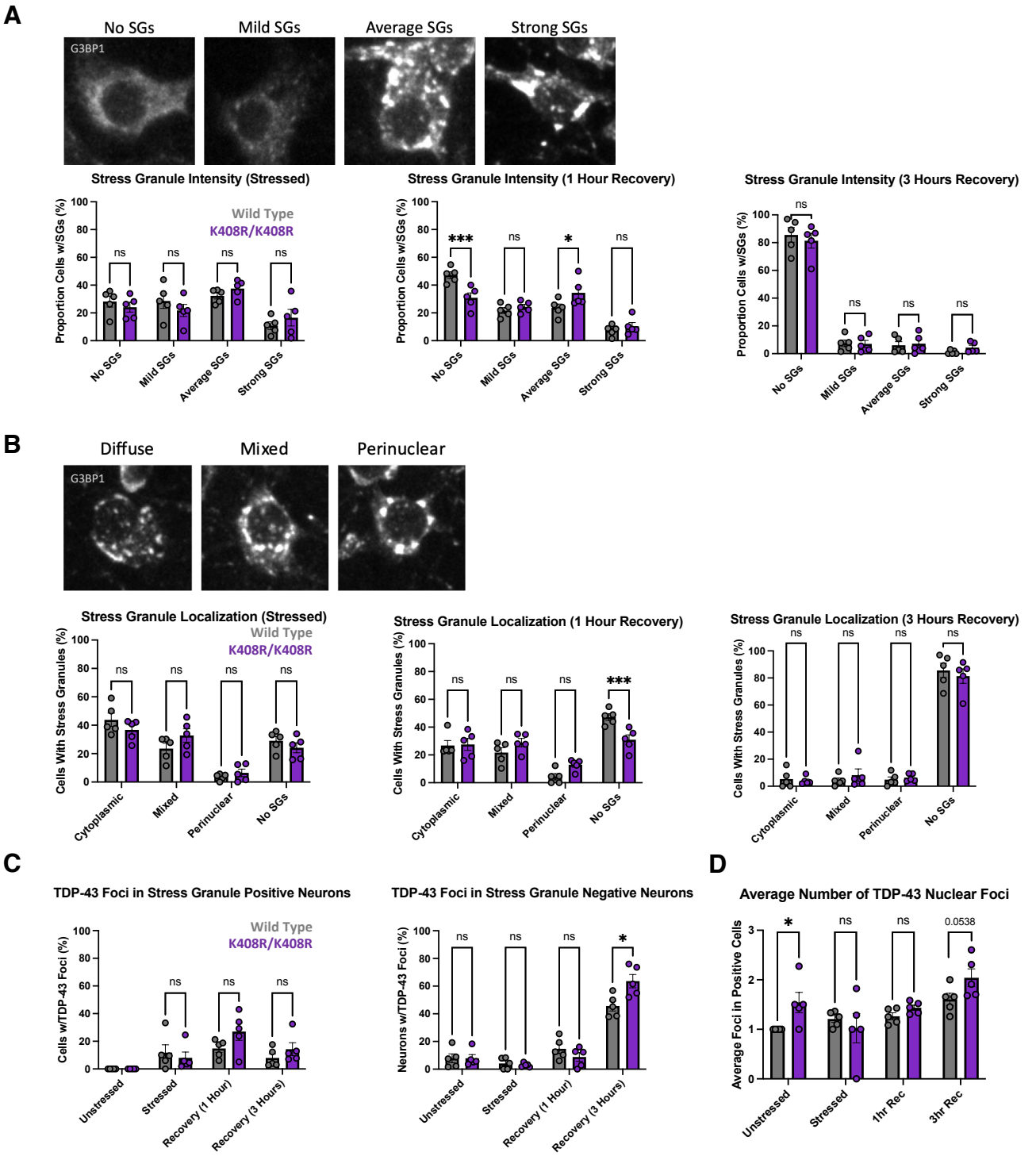

Fig. S5: Characterizing the stress response in TDP-43^{K408R} primary cortical neuron cultures.

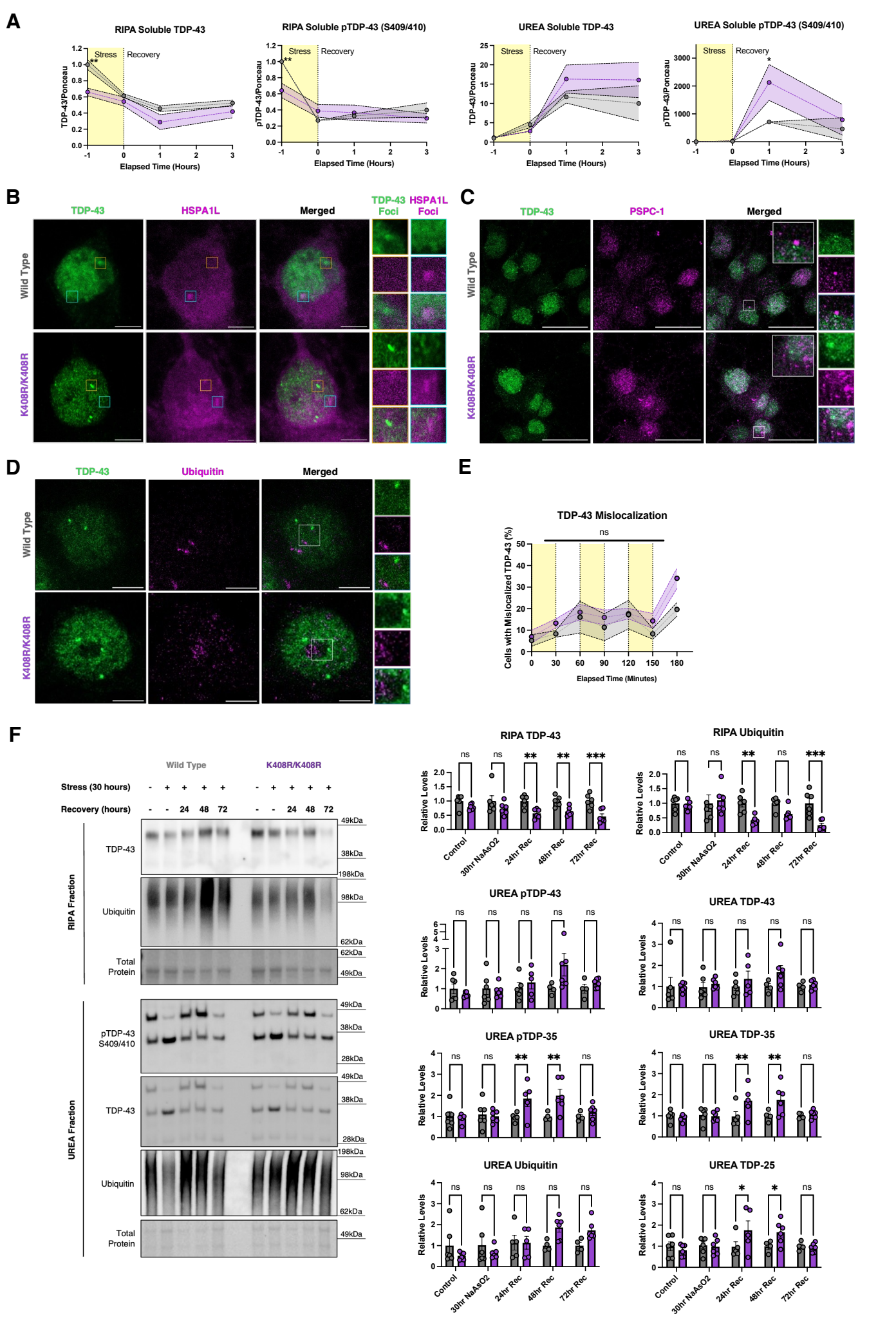

Fig. S6: Characterizing the effect of blocking TDP-43 SUMOylation in primary cortical neurons.

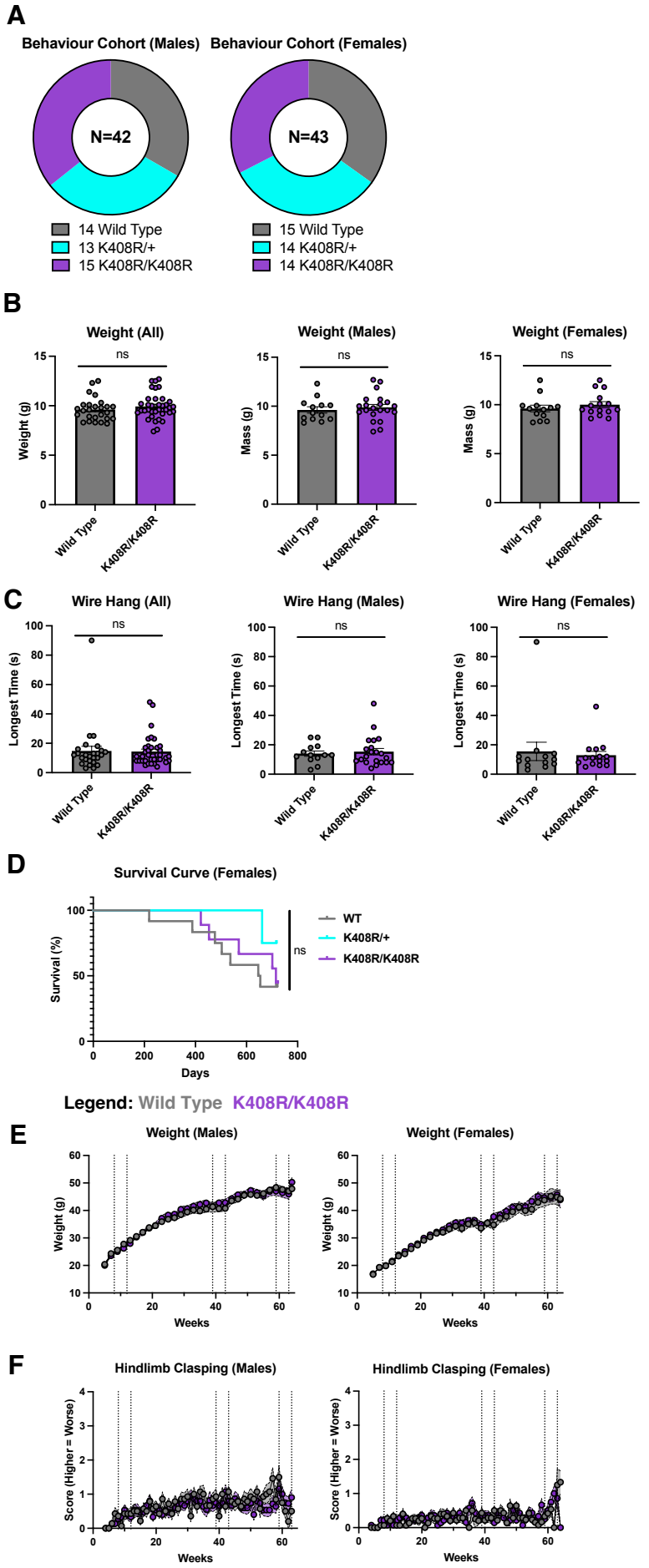

Fig. S7: General wellness of TDP-43^{K408R} mice during development and aging.

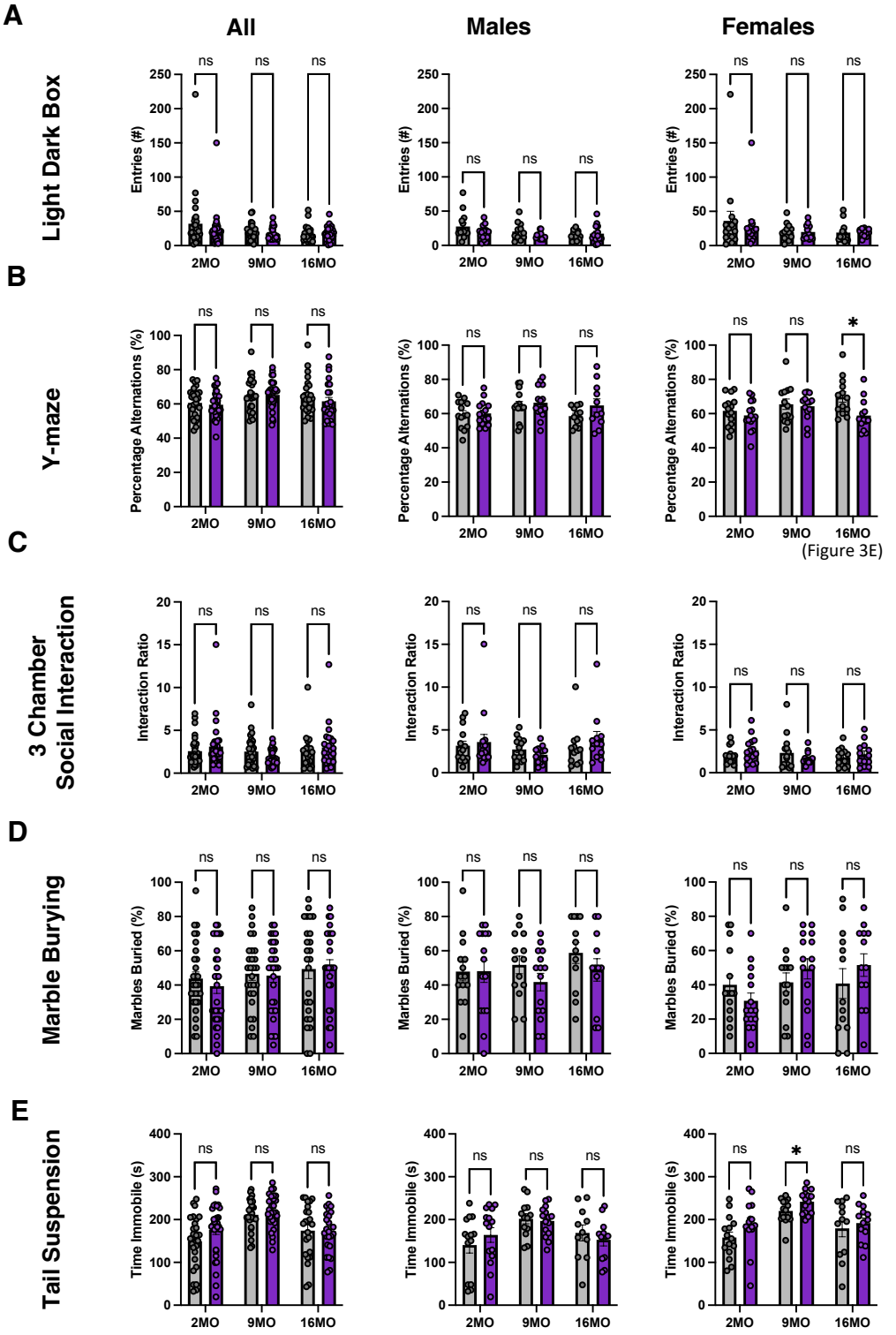

Fig. S8: Characterizing the cognitive and social behaviour of TDP-43^{K408R} mice.

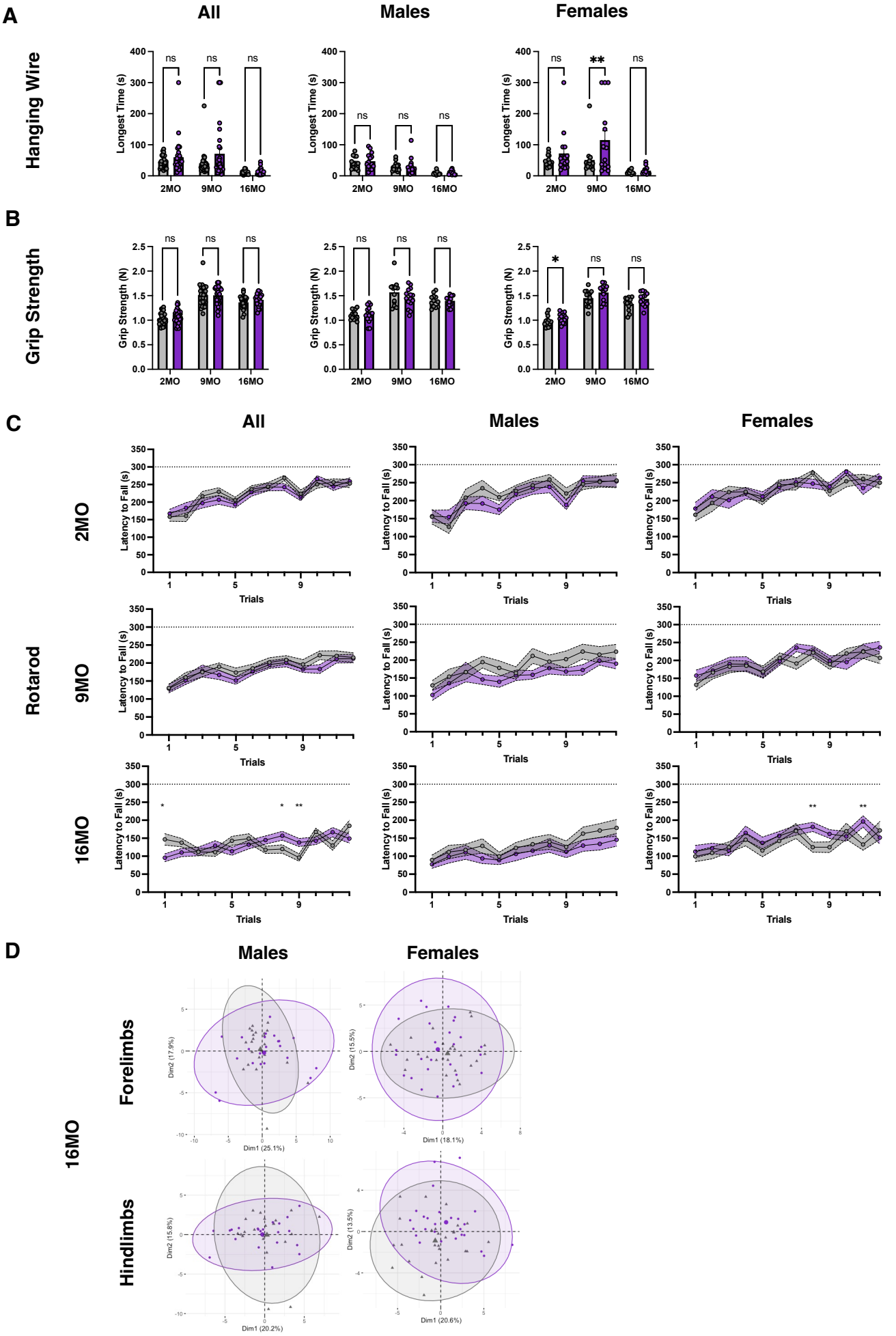

Fig. S9: Characterizing the motor behaviour of TDP-43^{K408R} mice.

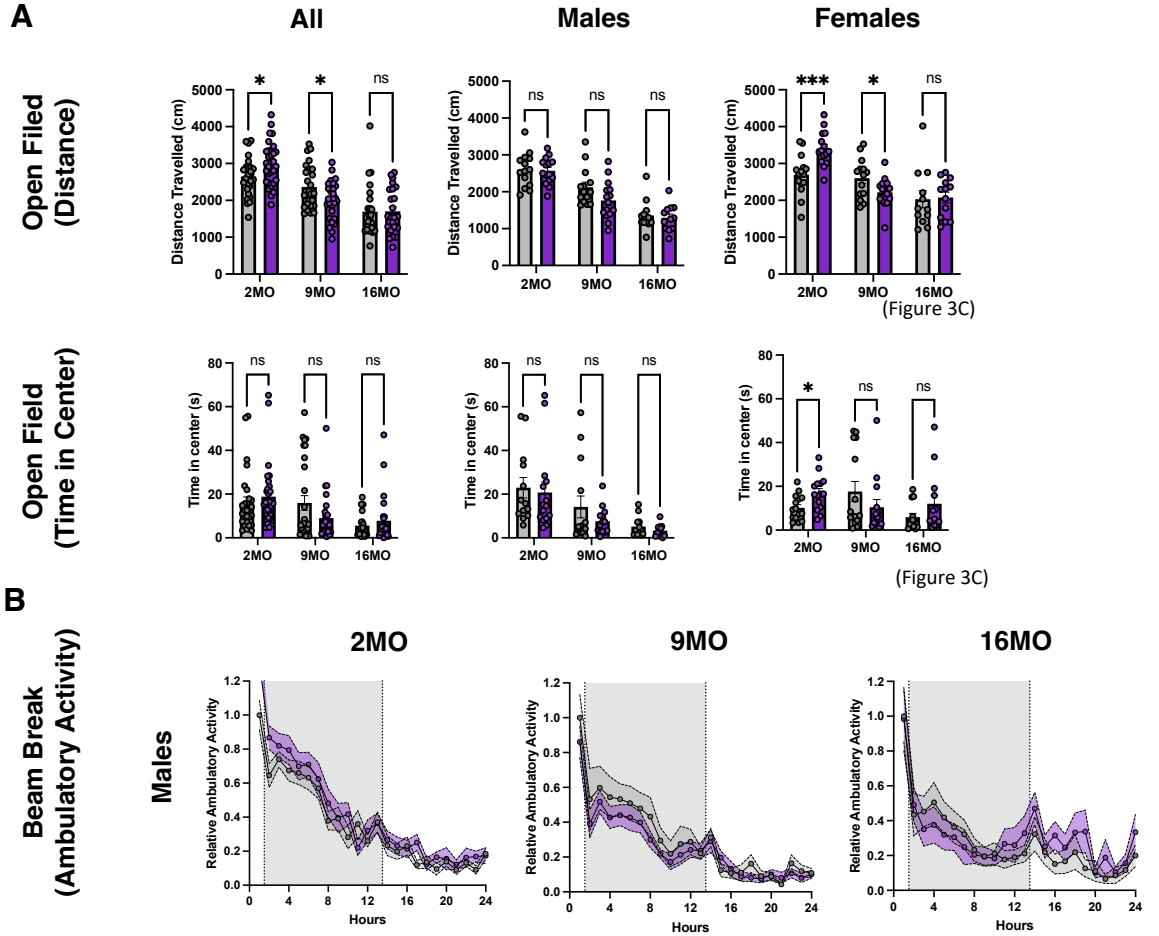

Fig. S10: Characterizing the activity of TDP-43^{K408R} mice.

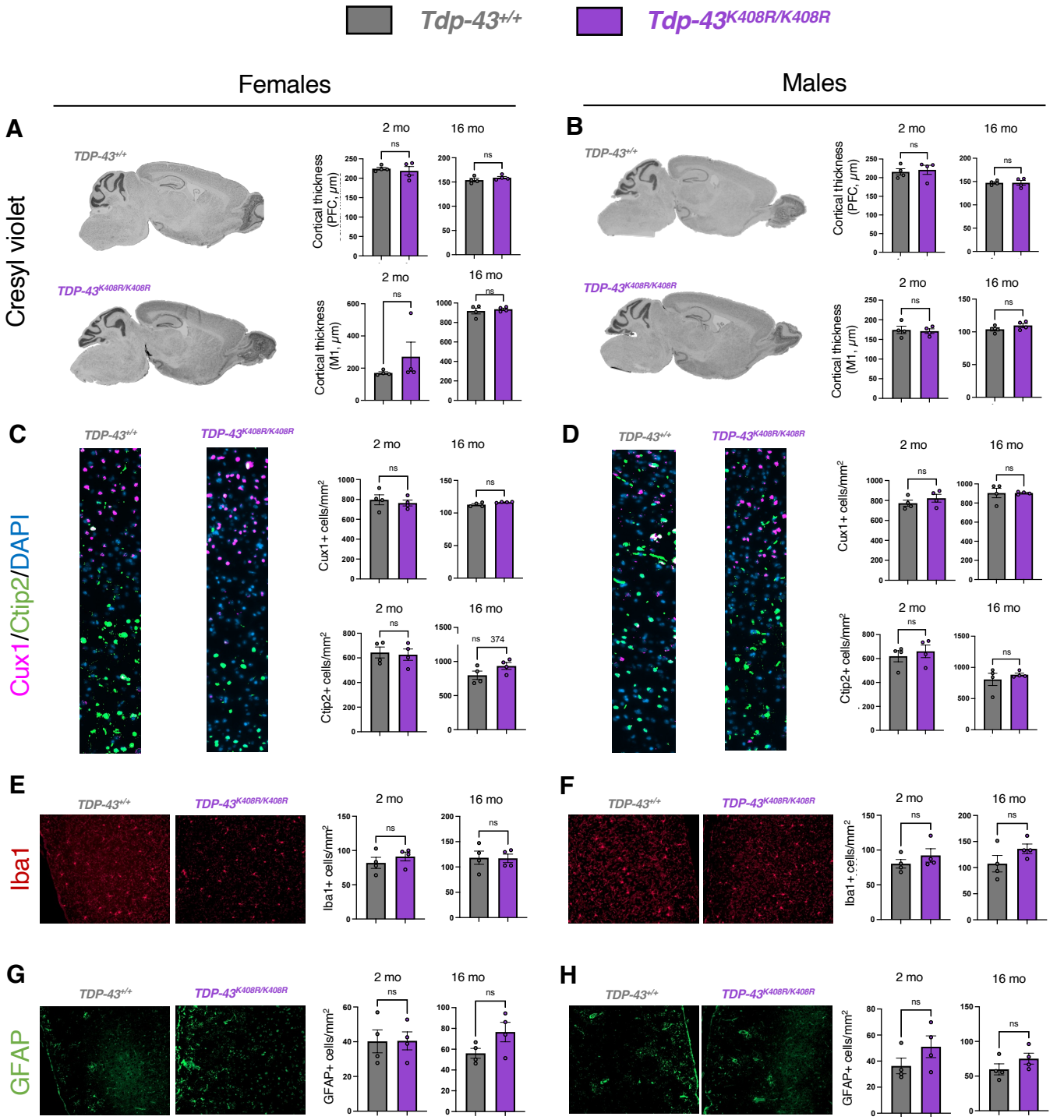

Fig. S11: Absence of overt neurodegenerative or neuroinflammatory phenotypes in TDP-43$^{K408R/K408R}$ mice.

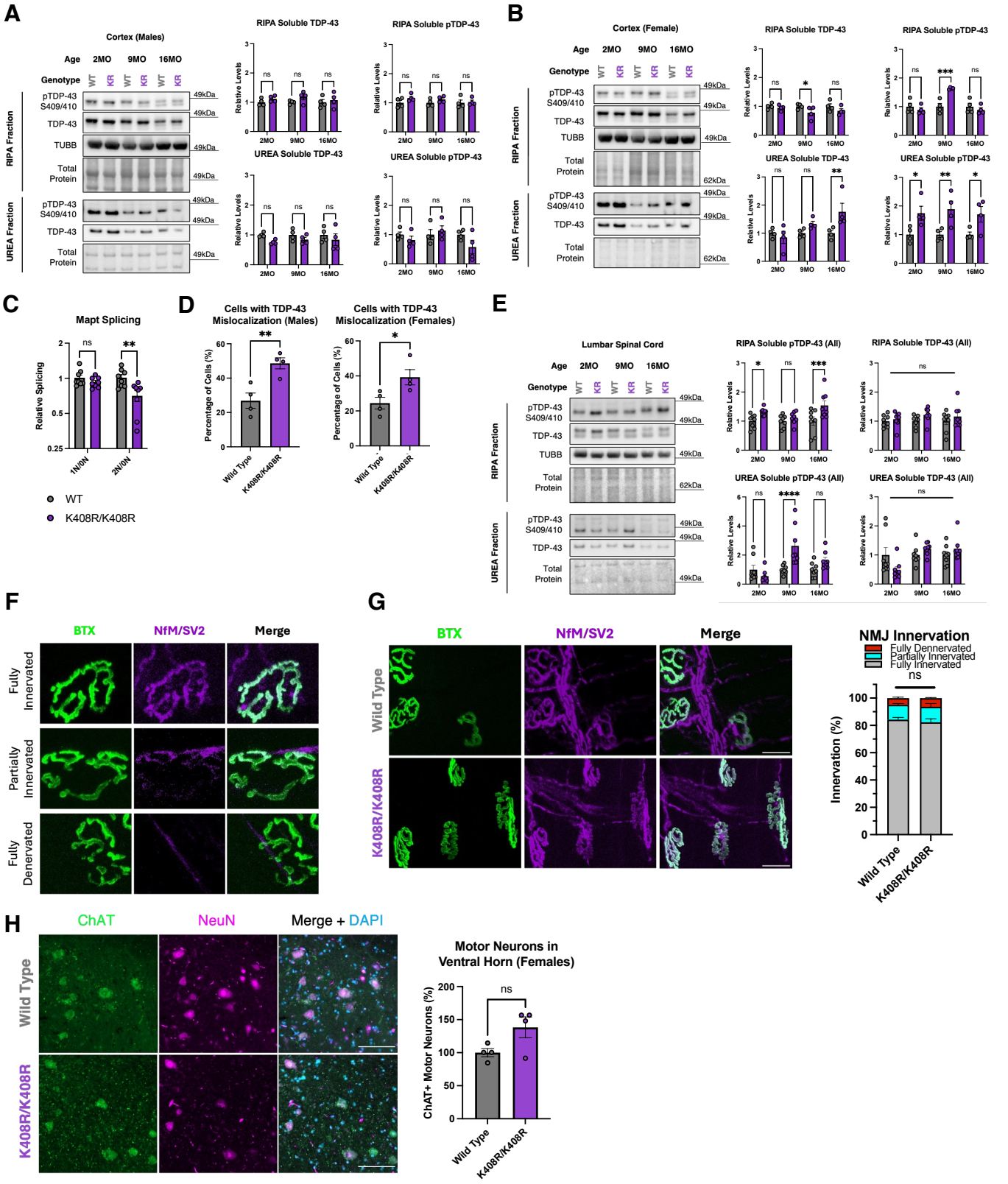

Fig. S12: Characterizing the molecular and histological affects of blocking TDP-43 SUMOylation in vivo.

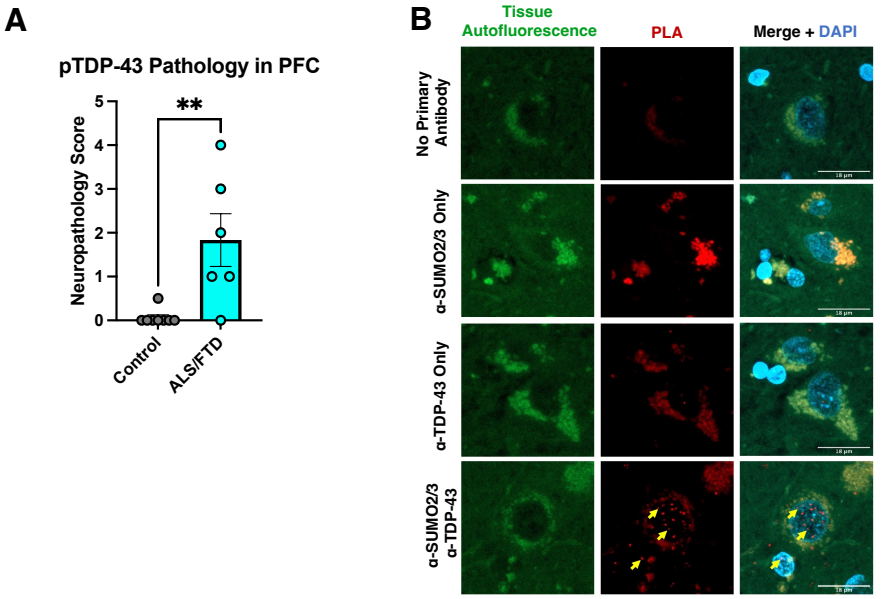

Fig. S13: Optimization of proximity ligation assay in human tissue.